ENGINEERING THE MECHANICAL PROPERTIES OF OCULAR TISSUES

Thesis by

Charles Sellers Nickerson

In Partial Fulfillment of the Requirements for the

degree of

Doctor of Philosophy

CALIFORNIA INSTITUTE OF TECHNOLOGY

Pasadena, California

2005

(Defended November 1, 2005)

ACKNOWLEDGEMENTS

I wish that I had space to thank everyone who has supported me and contributed to this work directly and indirectly, but I will have to limit this to just a few of the people who have done the most. It would be unjust to thank anyone before my wife, Pamela, for her love, support, and patience. She and my children, Rosemary and Samuel, have kept me on the narrow path between high productivity and work-a-holism. I would also like to acknowledge the contribution of my parents for encouraging my creativity, feeding my ravenous appetite for new challenges, and teaching me how to work. My siblings, James, Dawn, Kenny, Lee, and Suzie have also made numerous indirect contributions. My late grandmother has also been a very important influence in all of my accomplishments because she always expected a superior performance and taught me the value thereof. My achievements are the product of divine providence, the sacrifice of my parents, and the influence of my family, and I hope that they recognize the significance of their contributions. Additionally, I wish to thank Pam's family for all of their support while we have been here. Our many friends have also provided much-needed moral support through the ups and downs along the way.

On a professional level, I would first like to acknowledge my advisor, Professor Julie Kornfield, for her tremendous intellectual contributions to this work, for giving me room to think and create, and for her kindness. I don't know which of those things has been most important but they combined to create a wonderful graduate experience for which I will forever be grateful. I must also thank Anne Hormann in the same breath. Anne keeps the group on track, which is no minor task, and does it with a fantastic attitude.

I would also like to express deep gratitude to Dr. John Park of Vitreoretinal Technologies, Inc. He made tremendous scientific contributions to this work and was a mentor for me throughout. Mr. Hampar Karageozian and Dr. Vicken Karageozian at Vitreoretinal Technologies provided key ideas that inspired this research; Vitreoretinal Technologies funded most of this work. Professor Vincent Monnier of Case Western Reserve University has also been a key collaborator in our cornea work and provided ongoing academic and financial support. I would also like to thank the Achievement Rewards for College Scientists (ARCS) Foundation for providing me with the additional financial support necessary to attend graduate school while raising a family.

Former Kornfield group members, Dr. Frederic Tessier and Dr. Giyoong Tae, laid the foundation for the cornea work and spent a great deal of time teaching me about analytical biochemistry, tissue handling, and rheology. Dr. Maria Lujan Auad and Dr. Mike Kempe gave me further guidance in the techniques of rheometry and interpretation of rheological data. Ame DeLeon also contributed to the vitreous work during her summer research program.

I wish to thank everyone involved with our collaborative work in Mexico. I enjoyed and benefited immensely from working with Prof. Hugo Quiroz-Mercado directly and with his students, Dra. Nayeli Ibarra, Dr. Daniel Moreno, and Dra. Griselda Alvarez-Rivera, at the Hospital “Dr. Luis Sánchez Bulnes” de la Asociación Para Evitar la Ceguera (APEC) en México. Dr. Jorge Rivera and Dr. Jose Luis Garrero also contributed to those studies. Their willingness to share their clinical expertise and teach me their techniques allowed me to gain an understanding of the practical aspects of ophthalmic research. Professor Alberto

Tecante at the National Autonomous University of Mexico (UNAM) graciously opened his rheology lab to me while in Mexico. His student, Dra. Mariana Ramirez, was also very kind to help me in every aspect of my visit.

I would like to thank the current members of the Kornfield group, Eric Pape, Derek Thurman, Lucia Fernandez-Ballester, Rafael Verduzco, Neal Scruggs, Mike Mackel, Ameri David, Ryan Turner, Zulie Kurji, Dr. Shuichi Kimata, and particularly Matthew Mattson. Matthew has been an invaluable sounding board for ideas and source of suggestions. I would also like to thank former group members not mentioned above, including Wei Shen, Rob Lammertink, and Erica Thompson.

There are several other members of the Caltech community who deserve thanks: Professor Zhen-Gang Wang and Jennifer Whitman for fruitful discussions regarding network tension, Dr. Scott Ross for help with the difficult problem of conducting nuclear magnetic resonance (NMR) analyses of cornea lysates, and Professor John Brady for discussions regarding flows near permeable boundaries and surface features. I also wish to thank my committee members, Professors Robert Grubbs, David Tirrell, and Linda Hsieh-Wilson, for their help throughout this process. Graduate school has been a wonderful experience and I wish to thank the Institute for admitting me and providing this nurturing and stimulating academic environment. Finally, I would like to thank my first Chemistry teacher, Mr. Bill McKinney. He was the first to explain to me what I consider to be the most universal truth of chemistry—that structure yields function.

ABSTRACT

The mechanical properties of the structural tissues of the eye (cornea, sclera, and vitreous) are critical for vision. Age and disease can cause changes in their physical properties and compromise visual acuity; in the extreme, such changes can lead to blindness. Thus, there is great interest in understanding the mechanical properties of ocular tissues and in developing appropriate therapeutic strategies.

The goal of this thesis is to discover and manipulate the molecular mechanisms that determine the bulk physical properties of the vitreous and the cornea. These tissues are both ordered biocomposites of fibrous collagen embedded in soft matrices of proteoglycans (PGs) and glycosaminoglycans (GAGs). The hydration state, mole fraction, and particularly the organization of these components determine the mechanical properties of the respective tissues. Whereas the mechanical strength of these tissues has traditionally been attributed to their collagenous components, we present evidence that the PGs and GAGs also make significant contributions. We also suggest hypotheses regarding the mechanisms by which the carbohydrate components contribute and how they can be utilized for therapeutic purposes.

In order to study the unique physical properties of the vitreous, novel instrumentation was developed. We describe the use of cleated surfaces on parallel disk tools to quantitatively measure the rheological properties of diverse slip-prone fluids and soft materials. Densely-packed protrusions (0.45mm x 0.45mm cross section x 0.6mm length, 0.9mm apart) penetrate the slip layer, preventing significant flow between cleats. This creates a no-slip boundary ~ 0.16mm below their tips, which serves as the sample gap boundary, in direct analogy to the parallel plate geometry. This “cleat” geometry suppresses slip without application of significant normal force, it imposes well-defined shear to enable absolute measurements, and is compatible with small sample volumes. The geometry was validated in steady and oscillatory shear using a series of materials not prone to slip (Newtonian oils and an entangled polymer melt). The advantage of cleated tools over other slip-prevention

methods was demonstrated using slip-prone materials, including an emulsion, a suspension, and porcine vitreous humor.

The vitreous humor is a transparent gel comprised of a delicate, swollen double network of 10 – 20 nm collagen type II fibrils and charged GAG chains (hyaluronic acid). While extensive progress has been made in identifying the components and biochemistry of the vitreous, prior to the "cleat geometry" experimental limitations hampered quantitative determination of its mechanical properties. With cleated tools we overcame wall slip and avoided tissue compression during measurements of the dynamic moduli of fresh porcine and bovine vitreous. Shear moduli decreased five-fold from initial to steady-state values in the first hour after dissection. Steady-state values (Porcine: $G' = 2.6 \pm 0.9$ Pa and $G'' = 0.6 \pm 0.4$ Pa, $n = 9$; Bovine: $G' = 6.5 \pm 2.0$ Pa and $G'' = 2.0 \pm 0.6$ Pa, $n = 17$) are significantly greater than previously reported. The decrease in modulus after removal from the eye correlates with a decrease in mass: porcine vitreous expels ~5% of its mass within 5 minutes and continues to decay to a steady-state mass ~10% lower than its initial mass in the absence of external driving forces. The expelled fluid has a substantial hyaluronan concentration but a very low protein content. These results indicate that the vitreous network is under tension at its native volume, and its high initial modulus results from this state of tension. We hypothesize that hyaluronan plays a role in sustaining the "internal tension" by Donnan swelling.

The therapeutic goal in vitreous engineering is liquefaction: we seek pharmacological agents capable of gently separating the vitreous from the retina and destabilizing the network without damaging the adjacent tissues (retina and lens). We measured the stability of the vitreous against agents designed to target covalent bonds, hydrogen bonds, electrostatic attractions, and hydrophobic interactions using a simple weighing procedure. We found that in addition to covalent bonds, hydrogen bonds appear to play a particularly important role in stabilizing the vitreous network. This is in agreement with clinical observations that treating eyes with urea prior to vitrectomy provided a significant therapeutic benefit. We found that treating porcine vitreous with therapeutic doses of urea *in vitro* reduced the shear modulus by ~ 30%. Limited *in vivo* animal studies measured no

softening effect and indicated that the therapeutic benefit of urea may be a reduction of vitreoretinal adhesion.

The cornea is also composed of collagen fibrils embedded in a PG/GAG matrix. The cornea, however, contains far more collagen, PG, and GAG than vitreous, and its components are also more ordered: the collagen (type I) is in the form of 30 nm fibrils, precisely arranged lamellae and evenly spaced in a keratin sulfate-rich matrix. Our therapeutic goal in the cornea is to stabilize its nanostructure and mechanical properties against keratoconus, a degenerative disease in which the cornea softens and bows outward under the force of intraocular pressure.

We present coordinated biomechanical and biochemical analyses of corneal tissue that has been crosslinked using glycation. Non-enzymatic crosslinking alters the viscoelastic properties of protein-rich tissues, but a quantitative correlation between the formation of specific advanced glycation end products (AGEs) and physiologically relevant mechanical property changes has not previously been established. We report that corneas treated with 1% and 2% glyceraldehyde solutions produce a 300% and 600% rise in shear modulus, respectively, which strongly and linearly correlates with increased fluorescence and the formation of the AGEs argpyrimidine, lys-hydroxy-triosidine, and arg-hydroxy-triosidine (R^2= 0.999, 0.970, and 0.890 respectively). NMR studies are used to demonstrate that enzymatic digestion does not alter AGEs and has some advantages over acid hydrolysis. The level of mechanical reinforcement observed in these studies is probably sufficient to stabilize keratoconus corneas, based upon successful treatments with other crosslinking strategies.

Comparing quantitative correlations between modulus and AGE accumulation in corneas with analyses of collagen fibers isolated from mouse tail tendons suggests that glycation-induced corneal stiffening cannot be attributed solely to changes in collagen. We present a novel hypothesis that the mechanically-relevant AGE crosslinks are those that change the properties of the soft PG/GAG matrix and its coupling to the collagen fibrils, rather than the much more numerous AGEs that crosslink amino acids within fibrils.

TABLE OF CONTENTS

LIST OF ILLUSTRATIONS AND TABLES

SYMBOLS AND ABBREVIATIONS

AGE Advanced Glycation Endproduct

δ Penetration depth / Phase angle

G′ Storage Modulus

G″ Loss Modulus

GA Glyceraldehyde

GAG Glycosaminoglycan

G-3-phosphate Glyceraldehyde-3-phosphate

HA Hyaluronic acid

HPLC High Performance Liquid Chromatography

L_c Cleat length

MGO Methylglyoxal

MW Molecular Weight

NMR Nuclear Magnetic Resonance

PBS Phosphate-buffered Saline

PG Proteoglycan

PVD Posterior vitreous detachment

TBT Tendon breaking time

η Viscosity

η^* Complex Viscosity

σ Shear stress

γ Shear Strain

$\dot{\gamma}$ Strain Rate

C h a p t e r 1

INTRODUCTION

1.1 Background

The ability to create and maintain fixed spatial relationships between cells and organs is vitally important for higher organisms. Residing in fixed locations allows cells and tissues to work cooperatively through specialization and division of labor.[1] One illustration of the importance of precise physical properties and arrangements is mammalian vision, which relies on the precise geometry of the cornea, the mechanical strength of the sclera to support the retina, and the orbital ligaments to control the line of sight.

The mechanical properties of structural tissues such as these are derived from the nanoscale architecture and properties of their constituent molecules. Most structural tissues are biocomposites of fibrous proteins embedded in soft carbohydrate matrices. Collagen is the primary fibrous component; proteoglycans and glycosaminoglycans act as the matrix. The hydration state, mole fraction, and organization of these components vary between tissues and species, but the basic structure—high tensile-strength fibrils organized in soft matrices—is highly preserved. Rare genetic mutations that weaken collagen fibrils or

disrupt other aspects of this molecular pattern lead to devastating systemic diseases.[2-6] A number of more common diseases, such as arthritis and diabetes, are also associated with degeneration of collagenous tissues.

The debilitating nature and prevalence of heritable and degenerative disorders that affect connective-tissues has stimulated considerable biochemical and biomechanical research. Unfortunately, the molecular (biochemical) and biomechanical aspects of this important field have been investigated independently rather than in concert. We will present significant advancements that have come as a result of combining biochemical analyses with novel bulk characterization techniques.

Broadly stated, the goal of the present research is to discover and manipulate the molecular mechanisms that determine the bulk physical properties of the cornea and vitreous humor (Figure 1). This goal can be divided into three specific objectives:

1) To quantitatively determine the mechanical properties of connective tissues

2) To understand the molecular basis of these mechanical properties and their implications for disease and tissue engineering

3) To create therapeutic changes in the mechanical properties of the cornea and vitreous

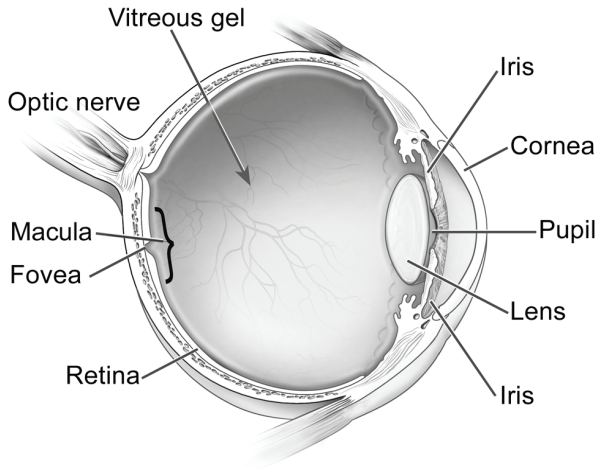

Figure 1. Diagram of the eye illustrating normal eye anatomy, including the vitreous humor (gel) and cornea. This figure reproduced by permission from the National Eye Institute, National Institutes of Health.

Our approach to these objectives is to combine analytical chemistry, rheology, and polymer physics with *in vivo* animal studies and the clinical experience of collaborators from industry and medicine. Biochemical and biomechanical investigations were conducted in parallel with drug discovery and clinical research, providing feedback between clinical and laboratory work. Clinical research identified potential therapeutics and evaluations of efficacy, while laboratory research addressed fundamental questions regarding the basis of the mechanical properties of collagenous tissues and how they can be engineered. The success of this approach in exploring potential therapeutics for the vitreous humor and cornea demonstrates the utility of an integrated approach to understanding and engineering connective tissues in general.

1.2 The Vitreous Humor

The vitreous is a transparent, collagenous gel that fills the posterior chamber of the eye. It is more than 98% water, avascular, and nearly acellular; thus, the vitreous was historically considered an inert space-filler.[7] However, over the past few decades it has become clear that the vitreous plays an essential structural role in the development, maintenance, and pathologies of vision. Sebag has summarized the functions of the vitreous as developmental—mediating proper growth of the eye; optical—maintaining a clear path to the retina; mechanical—supporting the various ocular tissues during physical activity; and metabolic—providing a repository of various small molecules for the retina.[8] Proper performance of these functions depends upon the unique physical properties of the vitreous.

The vitreous is thought to derive its physical properties from its hydrated double network of collagen type II fibrils and high molecular-weight, polyanionic hyaluronan macromolecules (Figure 2).[8-10] Heterotypic collagen fibrils (10 – 20 nm diameter) are composed of a small, collagen type V/XI core surrounded by collagen type II. Human vitreous hyaluronan (HA) is polydisperse with an average molecular weight that is estimated to be ~ 5,000,000.[9] Prior literature indicates that the vitreous completely liquefies when digested with collagenase enzyme, whereas it only shrinks when digested with hyaluronidase.[8, 9, 11] On this basis it has been presumed that the network of collagen fibrils provides mechanical strength, and the swollen HA macromolecules simply fill the space between fibrils to prevent aggregation. In Chapter 3 we will discuss the collagen-HA double network in greater depth and present rheological and biochemical evidence that hyaluronan *does* contribute

profoundly to the elastic character of the vitreous. This realization changes the way we view the network, particularly in the context of vitreous degeneration and engineering.

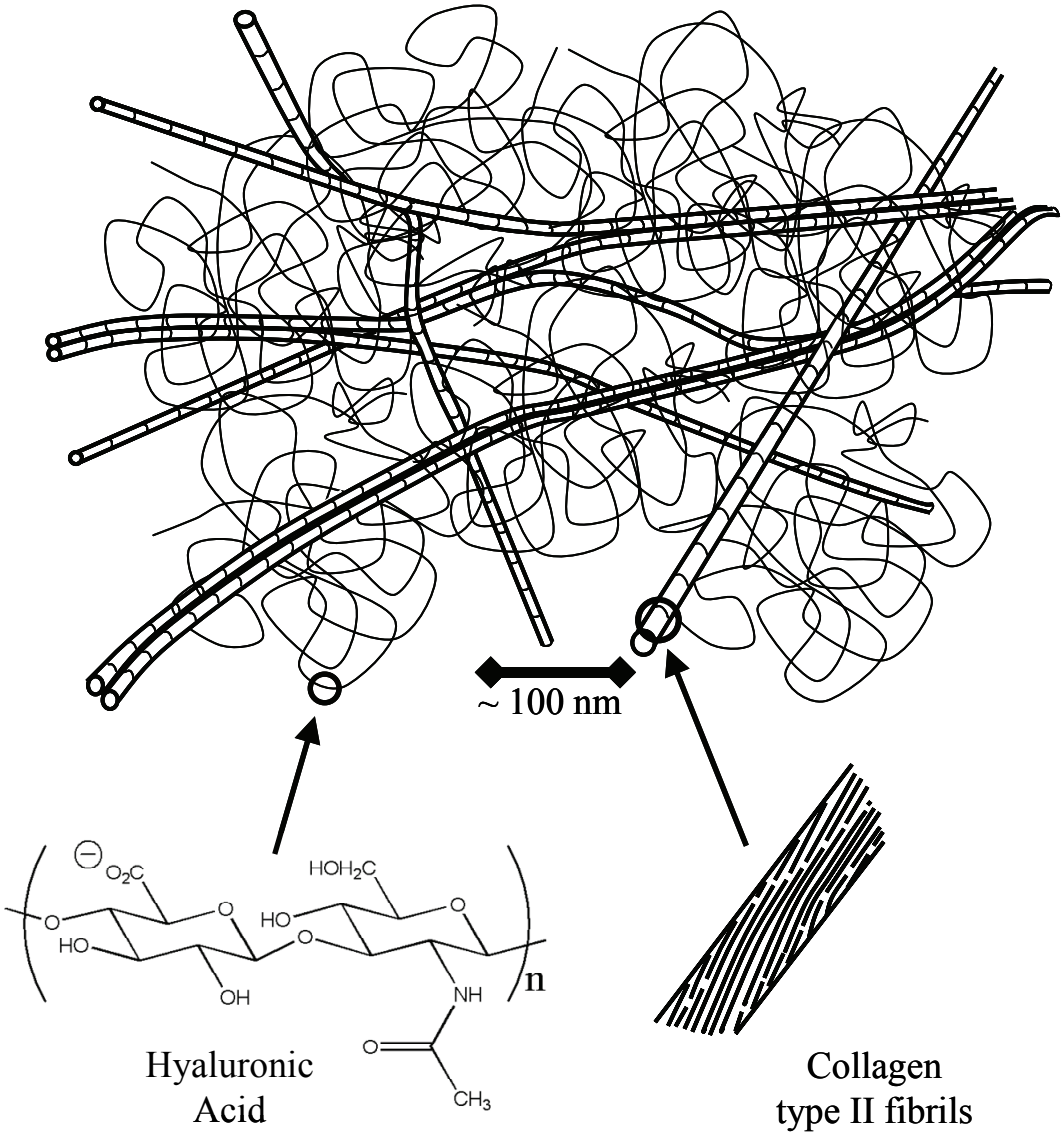

Figure 2. Schematic depiction of the network structure of the vitreous. The vitreous is composed of a highly-swollen double network of collagen type II fibrils (~ 15 nm in diameter) and hyaluronic acid (~ 5M MW).

With age the collagen-HA network degrades and loses mechanical integrity: pockets of fluid (lacunae) form near the retina as the components of the vitreous network aggregate and pull away from the retina.[8] Posterior vitreous detachment (PVD) is normally inhomogeneous, leaving points of adhesion that cause localized traction on the retina. Incomplete PVD and the resultant vitreoretinal traction are thought to play a role in a number of diseases, including macular holes, macular edema, vitreous hemorrhage, retinal tears, and retinal detachment.[8] The only treatment currently available for alleviating vitreoretinal traction is surgical removal of the vitreous (vitrectomy).[12] Motivated by the need for a less invasive and traumatic treatment, efforts have been made to find "pharmacological vitrectomy agents" capable of inducing PVD and liquefying or significantly softening the vitreous, thereby alleviating traction without surgery.[13] Proposed therapeutics from the literature will be discussed in detail in Chapter 4, but they generally consist of enzymes designed to cleave the proteins responsible for the mechanical integrity of the vitreous. Little attention has been given to the possibility of targeting noncovalent intermolecular interactions. We present results that indicate that disruption of hydrogen bonds strongly destabilizes the vitreous network, whereas disruption of electrostatic or hydrophobic interactions has a much weaker effect.

In addition to collagen type II and HA, 15 "minor" proteins and proteoglycans have been identified in the vitreous (Table 1). These components are minor in terms of mass, but may be crucial for the structure and stability of the vitreous, much as nails are a "minor" component of a wood-framed house. A number of these components, including link protein, fibronectin, and vitronectin, are known to connect proteins with polysaccharides in

other tissues. They may perform a similar function in the vitreous, stabilizing the collagen-HA network and linking it to other structures in the eye; however, little is known about the role of minor components in the molecular architecture of the vitreous network.

Given the importance of the viscoelastic properties of the vitreous to its function and to pathology, it is striking that there is no consensus on the value of its modulus in the prior literature. This is due in part to a lack of sufficient experimental methods for quantitatively measuring the mechanical properties of the vitreous and how they change as a result of various treatments.[14] To address this need we developed a novel rheological tool that enabled us to make the first quantitative measurements of the mechanical properties of the vitreous. We discovered that the modulus of the vitreous is significantly higher *in situ* than after removal from the eye. Further exploration of this discovery led us to a novel hypothesis regarding the mechanical properties of the vitreous: that HA increases the modulus of the vitreous by swelling the collagen network to a state of tension.

The novel tool also allowed us to measure modulus changes that resulted from treating the vitreous with a particular proposed pharmacological vitrectomy agent—urea. Clinical observations that urea may facilitate vitreous removal[15, 16] led us to investigate its influence on the mechanical properties of the vitreous *in vitro* and *in vivo*. Slit lamp observations of urea-treated vitreous, together with reduced surgical time during vitrectomy, suggested to the clinicians that urea "liquefied" the vitreous. By quantitatively characterizing the modulus of the vitreous, our work showed that treatment did not liquefy vitreous *in vitro* or *in vivo.* By working side-by-side with a team of eye surgeons working under the direction

of Professor Hugo Quiroz-Mercado at the Hospital "Dr. Luis Sánchez Bulnes" de la APEC in Mexico, we were able to reconcile clinical observations with rheological measurements. The clinical benefit was more likely the result of reduced vitreoretinal adhesion and phase separation as the collagen network contracted away from the retina to relieve tension. We also explored the effects of other agents on vitreous and found that hydrogen bonding plays a more significant role in stabilizing the vitreous network than electrostatic or hydrophobic effects. Taken together, these results provide a basis for rational design of future pharmacological vitrectomy agents.

Component	**Concentration** Human/Pig [μg/ml]	**Location**	**Proposed functions**
Water	>980,000[9]/ same	Throughout	Maintains vitreous mechanical properties and facilitates transport[7]
Salts (NaCl, KCl, $CaCl_2$, and $MgCl_2$)	~9,000[9]/same	Throughout	Global charge balance, Donnan swelling; vitreous is isotonic with blood and most other tissues[7]
Total Protein	800[7]/700[17]	Throughout	—
Total polysaccharide	240[18]/~250[17]	Throughout	—
Collagen type II	~225[9]/150[17]	Throughout as heterotypic fibrils	Resist elongation of the eye and provide structural framework for the vitreous body[7]
Hyaluronic acid	65-400[9]/165[17]	Throughout	Resist compression of the eye, hydrate tissue, space collagen fibrils[7]

Albumin	293[19]/	Throughout	Soluble protein, no known structural role
Link protein	0.6(bovine)[20]	Unknown	1:1 with versican; it may be there to link versican to HA[20]
Collagen V/XI	~30[9]/ Unknown	Throughout	Form the core of heterotypic collagen II fibrils[9]
Collagen IX	<30[9]/ Unknown	Throughout	Decorate surface of heterotypic collagen II fibrils, prevent fibril aggregation, possibly link fibrils to noncollagenous components[9]
Collagen VI[21]	Unknown	Concentrated on the zonular fibers	Bind collagen fibrils to HA and other species (has been shown to bind von Willebrand factor, collagen II fibrils, decorin and HA)[22, 23]
Collagen XVIII[9]	Unknown	Vitreoretinal interface	Vitreoretinal adhesion; has been co-localized with opticin at vitreoretinal interface; contains endostatin as a non-collagenous domain[9]
Cartilage oligomeric matrix protein (COMP)[24]	Unknown	Unknown	Unknown, but also found in cartilage and tendon; contains von Willebrand factor domains (see collagen VI)[25]
Microfibril-associated glycoprotein-1 (MAGP1)[26]	Unknown	Unknown	Decorate exterior of zonular fibers[26]
Opticin[9]	Unknown	Vitreous base and lamina cribrosa	Acts in conjunction with collagen XVIII to mediate vitreoretinal adhesion[9]
Fibrillin	Minor but probably > [coll VI][9]	Attached to lens capsule	Structural fibrils for lens capsule anchoring & articulation[9]
Fibronectin	6[9]/ >76(bovine)[27]	Throughout	Mediate binding between collagen and polysaccharides[25]

Vitronectin	4[28]/ Unknown	Unknown	Mediate collagen-polysaccharide binding; sensitive to denaturation[25]
Versican	60[29]/ 22(bovine)[20]	Unknown	1 per 150 moles of HA; possible link between HA and collagen and has been show to dissociate (if it was associated) in 4M guanidinium HCL; HA binding has been demonstrated[17, 25]
VIT1[30]	Unknown	Unknown	May have structural role[30]
Laminin/ Collagen type IV[31]	Unknown	Inner limiting membrane surrounding vitreous	While not components of the vitreous proper, they may participate in peripheral vitreous adhesion

Table 1. Known components of the vitreous humor listed with available information regarding concentration (μg / mL), distribution, and proposed function.

1.3 The Cornea

Like the vitreous, the cornea is composed of collagen fibrils embedded in a proteoglycan (PG) and glycosaminoglycan (GAG) matrix; however, unlike the vitreous, the cornea has a highly-ordered structure. The major structural element of the cornea (~ 90% of its thickness) is the stroma, which is composed of approximately 200 lamellae of oriented collagen type I fibrils embedded in a hydrated PG/GAG[12] (Figure 3). The precise arrangement of collagen fibrils allows the cornea to retain optical clarity in spite of the relatively high density of collagen fibrils (30 nm diameter) required to retain the shape of the cornea.

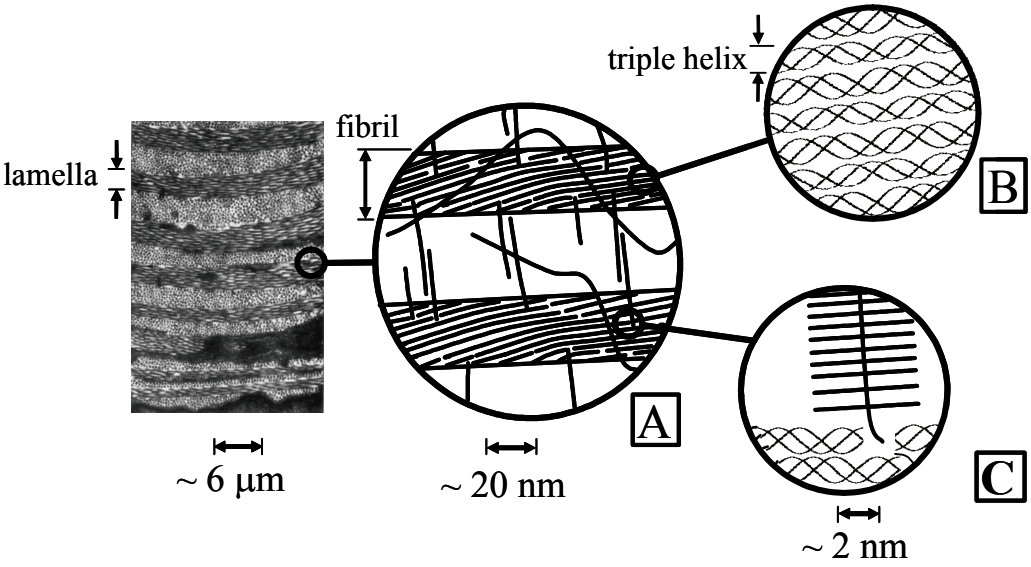

Figure 3. Stroma microstructure. [A] Represents the rigid collagen type I fibrils and smaller strands of proteoglycan that compose the lamellae of the corneal stroma. [B] Shows an enlargement of part of one of the fibrils, displaying the collagen triple helices aligned within a fibril. [C] Depicts the protein core of a proteoglycan non-covalently associated with the surface of a collagen fibril and decorated with polysaccharide chains. Micrograph was used by permission from Prof. K. Kadler, U. Manchester.

Whereas a primary therapeutic objective in the vitreous is softening and inducing PVD to alleviate vitreoretinal traction, a major, unmet clinical need in the cornea is enhancing its mechanical stability to prevent the progression of keratoconus. Keratoconus ("cone-shaped cornea") is a condition in which the cornea softens and slowly begins to protrude outward under the force of intraocular pressure.[12] It affects roughly 1 in 2,000 people, normally beginning in the teens or early twenties, and causes progressive loss of visual acuity, eventually leading to blindness.[32] In early stages, keratoconus is treated by application of hard contact lenses that correct vision and help maintain the shape of the cornea. If keratoconus progresses further, cornea transplantation is the only known treatment. The expense and difficulty of obtaining transplant tissue and the invasive nature of the surgery motivate our efforts to find a chemical treatment for keratoconus.

Collaborators at ISTA Pharmaceuticals, Inc. (Irvine, CA) developed a non-toxic, glycation-based crosslinking strategy to stabilize the cornea against keratoconus using glyceraldehyde (GA). Glyceraldehyde reacts with primary amines to form several known advanced glycation endproducts (AGEs), including two crosslinks and three AGEs that are also formed in reactions with methylglyoxal (MGO), another species investigated in this work (Figure 4). We have demonstrated that therapeutic (nontoxic) doses of glyceraldehyde are capable of significantly increasing the shear modulus of porcine corneas. Equivalent increases in modulus, achieved through alternative crosslinking strategies, have been shown to stabilize keratoconus eyes in clinical trials.[33, 34]

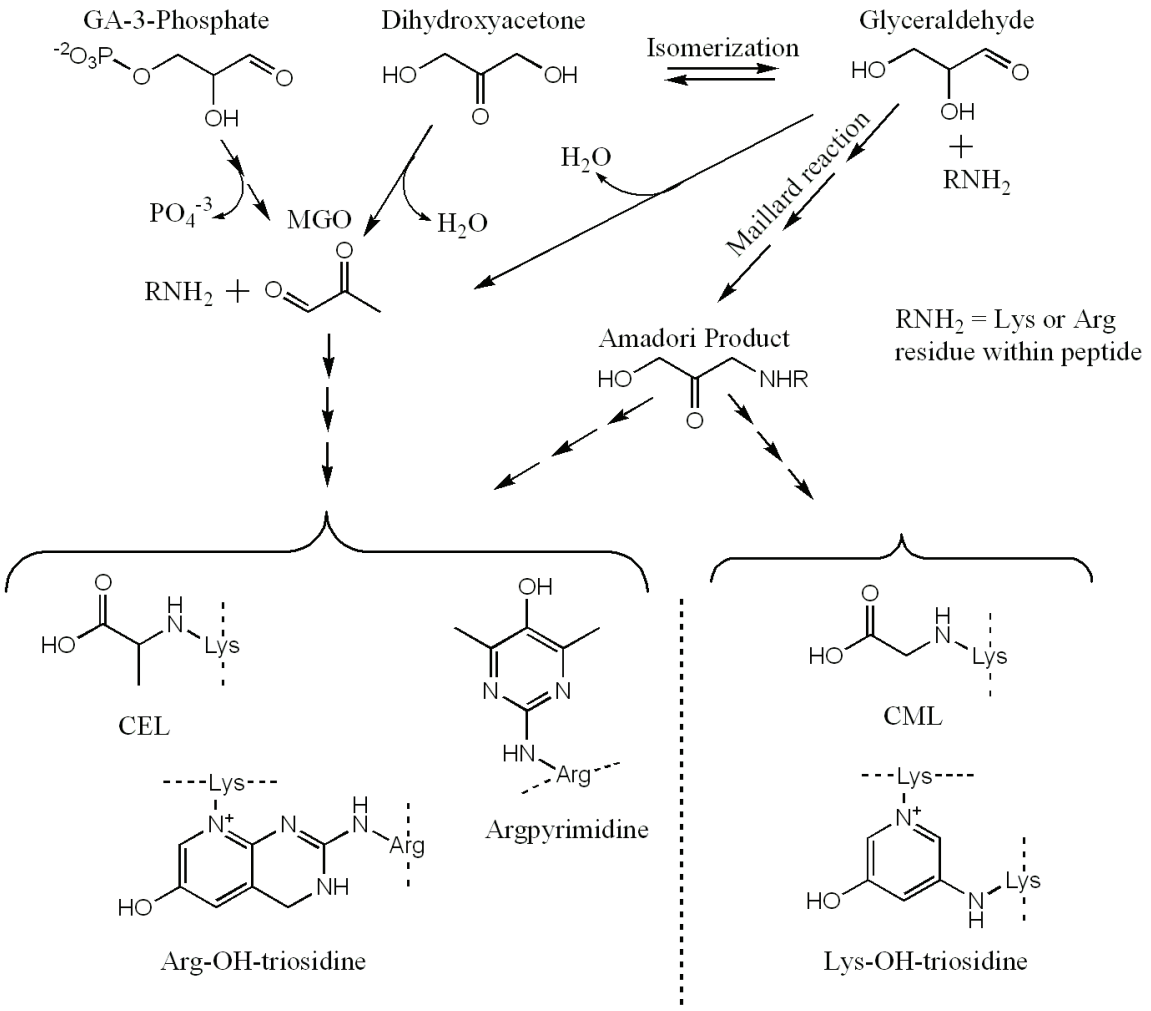

Figure 4. Glyceraldehyde, glyceraldehyde-3-phosphate (GA-3-phosphate), and methylglyoxal (MGO) all lead to similar AGEs, including argpyrimidine, arg-OH-triosidine, lys-OH-triosidine, and carboxyethyl lysine. RNH_2 indicates a primary amine on the side chain of an Arg or Lys residue within a peptide.

Biochemical analyses of GA-treated corneas revealed an additional protective effect of GA treatment: they are far less susceptible to proteolytic degradation (Chapter 5). This is particularly significant in light of the current hypothesis that keratoconus-induced softening comes as a result of overactive proteases in the cornea.[35] The enzyme protective effect also indicates that GA may be a suitable treatment for corneal ulcers, which have also been

linked to increased proteolytic activity and treated with crosslinking strategies.[36] The effect of GA on corneal ulcers has not yet been addressed.

Glycation-induced changes in enzyme resistance and modulus also correlate with increased fluorescence and AGE accumulation. We were able to isolate and quantify specific AGEs from glycated corneas and demonstrate that modulus increases linearly with accumulation of each of them, including argpyrimidine, a pendent adduct. Thus, it appears that crosslinking and noncrosslinking AGEs rise together and that various individual AGEs could serve as a surrogate to track tissue stiffening, whether or not the individual surrogate AGE is a crosslink. It may be possible to use an equivalent empirical relation to noninvasively measure (e.g., by fluorescence) the degree of tissue stiffening in clinical practice.

Quantitative correlations between the chemical and mechanical impact of glycation on corneal tissue also yield new insight into the molecular mechanisms of AGE-related tissue stiffening. The literature holds that glycation stiffens collagenous tissues by changing the properties of the constituent collagen fibrils;[37, 38] however, our results demonstrate that glycation-induced corneal stiffening cannot be attributed solely to changes in the properties of the collagen fibrils. We present a novel hypothesis that the mechanically relevant AGE crosslinks are those that change the properties of the soft PG/GAG matrix and its coupling to the collagen fibrils, rather than the much more numerous AGEs that crosslink amino acids within fibrils.

New insights into the increase in modulus associated with AGEs may also be broadly relevant to aging, diabetes, and tissue engineering research. The mechanisms by which glycation stiffens tissues *in vitro* may be relevant to certain pathologies of aging and diabetes. When properly understood, glycation has the potential to be turned from a pathologic process to a therapeutic strategy. The cornea is a good example, but it is merely a case-in-point. This strategy can be applied to a number of areas, from wound healing to bioadhesion to improving the mechanical properties of protein-based and polyamide synthetic tissues. Imparting strength to weakened connective tissue through glycation may provide an alternative to tissue transplants in diseases such as keratoconus.

1.4 Broader Implications

A unifying theme that emerges from both the vitreous and cornea work is that collagenous tissues depend integrally on the contributions of their carbohydrate components for mechanical strength. We hope that future efforts to engineer the mechanical properties of collagenous tissues will recognize the important mechanical role of carbohydrate components and apply this knowledge in the design of therapeutics.

The overarching goal of this thesis is to bridge the gap between the chemical, biomechanical, and clinical aspects of tissue engineering. Working closely with physicians to focus on these three aspects in parallel has allowed developments from the lab to rapidly influence therapeutic formulations for clinical trial (e.g., optimal pH of urea treatment), and feedback on the *in vivo* relevance of *in vitro* discoveries allowed us to rapidly verify the significance of new findings. We hope that the success we have had in elucidating the

molecular interactions that play a significant role in biomechanics will provide a model for productive cross-field collaborations.

1.5 Organization of Thesis

There were no rheological methods suitable for quantitative characterization of the vitreous prior to this work. Chapter 2 presents the novel "cleat geometry" developed specifically for this purpose.

Chapters 3 and 4 address the properties and network structure of the vitreous. In Chapter 3 the mechanical properties of the vitreous are defined. A novel hypothesis regarding a direct contribution of hyaluronic acid to the mechanical stiffness of the vitreous is also presented. In Chapter 4 the stability of the vitreous network in various chemical environments is examined as a basis for selecting potential pharmacological vitrectomy agents. Hydrogen bonding is shown to play a key role in stabilizing the vitreous network and urea is examined as a potential therapeutic for softening the vitreous.

Chapters 5 and 6 address glycation in the cornea. In Chapter 5 the chemical and mechanical impact of glycating corneal tissue with glyceraldehyde is examined. In Chapter 6 mechanical measurements of glycated collagen fibers from mouse tail tendons are used to demonstrate that the enhanced mechanical strength of glycated collagenous tissues cannot be attributed solely to the stiffening of collagen fibrils – the surrounding matrix (presumably proteoglycans) must also play a role.

BIBLIOGRAPHY

1. Scott JE. Extracellular-Matrix, Supramolecular Organization and Shape. *Journal of Anatomy.* Oct 1995;187:259-269.

2. Berg C, Geipel A, Noack F, et al. Prenatal diagnosis of Bruck syndrome. *Prenatal Diagnosis.* Jul 2005;25(7):535-538.

3. Baxter BT. Heritable diseases of the blood vessels. *Cardiovascular Pathology.* Jul-Aug 2005;14(4):185-188.

4. Chien S, Muiesan P. Spontaneous liver rupture in Ehlers-Danlos syndrome type IV. *Journal Of The Royal Society Of Medicine.* Jul 2005;98(7):320-322.

5. Glorieux FH. Caffey disease: an unlikely collagenopathy. *Journal Of Clinical Investigation.* May 2005;115(5):1142-1144.

6. Evereklioglu C, Madenci E, Bayazit YA, Yilmaz K, Balat A, Bekir NA. Central corneal thickness is lower in osteogenesis imperfecta and negatively correlates-vith the presence of blue sclera. *Ophthalmic And Physiological Optics.* Nov 2002;22(6):511-515.

7. Fatt I, Weissman BA. *Physiology of the Eye.* Second ed. Boston: Butterworth-Heinemann; 1992.

8. Sebag J. *The Vitreous - Structure, Function, and Pathobiology.* New York: Springer-Verlag Inc.; 1989.

9. Bishop PN. Structural macromolecules and supramolecular organisation of the vitreous gel. *Progress in Retinal and Eye Research.* May 2000;19(3):323-344.

10. Sebag J, Balazs E. Morphology and ultrastructure of human vitreous fibers. *Investigative Ophthalmology and Visual Science.* 1989;30:1867-1871.

11. Bos KJ, Holmes DF, Meadows RS, Kadler KE, McLeod D, Bishop PN. Collagen fibril organisation in mammalian vitreous by freeze etch/rotary shadowing electron microscopy. *Micron.* Apr 2001;32(3):301-306.

12. Oyster CW. *The Human Eye: Structure and Function.* Sunderland, MA: Sinauer Associates, Inc.; 1999.

13. Sebag J. Is pharmacologic vitreolysis brewing? *Retina.* Feb 2002;22(1):1-3.

14. Nickerson CS, Kornfield JA. A "cleat" geometry for suppressing wall slip. *Journal of Rheology.* 2005;49(4):865-874.

15. Karageozian HL. Determine the safety and efficacy of Vitreosolve administered intravitreally to induce a complete posterior vitreous detachment (PVD) in non proliferative diabetic retinopathy human subjects. *Investigative Ophthalmology & Visual Science.* 2005;46.

16. Ochoa-Contreras D, Romero-Castro RM, Rivera-Sempertegui JO, Karageozian V, Karageozian H, Quiroz-Mercado H. Anatomical and visual outcome of retinal detachment surgery in children with intravitreal carbamide previous a vitrectomy surgical procedure. *Investigative Ophthalmology & Visual Science.* May 2003;44:U94-U94.

17. Noulas AV, Theocharis AD, Feretis E, Papageorgakopoulou N, Karamanos NK, Theocharis DA. Pig vitreous gel: macromolecular composition with

particular reference to hyaluronan-binding proteoglycans. *Biochimie*. Apr 2002;84(4):295-302.

18. Gloor BPMD. The vitreous. In: Adler FH, Hart WM, eds. *Adler's Physiology of the Eye*. Ninth ed: Mosby-Year Book, Inc.; 1992:255-276.

19. Clausen R, Weller M, Wiedemann P, Heimann K, Hilgers RD, Zilles K. An Immunochemical Quantitative-Analysis Of The Protein Pattern In Physiological And Pathological Vitreous. *Graefes Archive For Clinical And Experimental Ophthalmology*. 1991;229(2):186-190.

20. Reardon A, Heinegard D, McLeod D, Sheehan J, Bishop P. The large chondroitin sulphate proteoglycan versican in mammalian vitreous. *MATRIX BIOLOGY*. 1998;17(5):325-333.

21. Bishop P, Ayad S, Reardon A, McLeod D, Sheehan J, Kielty C. Type VI collagen is present in human and bovine vitreous. *Graefes Archive For Clinical And Experimental Ophthalmology*. Nov 1996;234(11):710-713.

22. Bidanset DJ, Guidry C, Rosenberg LC, Choi HU, Timpl R, Hook M. Binding Of The Proteoglycan Decorin To Collagen Type-VI. *Journal Of Biological Chemistry*. Mar 15 1992;267(8):5250-5256.

23. Kielty CM, Whittaker SP, Grant ME, Shuttleworth CA. Type-Vi Collagen Microfibrils - Evidence For A Structural Association With Hyaluronan. *Journal Of Cell Biology*. Aug 1992;118(4):979-990.

24. Nguyen BQ, Fife RS. Vitreous Contains A Cartilage-Related Protein. *Experimental Eye Research*. Sep 1986;43(3):375-382.

25. Ayad S, Boot-Handford RP, Humphries MJ, Kadler KE, Shuttleworth CA. *The Extracellular Matrix FactsBook*. second ed. London: Academic Press Limited; 1998.

26. Henderson M, Polewski R, Fanning JC, Gibson MA. Microfibril-associated glycoprotein-1 (MAGP-1) is specifically located on the beads of the beaded-filament structure for fibrillin-containing microfibrils as visualized by the rotary shadowing technique. *Journal Of Histochemistry & Cytochemistry*. Dec 1996;44(12):1389-1397.

27. Menasche M, Dagonet F, Ferrari P, Labat-Robert J. Fibronectin in the vitreous body - distribution and possible functional role. *Pathologie Biologie*. May 2001;49(4):290-297.

28. Esser P, Bresgen M, Weller M, Heimann K, Wiedemann P. The Significance Of Vitronectin In Proliferative Diabetic-Retinopathy. *Graefes Archive For Clinical And Experimental Ophthalmology*. Aug 1994;232(8):477-481.

29. Theocharis AD, Papageorgakopoulou N, Feretis E, Theocharis DA. Occurrence and structural characterization of versican-like proteoglycan in human vitreous. *Biochimie*. Dec 2002;84(12):1237-1243.

30. Mayne R, Liu J, Ren ZX, Mayne PM, Cook T. Genomic structure and chromosomal location of a novel extracellular matrix protein from mammalian vitreous. *Investigative Ophthalmology & Visual Science*. Mar 15 1999;40(4):S12-S12.

31. Dunker S, Kleinert R, Faulborn J. Immunohistological staining of the vitreous. *Ophthalmologe*. Jan 1998;95(1):8-12.

32. NKCF. National Keratoconus Foundation. http://www.nkcf.org/.

33. Spoerl E, Seiler T. Techniques for stiffening the cornea. *J Refract Surg.* Nov-Dec 1999;15(6):711-713.

34. Wollensak G, Sporl E, Seiler T. Treatment of keratoconus by collagen cross linking. *Ophthalmologe.* Jan 2003;100(1):44-49.

35. Kao WWY, Vergnes JP, Ebert J, Sundarraj CV, Brown SI. Increased Collagenase And Gelatinase Activities In Keratoconus. *Biochemical And Biophysical Research Communications.* 1982;107(3):929-936.

36. Spoerl E, Wollensak G, Seiler T. Increased resistance of crosslinked cornea against enzymatic digestion. *Current Eye Research.* Jul 2004;29(1):35-40.

37. Duquette JJ, Grigg P, Hoffman AH. The effect of diabetes on the viscoelastic properties of rat knee ligaments. *J Biomech Eng.* Nov 1996;118(4):557-564.

38. Wollensak G, Spoerl E. Collagen crosslinking of human and porcine sclera. *Journal Of Cataract And Refractive Surgery.* Mar 2004;30(3):689-695.

C h a p t e r 2

THE "CLEAT" GEOMETRY: A NOVEL RHEOLOGICAL TOOL

A significant portion of the text and figures in this chapter have been published by C. S. Nickerson and J. A. Kornfield in the *Journal of Rheology* and are reproduced here with their permission.[1]

2.1 Wall Slip – A Classical Problem with Implications in Biorheology

Accurate rheological characterization using rheometric flows depends critically upon the "no-slip" boundary condition, which essentially requires that the sample adhere to the surfaces of the rheometer. Stated more specifically, the velocity of the sample at the sample boundary must be equal to the velocity of the adjacent tool surface (Figure 1) so that the deformation rate of the sample is known. Unfortunately, a wide range of materials violate this boundary condition. For example, in suspensions and emulsions (e.g., creams, lotions, and pastes) a thin "depletion" layer can form as particles/droplets migrate away from the boundary. The depletion layer forms a planar region with reduced viscosity and so the deformation becomes inhomogeneous. Polymers in solution are entropically driven away from solid boundaries; in this case, depletion layers form even in the absence of flow.

Many biological specimens slip due to the formation of lubricating layers at their surfaces. Elastomers are susceptible to slip even without lubricating fluid layers, sliding at the tool interface if there is insufficient friction.

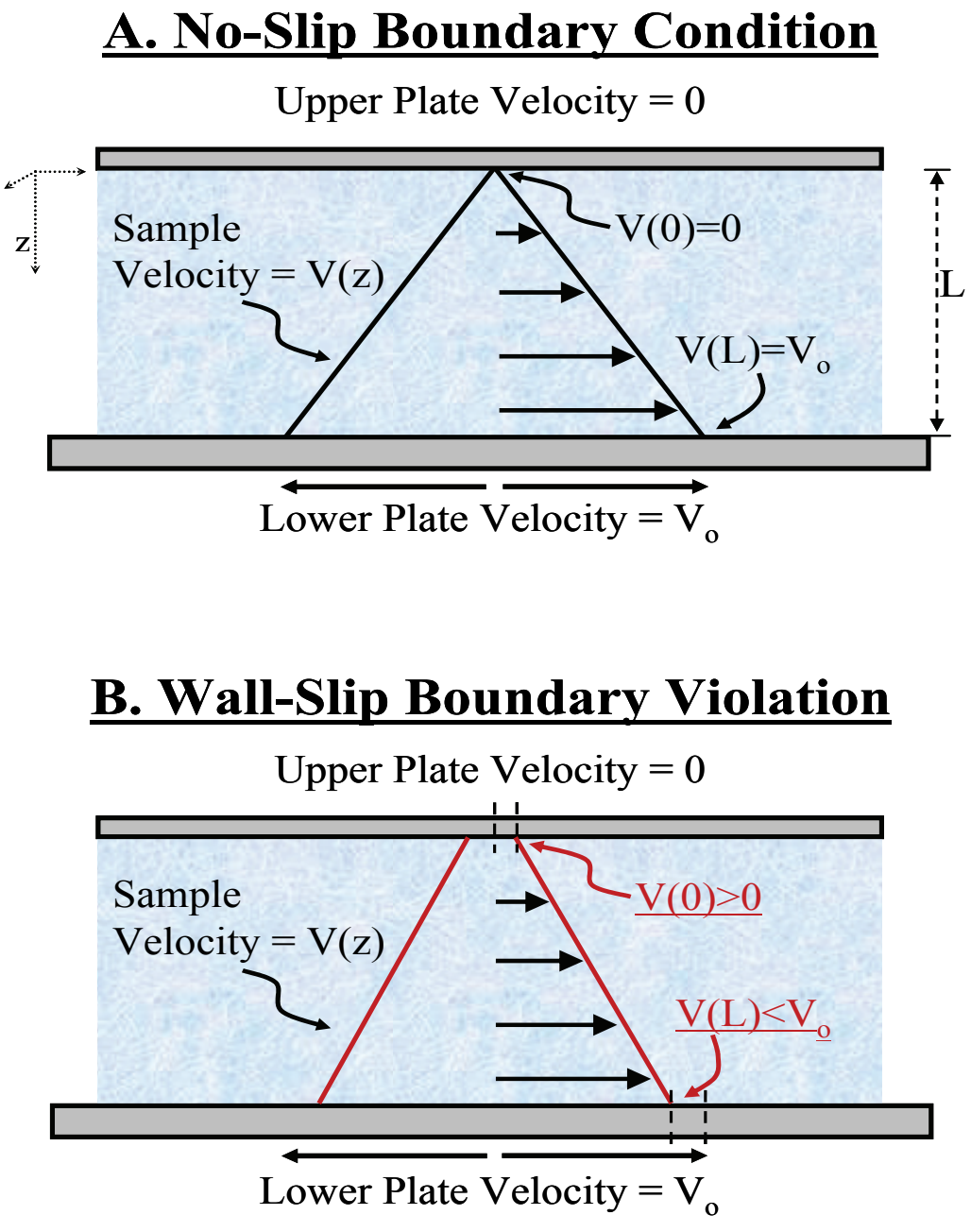

Figure 1. Schematic representation of the velocity field in a sample experiencing shear deformation between parallel plates when the no-slip boundary condition holds (A) and when it is violated (B).

Thus, wall slip is a constant concern for rheologists working in fields ranging from biomaterials and gels to paints and industrial products to foods and personal-care items. A number of useful solutions to the wall-slip problem in its various forms have evolved for specific cases.[2-9] We have divided these wall-slip prevention methods into three general approaches: mathematical methods, surface modifications, and alternative geometries (Table 1). Each method has made important contributions to the field, but each has significant limitations as explained below.

Approach	Examples (from the literature)	Problems
Mathematical	Determine the contribution of the slip layer empirically, then account for it	Labor intensive, Large sample requirement
Modify the Surface of Standard Fixtures	Sandpaper, Porous frit, Serrated / Grooved plates, Chemical treatment	Not useful with thick or lubricating slip layers, usually requires compression
Alternative Geometries	Vane, Helix	Large sample volumes, Comparative (not in absolute units), destroy delicate networks

Table 1. Existing approaches to the wall slip problem are listed with specific examples. Each approach has significant limitations as shown.

The first approach involves empirically or mathematically estimating the magnitude of the wall slip and accounting for its contribution to rheological measurements, as explained by Yoshimura and Prud'homme[10] and Barnes.[3] When possible, mathematical methods can be

very useful because they characterize wall-slip rather than simply eliminating it. However, mathematical methods require repetitive experiments and large sample volumes, which can be prohibitive. Also, these methods are essentially perturbation analyses; therefore, when slip dominates the material response, they are not applicable.

Another approach is to prevent slip by modifying the surfaces of standard rheological tools. This is usually accomplished by either roughening the surfaces or by attaching a rough material such as sandpaper or serrated surfaces, although chemical modifications have also been described; examples of this are Mhetar and Archer[11], Rosenberg, et al.[6], and Walls, et al.[9] Surface methods have been successfully applied to systems that form thin slip layers. Unfortunately, slip can still persist with surface modified tools in many systems, particularly gels and elastomers. Also, to be effective in gels and solids (which includes nearly all biological tissues), most surface-modified tools require compression or significant normal force as described by Jin and Grodzinsky[12] and Liu and Bilston[13]. Typical samples are compressed a minimum of 5 – 10%, which can alter the structure of the material. We observe that small compression (5%) causes the apparent modulus and properties to increase for two biological specimens (cornea and vitreous humor) and that delicate specimens, like the vitreous humor, are irreversibly damaged by compression of 10% or more, giving an artificial decrease in the apparent modulus.

The third approach to the wall slip problem is to use alternative geometries such as the vaned and helical tools recently reviewed by Barnes and Nguyen[2] and Cullen, et al.[4], which either prevent the formation of slip layers through mixing or measure the properties of the sample in spite of the slip layer. The flow fields in these geometries depend upon the nature

of the fluid; consequently, the measurements are comparative, rather than yielding absolute modulus or viscosity values. Most alternative geometries, particularly vaned and helical tools, are also unsuitable for delicate samples that are altered by loading into a highly non-uniform gap.

We present a novel "cleat" test geometry that overcomes many of the limitations mentioned above (Figure 2). The geometry is a modified parallel plate tool with a large number of uniform protrusions, or "cleats", extending from the faces of the plates. A key feature of the new tool is the constant cleat length (L_c, distance from plate face to cleat tip). The significance of uniformity is that the cleat tips create a well-defined plane within the sample that is parallel to the plate face. Motion of fluid between the cleats is restricted and decays to zero a short distance (δ) into the tool. The depth at which fluid motion is stopped establishes the effective sample gap boundary. The position of this effective sample boundary was found to be independent of the material over the wide range of materials examined. The penetration depth δ can be estimated from the geometric parameters of the cleats and verified empirically, as will be discussed below. The only procedural difference between cleat geometry and smooth plate experiments is the use of the effective sample gap ($gap_{eff} = gap_{meas} + 2 \bullet \delta$) rather than the measured sample gap (gap_{meas}).

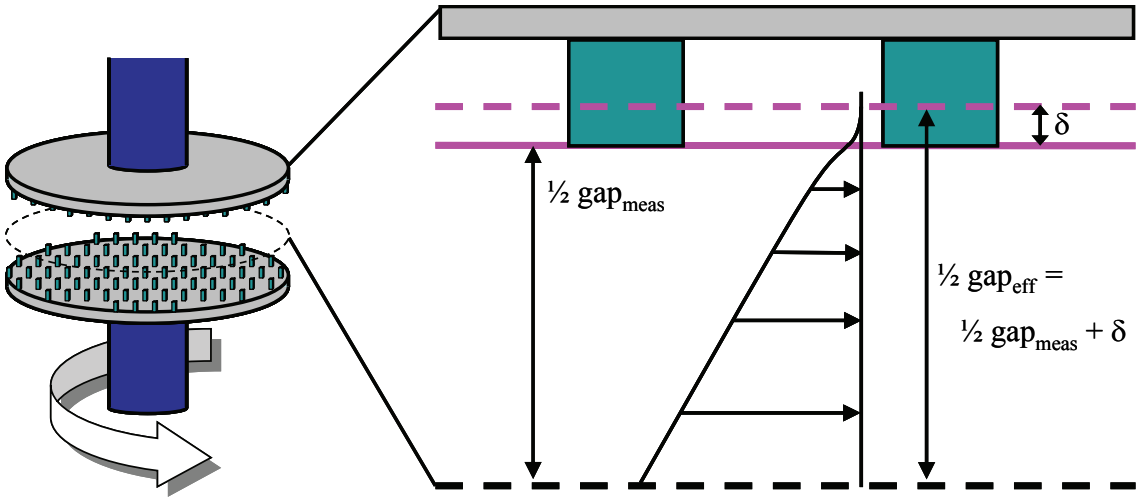

Figure 2. Schematic representation of two cleated fixtures placed opposite each other. Sample motion penetrates only a short distance δ into the cleat array. The actual cleat density is high: approximately 100/cm^2.

The effective sample gap is estimated by treating the array of cleats as a porous medium and determining the flow field within it. From measurements of the in-plane, pressure-driven flow through an array of cleats analogous to the tool, the permeability of the cleat geometry was determined using Darcy's law ($k = 8.7 \times 10^{-10}$ m^2). Flow of Newtonian fluids over porous media has been analyzed extensively, starting with the work of Beavers and Joseph[14] and Neale and Nader,[15] who showed that the resulting motion of fluid within the porous medium is attenuated over a short distance that is related to the permeability k ($\delta \propto k^{1/2}$) and is independent of the viscosity of the fluid. In highly porous media such as the cleat geometry, Neale and Nader[15] predict an exponential velocity decay profile such that the fluid velocity in the porous region will be reduced to < 1% of the boundary velocity when $\delta \sim 5 \bullet k^{1/2}$ (~ 150 μm in the present cleat geometry). Since the attenuation depth is

insensitive to fluid properties, the value of δ for Newtonian fluids provides a good approximation for viscoelastic materials as well.

The present study demonstrates the accuracy and utility of the cleat geometry. We show that this unique geometry for slip prevention accommodates small sample volumes and allows direct measurement of shear modulus using a gentle loading procedure and negligible normal force. Results obtained with the cleated tools are compared with those obtained using smooth and roughened parallel plate geometries. First, for fluids that do not exhibit slip, the results confirm that quantitative measurements can be obtained using a single value of the gap correction δ. The empirical value for δ based on these fluids is compared with $k^{1/2}$ to evaluate the applicability of the porous medium analogy. Next we show that the tool performs well when applied to two fluids that exhibit moderate slip, and we validate the results independently using roughened plates. Finally, the power of the new geometry is illustrated by obtaining modulus measurements for porcine cornea and vitreous humor, two biological tissues that are difficult or impossible to handle successfully with prior tools. More comprehensive rheological characterization of cornea and vitreous tissue will be presented in conjunction with chemical analysis in subsequent chapters.

2.2 Methods and Materials

Four different tools were used to measure the shear moduli and viscosities of a variety of materials, from low viscosity Newtonian oils to slippery biological tissues. The primary reference tool was a smooth 25 mm titanium parallel plate test geometry. A rough tool was made by attaching fine emery cloth to the surface of a 25 mm aluminum parallel plate

geometry. Two of the cleated tools were likewise 25 mm in diameter. Cleats were machined into an aluminum disk, leaving protrusions with a square cross section 0.45 mm x 0.45 mm, evenly spaced 1.35 mm apart (center to center). Two L_c values were used: 0.6 mm and 1.3 mm. A second set of smooth, rough, and cleated tools with 0.6 mm cleats and 8 mm diameters were used for measurements on cornea. In addition, a vaned fixture and porous plates were used when roughened plates failed (on vitreous humor), but they were unsatisfactory. The 25 mm tools were mounted on an ARES-RFS fluids rheometer, while the 8 mm tools were mounted on an AR2000 rheometer (both from T.A. Instruments, Inc., New Castle, DE) with sample gaps ranging from 2.25 mm to 0.3 mm. The in-plane permeability of the cleated tools was measured by Porous Materials, Inc. (Ithaca, NY).

Four of the test fluids were selected specifically because they are not prone to slip: a series of three silicone oils, (η = 10, 1.0, and 0.1 Pa·s respectively) and GE Silicones SE-30 polydimethylsiloxane (PDMS) putty (Waterford, NY). The 10 Pa·s fluid was methyl silicone oil purchased from Nye Lubricants, Inc. (New Bedford, MA); the 1.0 and 0.1 Pa·s oils were silicone viscosity standards from Brookfield Engineering Laboratories, Inc. (Middleboro, MA). In experiments on these fluids the upper tool was cleated and the lower surface was smooth. Using a smooth lower plate allowed us to validate the cleats at large sample gaps with low viscosity fluids. Each fluid was tested at least three times per sample gap at 22° C and multiple shear rates (1 – 80 s^{-1}) or frequencies (10^{-1} – 10^{2} rad/s); the PDMS putty was tested in the linear viscoelastic regime (γ = 0.2%).

To demonstrate the utility of the cleated geometry for samples that slip, two food products and two biological tissues were characterized using smooth, rough, and cleated tools (both

upper and lower fixtures). The foods used were Kroger brand "Real Mayonnaise" (Kroger Co., Cincinnati, OH), an oil in water emulsion, and Winn-Dixie brand "Creamy Peanut Butter" (Winn-Dixie Stores, Inc., Jacksonville, FL), a suspension, both of which exhibit slip on smooth tools. Samples were tested at least three times at 5° C and multiple shear rates (10^{-2} – 10 s^{-1}). The biological tissues were fresh porcine eyes (< 36 hours *post mortem*, stored at 5° C in physiological saline prior to arrival) were acquired through Sierra for Medical Science (Santa Fe Springs, CA). All pigs were 3 – 6 month old Chester Whites, weighing 50 – 100 kg and in good health at the time of slaughter. Cornea is a slip-prone biological elastomer with a complex network structure, as will be discussed in subsequent chapters. The vitreous humor is an example of a delicate hydrogel that exhibits slip even on rough tools. Eyes from 3 – 6 month old swine were enucleated immediately after the animals were sacrificed and shipped at ~ 5˚ C in physiological saline. Fresh eyes were gently dissected between 24 and 36 hours *post mortem* (no cornea or vitreous degradation is seen within ~ 48 hours when the eye is maintained in Dulbecco's phosphate buffered saline at 5° C), and the vitreous was removed with minimal disruption, leaving the cornea for parallel analysis. From the intact vitreous, a disc-like section approximately 25 mm in diameter was cut with the axis of the disc coinciding with the anterior-to-posterior axis of the eye (typically 1.5 – 2.5 g). 8 mm discs were cut from the central cornea ($n \geq 4$ for each tool). To mitigate the effects of drying, a vapor trap was used in all experiments. Vitreous time-dependent shear modulus measurements were made at 20° C with zero normal force on the samples at a fixed strain and frequency (γ = 3%, ω = 10 rad/s), while variable stress, fixed frequency cornea (5° C) measurements were made at σ = 1 – 30 Pa, ω

= 1 rad/s. More extensive rheological analysis of these materials will be presented in subsequent chapters.

2.3 Quantitative Validation

Newtonian Oils: The viscosities of three silicone oils were measured with the smooth parallel plate geometry and with one of the parallel plates replaced by a cleated tool. Two different cleat lengths (600 μm and 1300 μm) were compared. At least four different sample gap values were tested for each tool configuration. For smooth tools, the measured viscosity is independent of gap (Figure 3). The viscosity obtained with cleated tools is insensitive to gap thickness when $gap_{meas} \geq 1$ mm, indicating $\delta << 1$ mm. The results are also insensitive to cleat length (cf. $L_c = 0.6$ and 1.3 mm), which indicates $\delta < 600$ μm, in accord with the porous-medium prediction of $\delta \sim 150$ μm.

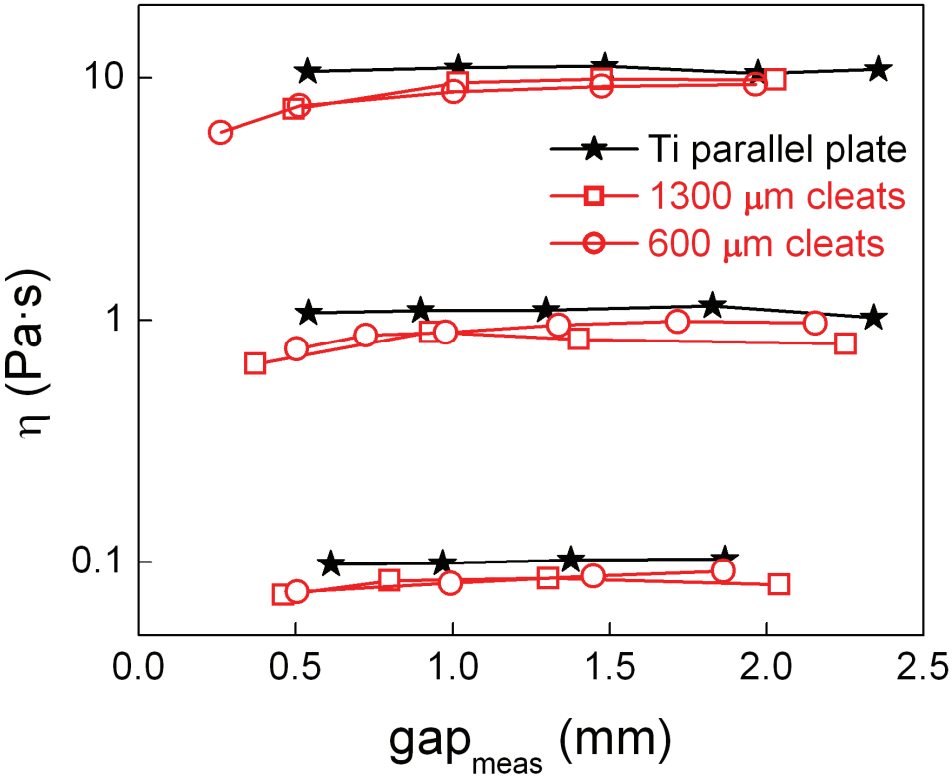

Figure 3. The viscosity of three Newtonian oils was measured at multiple gaps with two cleated tools and compared with measurements made with a smooth titanium plate. At small gaps cleat geometry values diverge from smooth plate values.

Experimentally-determined correction values also compare favorably with predictions. Based on the porous-medium analogy, the gap-dependent disparity between viscosity measurements from smooth (η_{true}) and cleated tools (η_{meas}) is predicted to be:

$$\eta_{meas} / \eta_{true} = gap_{meas} / (gap_{meas} + \delta)$$

Note that δ would be replaced by 2 • δ if both faces were cleated rather than just the upper tool. This expression accords well with the experimental results as a function of gap

(Figure 4). A single value of δ holds for all three Newtonian oils. Non-linear least squares fitting of η_{meas}/η_{true} to $\left(1+\delta/gap_{meas}\right)^{-1}$ yields an empirical value of δ = 157 μm (95% CI = 141 – 173 μm), in remarkably good agreement with the predicted value above. Application of the 157 μm correction factor to the Newtonian oil data (Figure 3) demonstrates the accuracy of δ. Figure 5.

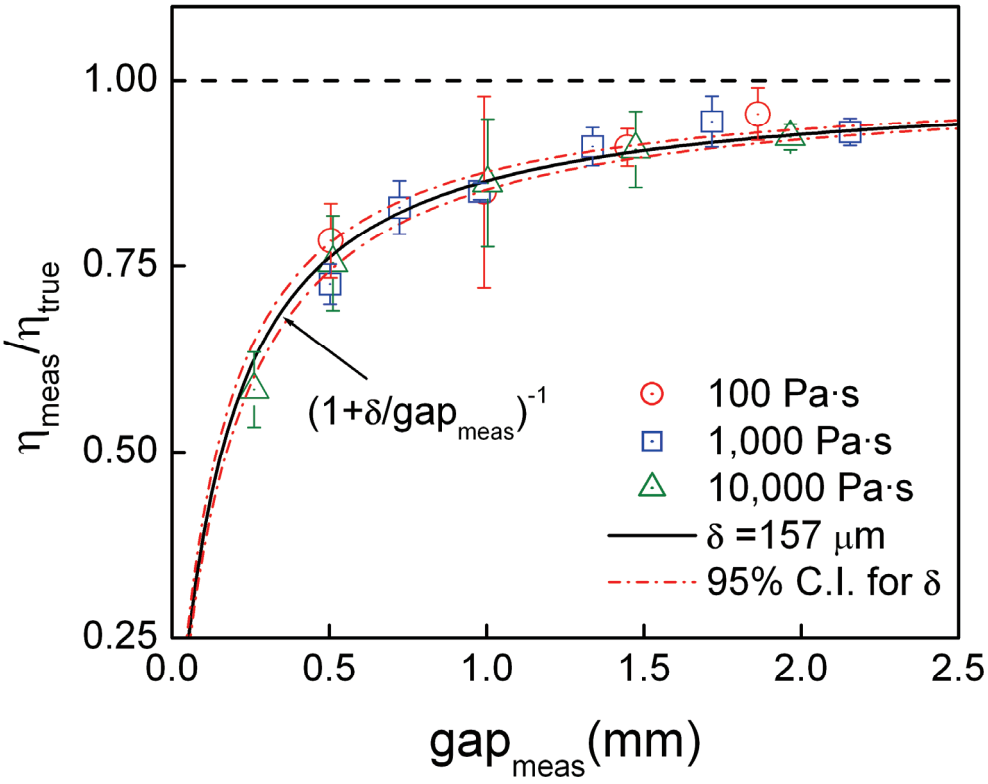

Figure 4. Viscosity measured using the cleat geometry divided by true viscosity, measured by the smooth plates. The solid curve shows the predicted gap dependence $(1+\delta / gap_{meas})^{-1}$ with a value of δ = 157 μm. Dashed curves bound the 95% confidence interval (141 μm < δ < 173 μm).

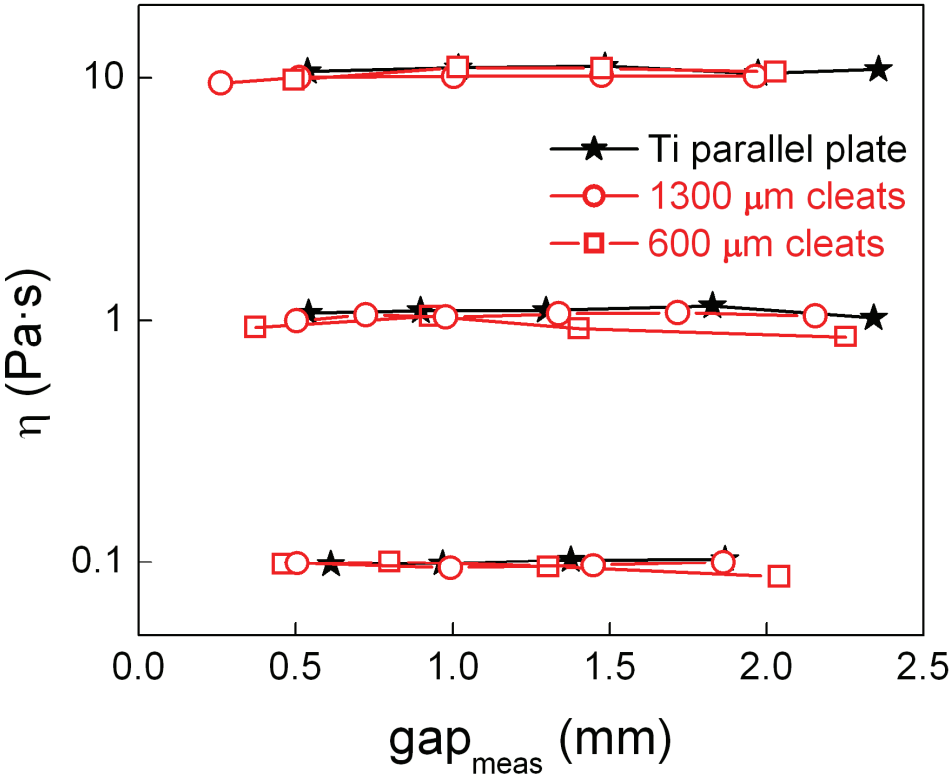

Figure 5. The cleat geometry viscosity data from Figure 3 plotted after gap correction with δ = 150 μm. Accurate measurements are obtained at all gaps and viscosities when the gap is accounted for correctly.

PDMS Putty: The uncorrected storage and loss moduli of PDMS putty ($\eta_o > 10^4$ Pa • s) measured with the two cleated tools were consistently lower than those measured using the smooth parallel plates; however, the 157 μm correction factor brings the cleat measurements within 1% of the parallel plate results (Figure 6). G′ and G″ measurements were accurate over the three decades of frequency examined, and the gap dependence matched that of the Newtonian oils. Thus, δ appears to be independent of material

properties for a wide range of soft materials and fluids, including a complex fluid, as anticipated from the porous medium analogy.

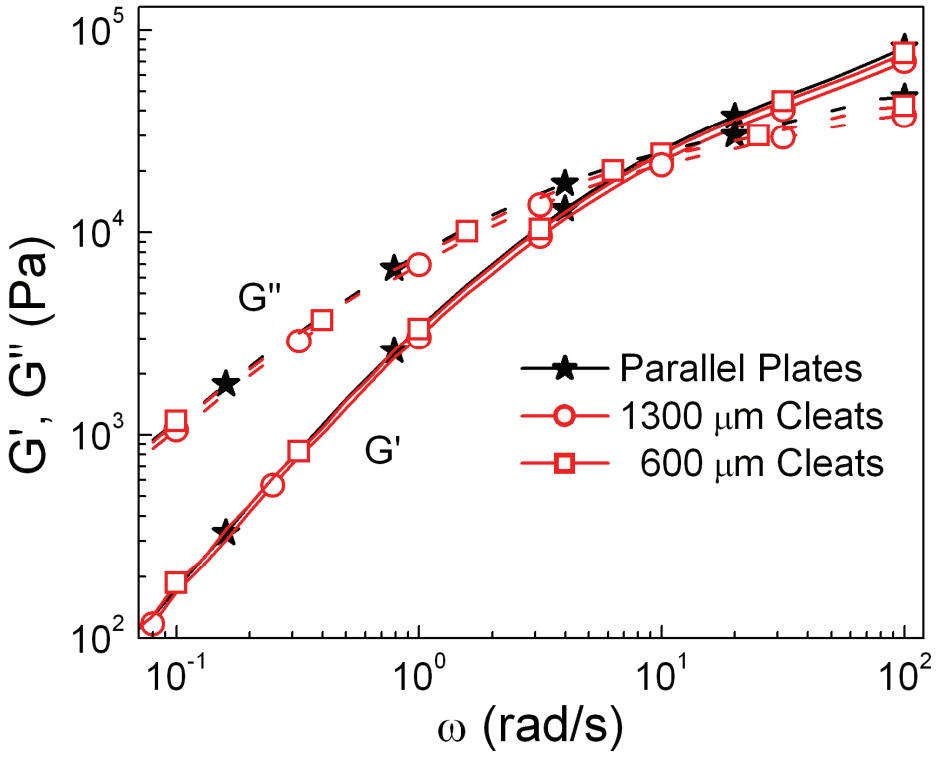

Figure 6. Gap corrected shear moduli of PDMS putty measured with the cleat geometry are within 1% of values obtained using a titanium parallel plate over three decades of frequency and modulus (γ = 0.2%, gap_{meas} = 2 mm).

The experimental results for Newtonian oils support our hypothesis that the cleats create an effective no-slip boundary that is close to the plane of the cleat tips. Furthermore, the observation that the ratio of the apparent viscosity observed using cleated tools, η_{meas}, to actual viscosity, η_{true}, is independent of the viscosity of the fluid accords with a model that

treats the array of cleats as a porous medium. The attenuation distance $\delta = 157\ \mu m$ inferred from the ratio of η_{meas}/η_{true} is similar to $5 \bullet k^{1/2}$ determined independently. The experimental observation that the correction factor determined for a series of Newtonian fluids also applies for a viscoelastic fluid (an entangled polymer melt, Figure 6) over a frequency range that spans from near terminal behavior ($G' < G''$) to elastic behavior ($G' > G''$) suggests that the attenuation depth continues to be governed by the geometry of the cleat array even for some non-Newtonian fluids.

The gap dependence of η_{meas} is reminiscent of slip phenomena; however, the fluid independence of the value, combined with the improbability of slip with the samples chosen, demonstrate that δ represents a true sample gap boundary—not a slip length. The cleat geometry creates a secondary boundary at a distance δ below the cleat tips where the no-slip condition effectively holds. The dependence $\eta_{meas}/\eta_{true} = \left(1 + \delta/gap_{meas}\right)^{-1}$ corresponds to the "apparent gap" effect noted by Sanchez-Reyes and Archer.[8] We have shown that an empirical δ can be inferred that appears to be accurate for the samples investigated and is consistent with the observed dependence of η_{meas} on gap_{meas} down to the smallest gap tested ($gap_{meas} \approx 2 \bullet \delta$).

Optimization of the cleat parameters (height, width, length, and spacing) involves a trade off between minimizing the attenuation length and minimizing the disruption of the sample. Therefore, one can decrease δ by reducing k through an increase in the area of the cleated surfaces per unit area of the tool. However, increasing the cross-section of each cleat or the

cleat surface density hinders penetration into samples such as gels, elastomers, and biological tissue. The specific parameters of the cleat array we describe have the advantage that only 11% of the nominal surface area (area relevant to penetration) of the disk is occupied by the cleats themselves. This arrangement of well-spaced "pins" readily penetrates diverse complex fluids and certain soft solids. As stated previously, the permeability k of the cleat arrangement determines δ, which subsequently dictates the minimum value of L_c. Based on the findings of Sanchez-Reyes and Archer, the optimal length scale of the surface features will decrease as the modulus range of interest increases.[8] They observed that with increasing polymer concentration, i.e., decreasing size of entangled blobs, the optimal sizes of surface features decreases.

Peanut Butter and Mayonnaise: To validate that the cleat geometry is also accurate in moderately slip-prone systems, we compare results obtained for a model suspension and a model emulsion to results obtained using published methods. The viscosity of peanut butter (Figure 7) and mayonnaise (Figure 8) were measured using smooth, rough, and cleated tools at gap_{meas} = 2 mm. Prior literature, including work by Citerne, et al.[16] and Franco, et al.[17], shows that roughened plates are adequate to suppress slip for both of these complex fluids. Peanut butter, a typical suspension, and mayonnaise, an oil-in-water emulsion, both exhibit slip at low shear rates on smooth plates, giving apparent values of η considerably smaller than values measured with rough plates. The measured viscosity of both samples was essentially the same with cleated or roughened plates. Apparently, the characteristic feature sizes of both tools were larger than the thin depletion layers that cause slip. On a practical note, it was observed that, relative to emery cloth and porous glass, the cleated

tools were far easier to clean and more robust against physical damage, solvents, and high temperatures.

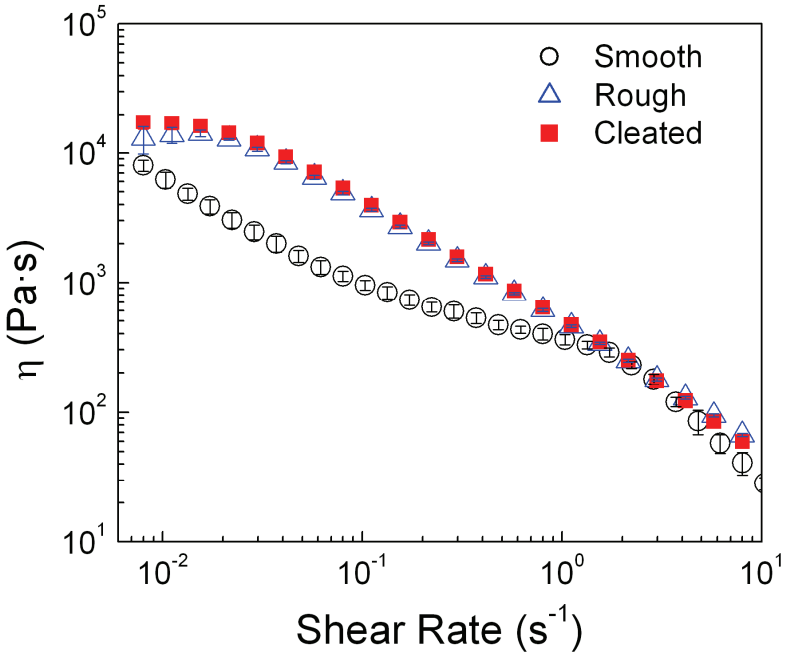

Figure 7. The corrected viscosity of peanut butter measured with cleated and rough plates. Smooth plates show slip at low shear rates (gap_{meas} = 2 mm).

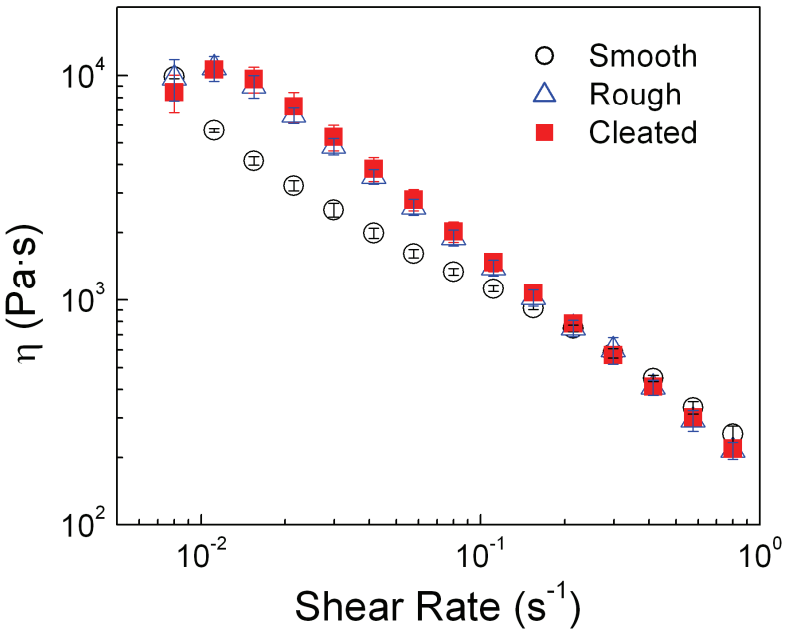

Figure 8. The corrected viscosity of mayonnaise measured with cleated and rough plates. Smooth plates show slip at low shear rates (gap_{meas} = 2 mm).

2.4 Applications in Biorheology

Cornea: Results obtained from cornea specimens demonstrate the utility of the cleat geometry for soft elastomeric materials. Corneal tissue is a valuable example in this regard because it can be characterized on smooth tools for comparison with results obtained in cleated tools. Immediately after dissection, corneal tissue is slippery and remains so even after the epithelial cell layer is removed. Fortunately, if the surfaces are briefly put in contact with an absorbent material, the surface is no longer slippery. There is negligible weight change (< 3%) in the process, so the viscoelastic properties of the tissue closely approximate the tissue *in vivo*. Thus, we regard results from the smooth tools as an accurate reference against which other tool surfaces can be compared. Gap-corrected shear modulus

measurements from the cleat geometry agree quantitatively with measurements obtained with smooth tools (Figure 9). The standard deviation (for n = 4) is, unfortunately, much greater on cleated tools than on smooth tools. This suggests a direction for future research: evaluation of the effect of cleat size relative to tool size. For example, on an 8 mm tool there are only 35 – 40 cleats, so that from one sample loading to the next, details of loading and azimuthal orientation of tools could lead to significant variations.

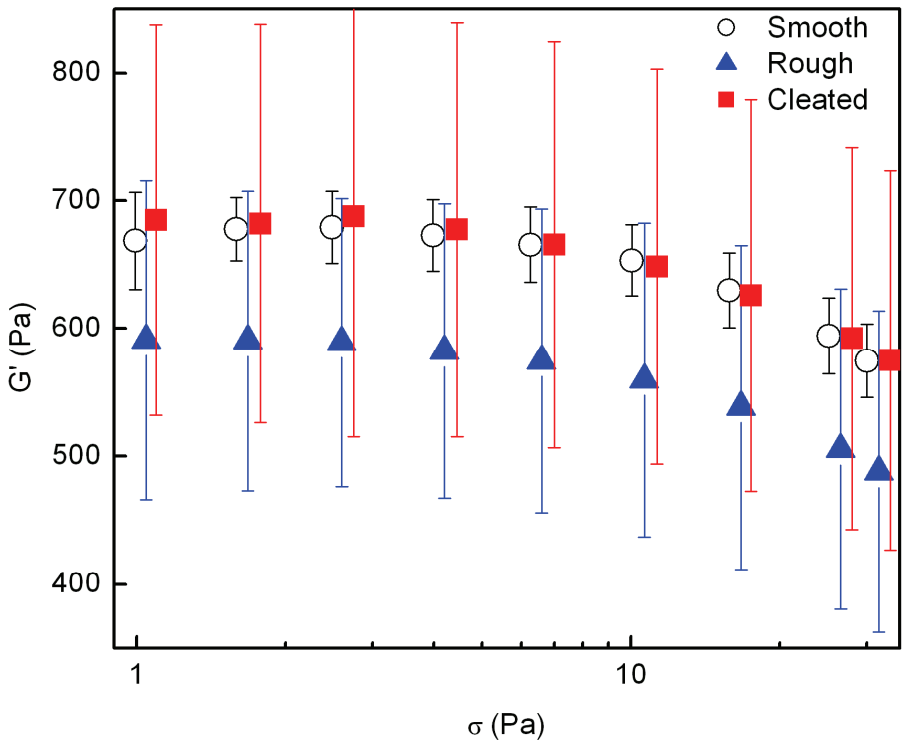

Figure 9. Gap corrected shear modulus of fresh porcine cornea at fixed frequency (w = 1 rad/s) and 5° C using smooth, roughened, and cleated tools. Tools were lowered until ~ 0.1 N of normal force was detected, then the sample was allowed to relax completely and tested (n = 4).

Values obtained with roughened tools are systematically too low (Figure 9). This comparison is made using the same normal force in all three cases, with a normal force small enough that the tissue is not damaged. Cornea samples were loaded by slowly lowering the upper fixture until the normal force was ~ 0.1 N. The normal force decayed to zero within seconds. Small amplitude oscillatory shear was used to observe relaxation of the sample to a steady state (~ 15 minutes was sufficient) and then measurements were made. This loading technique was sufficient to generate good contact between the smooth tool and the cornea and to allow adequate penetration by the cleats. However, in accord with prior literature, such low normal force is insufficient to allow the irregular surface features of the roughened tool to fully "grip" the sample. This demonstrates a significant advantage of the cleats over roughened tools – adequate measurements can be made using negligible normal force.

Vitreous Humor: Results obtained from the vitreous humor of the eye demonstrate the utility of the cleat geometry for more difficult samples. Previous efforts to measure the mechanical properties of the vitreous, including work by Bettelheim and Wang,[18] Lee, et al.,[19] Pfeiffer,[20] Tokita, et al.,[21] and Zimmerman,[22] have yielded unsatisfactory and sometimes conflicting results. The shear moduli of this delicate tissue were also impossible to measure using previously published geometries in our laboratory (Figure 10). Smooth plates slipped drastically, and roughened plates were insufficient because slip was not consistently prevented (as denoted by the large standard deviation). While some vitreous samples appeared to be measured accurately on the rough fixtures, other loadings appeared to fail (slip) from the first data point, yielding results similar to those obtained with the

smooth tools. The normal force required to obtain measurements with roughened tools artificially raised the apparent modulus in the initial data points. Over the course of a typical experiment, the apparent modulus decreased with the normal force as fluid was squeezed out of the tissue. In conjunction with fluid loss, a thick lubricating layer formed within five minutes, making it impossible to eliminate slip using roughened plates. In previous efforts to measure the modulus of the vitreous, the use of porous plates failed for the same reasons as roughened plates. The vane geometry was unsuitable because it destroyed the gel network and sample volume is limited to the size of a single eye.

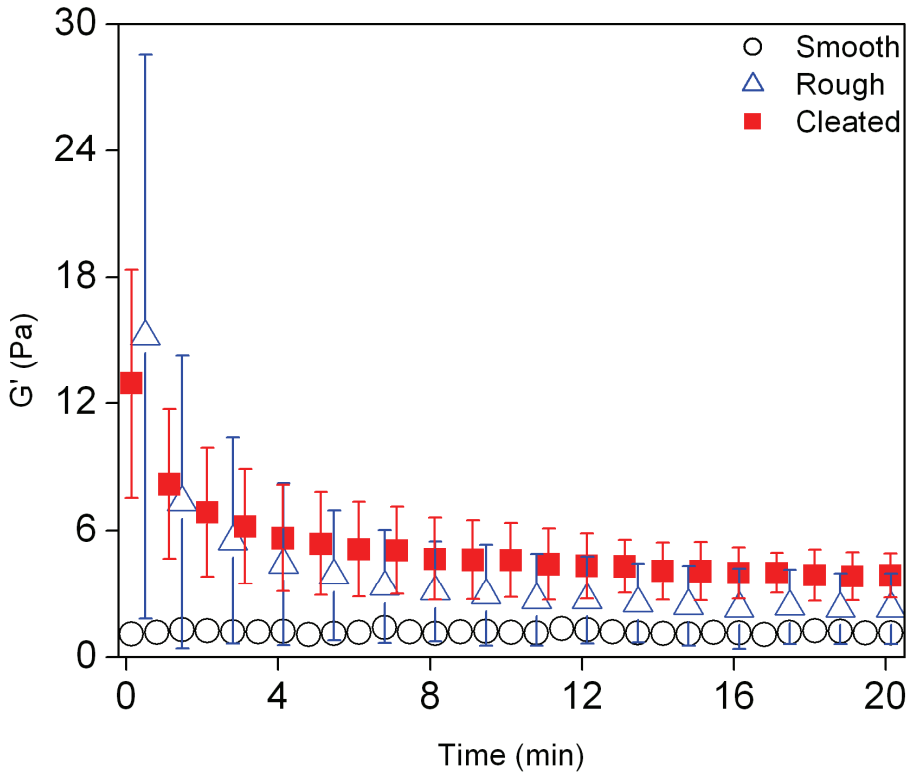

Figure 10. The corrected shear modulus of freshly-enucleated vitreous humor measured with the cleat geometry is far more consistent than rough plates and clearly more accurate than smooth plates (g = 3%, w = 10 rad/s, n = 9).

Using the cleat geometry, these obstacles appear to have been overcome and consistent shear moduli were measured. The modulus values measured with the cleat geometry are slightly greater than those obtained with roughened tools, but the most obvious improvement is the reduction in standard deviation (Figure 10). Comparing results obtained using the cleat geometry with literature values obtained using other methods suggests that the shear moduli of the vitreous are significantly higher than reported in the works mentioned above. The cleat geometry has also allowed us to quantify time-dependent modulus changes that were previously reported only as qualitative observations.

Results from the vitreous humor demonstrate some advantages of the cleat geometry. Highly-charged hyaluronic acid (HA), which draws water into the vitreous in vivo, seeps out of the vitreous when it is removed from the eye. The HA solution that blooms to the surface is a very efficient lubricant, similar to the synovial fluid that lubricates the joints. This HA solution causes the wall slip observed even on very rough surfaces such as sandpaper and porous plates. Note that the successful modeling of cleats as porous media does not imply that porous surfaces work as well as cleats: they do not. The advantage of using cleats over standard porous materials such as fritted disks is that the cleats protrude orthogonally from the tool face and engage the sample.

There is an important, transient decrease in modulus that occurs spontaneously after the vitreous is removed from the eye, captured in measurements using the cleat geometry. It is not possible to characterize this transient behavior using roughened plates due to the need to apply a substantial normal force; the strong effects of compression mask the natural decay. Thus, the cleat geometry is uniquely capable of measuring the time-dependent

changes in this sample, which is too slippery and fragile to be measured accurately using previously published methods. Because prior mechanical investigations of the vitreous are unsatisfactory, we have no way to independently verify the accuracy of our modulus values. The sample dictates the gap and is destroyed by compression; therefore, the usual procedure to test for slip (varying sample geometry) cannot be applied. The values we report represent a lower bound: potential sources of error in the cleat geometry (wall slip, insufficient surface contact, or increased flow between the cleats) would reduce the apparent modulus. We observed that near the tools heterogeneities in the tissue moved with the tool surface; therefore, we believe that the above errors are small.

The modulus values here pertain to the central vitreous, the bulk of the tissue. The work of Lee, et al. suggests that different moduli would characterize the tissue near the anterior pole (stiffer).[19] Regional variations in tissue properties will be discussed in conjunction with more complete rheological and structural analyses presented in subsequent chapters.

BIBLIOGRAPHY

1. Nickerson CS, Kornfield JA. A "cleat" geometry for suppressing wall slip. *Journal of Rheology.* 2005;49.

2. Barnes HA, Nguyen QD. Rotating vane rheometry - a review. *Journal of Non-Newtonian Fluid Mechanics.* Mar 15 2001;98(1):1-14.

3. Barnes HA. A Review of the Slip (Wall Depletion) of Polymer-Solutions, Emulsions and Particle Suspensions in Viscometers - Its Cause, Character, and Cure. *Journal of Non-Newtonian Fluid Mechanics.* Mar 1995;56(3):221-251.

4. Cullen PJ, O'Donnell CP, Houska M. Rotational rheometry using complex geometries - A review. *Journal of Texture Studies.* Apr 2003;34(1):1-20.

5. Klein B, Laskowski JS, Partridge SJ. A New Viscometer for Rheological Measurements on Settling Suspensions. *Journal of Rheology.* Sep-Oct 1995;39(5):827-840.

6. Rosenberg M, Wang Z, Chuang SL, Shoemaker CF. Viscoelastic Property Changes in Cheddar Cheese During Ripening. *J. Food Sci.* MAY-JUN 1995 1995;60(3):640-644.

7. Russel JL. Studies of thixotropic gelation. Part II. The coagulation of clay suspensions. *Proc. Roy. Soc. London, Series A.* 1936;154:550-560.

8. Sanchez-Reyes J, Archer LA. Interfacial slip violations in polymer solutions: Role of microscale surface roughness. *Langmuir.* Apr 15 2003;19(8):3304-3312.

9. Walls HJ, Caines SB, Sanchez AM, Khan SA. Yield stress and wall slip phenomena in colloidal silica gels. *Journal of Rheology.* Jul-Aug 2003;47(4):847-868.

10. Yoshimura A, Prud'homme RK. Wall Slip Corrections for Couette and Parallel Disk Viscometers. *Journal of Rheology.* JAN 1988 1988;32(1):53-67.

11. Mhetar V, Archer LA. Slip in entangled polymer melts. 2. Effect of surface treatment. *Macromolecules.* Dec 1 1998;31(24):8617-8622.

12. Jin MS, Grodzinsky AJ. Effect of electrostatic interactions between glycosaminoglycans on the shear stiffness of cartilage: A molecular model and experiments. *Macromolecules.* Nov 6 2001;34(23):8330-8339.

13. Liu Z, Bilston L. On the viscoelastic character of liver tissue: experiments and modelling of the linear behaviour. *Biorheology.* 2000;37(3):191-201.

14. Beavers GS, Joseph DD. Boundary Conditions At A Naturally Permeable Wall. *Journal Of Fluid Mechanics.* 1967;30:197-207.

15. Neale G, Nader W. Practical Significance of Brinkman's Extension of Darcy's Law: Coupled Parallel Flows within a channel and a Bounding Porous Medium. *Can. J. Chem. Eng.* August 1974 1974;52:475-478.

16. Citerne GP, Carreau PJ, Moan M. Rheological properties of peanut butter. *Rheol. Acta.* JAN 2001 2001;40(1):86-96.

17. Franco JM, Gallegos C, Barnes HA. On slip effects in steady-state flow measurements of oil-in- water food emulsions. *Journal of Food Engineering.* Apr 1998;36(1):89-102.

18. Bettelheim FA, Wang TJY. Dynamic Viscoelastic Properties of Bovine Vitreous. *Experimental Eye Research.* 1976;23(4):435-441.

19. Lee B, Litt M, Buchsbaum G. Rheology of the vitreous body: Part 2. Viscoelasticity of bovine and porcine vitreous. *Biorheology.* Jul-Aug 1994;31(4):327-338.

20. Pfeiffer HH. Zur analyse der fliess-elastizitaet durch spinnversuche am corpus vitreus. *Biorheology.* 1963;1:111-117.

21. Tokita M, Fujiya Y, Hikichi K. Dynamic viscoelasticity of bovine vitreous body. *Biorheology.* 1984;21(6):751-756.

22. Zimmerman RL. In Vivo Measurements of the Viscoelasticity of the Human Vitreous-Humor. *Biophysical Journal.* 1980;29(3):539-544.

Chapter 3

THE VITREOUS HUMOR: MECHANICS AND STRUCTURE

3.1 Primary Structure and Composition

As described in Chapter 1, the vitreous humor is a delicate, transparent gel composed of a highly-hydrated double network of protein fibrils and charged polysaccharide chains (Figure 1). By weight, vitreous is ~ 99% water and 0.9% salts.[1] The remaining 0.1% is divided between protein and polysaccharide components. Most of the protein is found in or associated with 10-20 nm heterotypic collagen fibrils composed of a small collagen type V/XI core wrapped in a thick layer of collagen type II (75% of the fibril by mass). The exterior of each fibril is decorated with covalently-bound collagen type IX and other glycoproteins. Collagen IX contains four short, coiled noncollagenous domains separated by three triple-helical collagenous domains. Two of the collagenous domains are aligned with, and crosslinked to, the axis of the fibrils, but the third strut-like collagenous domain is sterically forced to project out from the fibril by a heparin-sulfate glycosaminoglycan (GAG) chain that is covalently bound to the adjacent, hinge-like noncollagenous domain.[1]

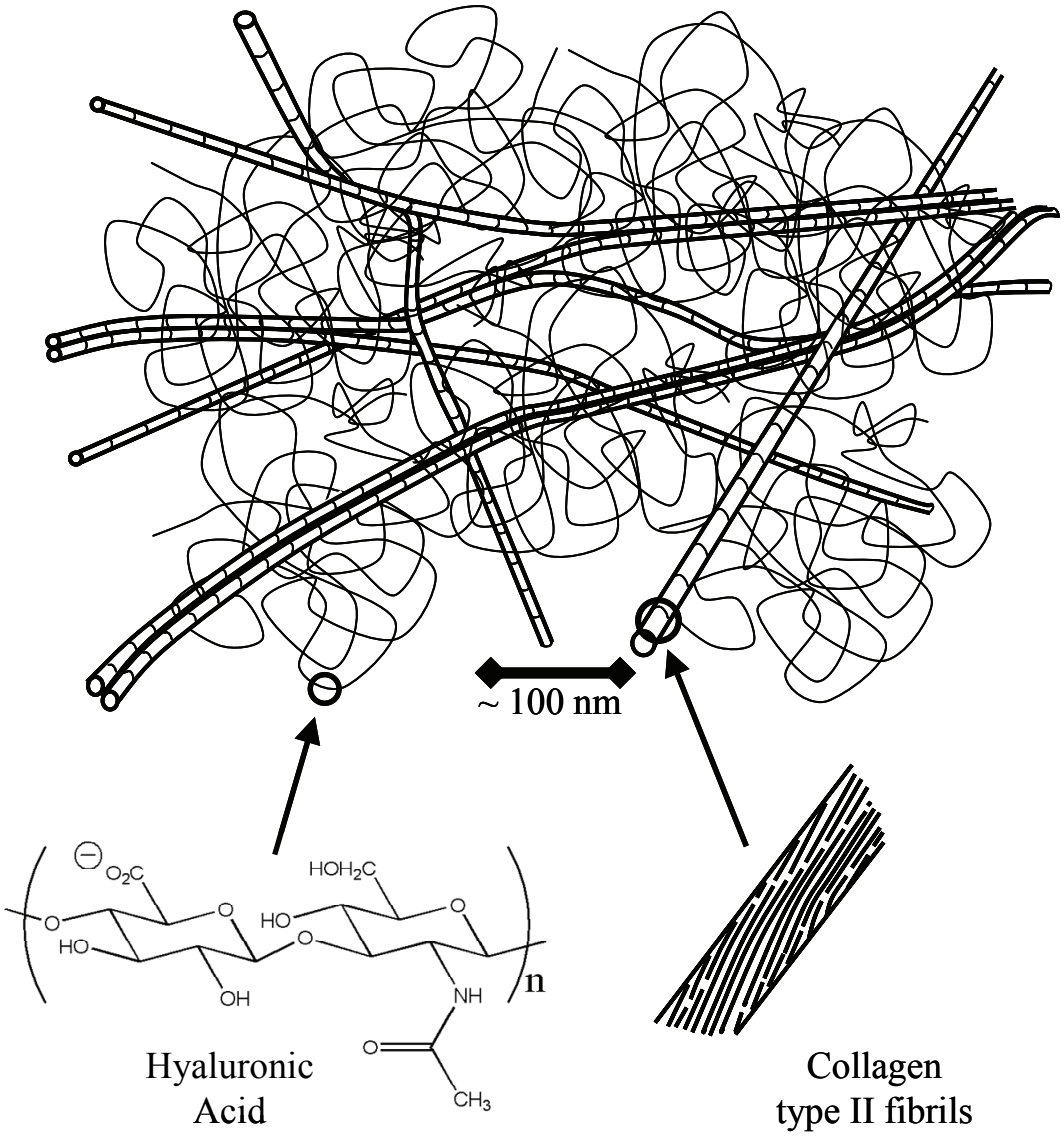

Figure 1. Schematic depiction of the network structure of the vitreous. The vitreous is composed of a highly-swollen double network of collagen type II fibrils (~ 15 nm in diameter) and hyaluronic acid (~ 5M MW).

Most of the collagen fibrils originate in the vitreous base – a band of peripheral vitreous that stretches from just behind the plane of the lens and zonules back to the meridian of the eye. The high concentration of protein fibrils in the vitreous base drops as the collagen fibrils fan out and fill the vitreous cavity. After the fibrils diverge they approach the retina

at various points around the periphery and insert into the inner limiting membrane where they turn and run in the posterior direction to the optic nerve, following the curvature of the eye.[2] Collagen fibrils are hydrophobic and adhere to each other when they come in contact; thus, the fibrils of the vitreous continuously merge with and diverge from lateral aggregates as they traverse the length of the eye.[3] A sufficient number of fibrils are also oriented nasal-temporally to form a fully crosslinked network.

While extensive progress has been made in identifying the components and biochemistry of the vitreous, lack of sufficient experimental methods has hampered previous efforts to quantitatively define its mechanical properties and nano-scale architecture. The lubricating ability of its constituent molecules and its fragile network structure have made reliable measurements extremely difficult. A number of creative methods have been devised to measure the gel character of the vitreous, including bulk measurements,[4-6] magnetic microrheology,[7-9] *in vivo* visual tracking for humans,[10] and more recently, acoustic techniques.[11] These techniques allow for comparative analyses, but cannot give insight into the molecular mechanisms responsible for the observed bulk behavior. A few of these authors estimate the moduli of the vitreous, but the present results suggest that these values are systematically low for bovine and porcine vitreous— in some cases by orders of magnitude.

The network of collagen fibrils has been presumed responsible for the mechanical properties of the vitreous because of the load-bearing capacity of collagen and because the vitreous does not fully collapse with enzymatic removal of hyaluronan.[1, 2, 12] It has been suggested that swollen hyaluronan (HA) polysaccharide chains play a passive role in the

vitreous by filling the space between the fibrils to prevent extensive aggregation. Prior literature indicates that the vitreous shrinks after removal of hyaluronan[1-3], and morphologically the collagen network "relaxes" from having relatively straight to significantly curved fibrils.[3]

These "relaxation" and shrinking observations appear to be more significant than previously thought: they are manifestations of an additional, structural role for hyaluronan. We present rheological and biochemical evidence that hyaluronan contributes significantly to the *elastic* character of the vitreous *in vivo*. Specifically, hyaluronan swells, stretching the network of rope-like collagen fibrils to a state of tension and increasing the rigidity of the network (Figure 2). When removed from the confines of the retina, HA is rapidly driven out of the vitreous to release the network tension. We present evidence that the shrinking that occurs after dissection is due to the loss of HA.

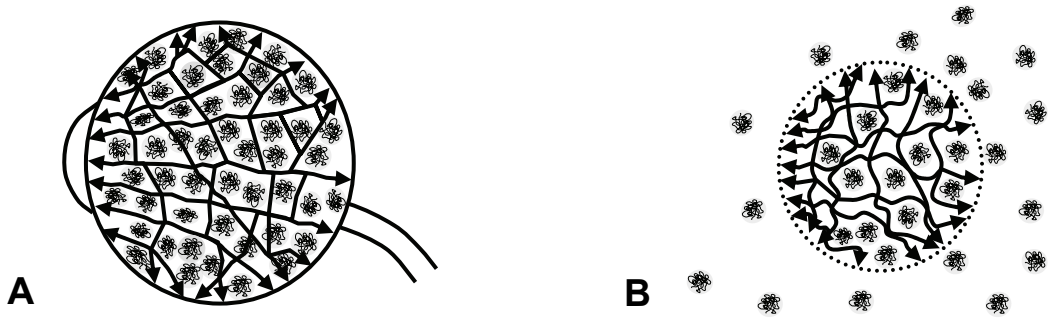

Figure 2. Schematic depiction of the collagen fibrils (heavy lines) of the vitreous network under tension and after relaxation. (A) Native state of the vitreous in the eye and (B) after relaxation by release of hyaluronan (thin coils) after removal from the eye.

To address wall-slip and accommodate the fragile vitreous tissue, two significant experimental challenges imposed by the structure of the network, we have employed the cleat geometry[13] for dynamic shear rheometry (Chapter 2). This tool has allowed us to quantitatively measure the shear moduli of the vitreous directly using a fluids rheometer. The cleat geometry suppresses wall slip while causing minimal disturbance to tissue structure (see Chapter 2). We have also used this tool to track the softening that occurs after the vitreous is extracted from the eye. These results, in conjunction with observations that HA is actively forced out of the vitreous after removal from the eye, suggest a modified view of the network structure of the vitreous in which internal tension from the swelling of HA significantly increases the stiffness of the tissue *in vivo*. Overcoming the obstacles to measuring the shear moduli of the vitreous is also an essential step forward in defining target mechanical properties for potential vitreous replacement materials and evaluating pharmacological vitrectomy agents. In addition to quantitative results for bovine and porcine vitreous, qualitative results for human vitreous are presented.

3.2 Materials and Methods

Fresh porcine eyes (< 36 hours *post mortem*, stored at 5° C in physiological saline prior to arrival) were acquired through Sierra for Medical Science (Santa Fe Springs, CA). All pigs were 3 – 6 month old Chester Whites, weighing 50 – 100 kg and in good health at the time of slaughter. Human donor eyes were obtained through the National Disease Research Interchange (a service of the NIH, Philadelphia, PA). Permission was obtained specifically for research use of the human eyes; they were unsuitable for cornea transplants. Approval

was also obtained from the Caltech Internal Review Board (Appendix A). Eyes were gently dissected to remove the vitreous with minimal disruption. All human specimens were tested between 28 and 48 hours *post mortem*; storage as an intact globe for up to 60 hours *post mortem* did not affect rheological results as previously observed.[14] Intact vitreous was either used directly or a disc-like section was cut with the axis of the disc coinciding with the anterior-to-posterior axis of the eye (typically 1.5 – 2.5 g). Some of the vitreous discs were loaded into a cleated 25 mm parallel disc geometry for mechanical characterization, and the remainder were used for network stability studies. Cone-and-plate geometries are inappropriate for chemically crosslinked gels because high compression near the center of the tool induces a non-uniform normal force profile and destroys the vitreous network.

Mechanical measurements were made on an ARES-RFS fluids rheometer from TA Instruments, Inc. (New Castle, DE) using our novel cleat geometry to overcome slip.[13] Previously reported methods for overcoming wall slip such as roughened plates or sandpaper were insufficient because the upper boundary of the vitreous develops a lubricating layer. Cleated tools succeed by penetrating the lubricating boundary layer to achieve an effective no-slip boundary condition (Chapter 2). All measurements were made in a closed, humid atmosphere at 20° C and with zero normal force on the samples. Shear moduli were monitored as samples were subjected to oscillatory strain ($\gamma = 3\%$) at a fixed frequency ($\omega = 10$ rad/s) for up to 90 minutes Longer experimental times were precluded by drying of the sample edges, which artificially raised the apparent modulus of the samples. The conditions for these experiments were chosen based on the results of variable

frequency (γ = 3%, ω = 1 - 50 rad/s) and variable strain (ω = 10 rad/s, γ = 0.5 – 100%) experiments. The initial modulus values are very sensitive to the length of time that elapses between dissection and rheological testing. Therefore, dissection time was kept as uniform as possible (2 – 3 minutes) and tissue was transferred to the instrument immediately after dissection was completed.

In addition to oscillatory tests, steady (shear) rate tests were conducted to determine the minimum shear stress and strain required to destroy the tissue. These "failure" tests were conducted after loading vitreous specimens and watching the moduli reach steady state in oscillatory shear (Figure 3). Then a steady shear rate ($\dot{\gamma}$ = 0.1 s^{-1}) was applied for 150 seconds while continuously monitoring the resulting shear stress. Higher and lower shear rates ($\dot{\gamma}$ = 0.3 and 0.01 s^{-1}) were also probed separately to demonstrate the rate dependence of the transient shear stress.

The discovery that vitreous loses elasticity and exudes fluid after dissection motivated us to measure the time-dependent mass loss and the composition of the exuded fluid. Post-dissection mass loss was measured in four different environments denoted A-D: (A) an intact vitreous body was placed in a dry Petri dish and covered; (B-D) central discs of vitreous were placed in covered Petri dishes that were either (B) dry, (C) filled with isotonic saline, or (D) filled with mechanically liquefied vitreous from other eyes. Liquefied vitreous was obtained by removing the vitreous of three to six fresh eyes of the same species immediately prior to the experiment and slicing them into small fragments, which caused much of the vitreous to liquefy. The mass of each vitreous sample was measured immediately after removal from the eye ($Mass_o$) and only once at the end of the

treatment period, which ranged from 5 to 120 minutes ($Mass_f$) – excess handling damages the vitreous and artificially accelerates weight loss. The treatment periods ranged from 5 to 120 minutes. One specimen was subjected to condition A and photographed at 1, 10, 30, and 90 minutes from the moment it was placed in the Petri dish. Using condition C, the components exuded into the saline solution were analyzed for hyaluronic acid (Hyaluronic Acid Test Kit; Corgenix, Inc., Denver, CO) and the presence of protein (ninhydrin assay). The circular dichroism spectrum of the bath solution of condition C was measured after 120 minutes and compared with spectra from solutions of purified collagen type II and hyaluronic acid obtained at room temperature with a model 62DS Circular Dichroism Spectrometer, AVIV Associates (Lakewood, NJ).

3.3 Mechanics of the Vitreous – the Key to Structure

In accord with prior literature, it appears that the connectivity of the gel network, while not completely homogeneous, is well distributed throughout most of the tissue.[1, 15] One consequence of this structural homogeneity is that central vitreous collapses at the same rate as intact, whole vitreous (i.e., removal of the peripheral tissue does not accelerate the shrinking rate). A second consequence is that the mechanical stability of a central disk of vitreous reflects the properties of the whole – a key assumption in our rheological experiments.

The dynamic moduli of vitreous sections decay monotonically to a significantly lower, steady-state value that persists thereafter (Figure 3). The average initial storage and loss moduli of bovine vitreous were $G'_{init} = 32 \pm 12$ Pa (mean ± SD) and $G''_{init} = 17 \pm 7.0$ Pa

(n=17); and for porcine vitreous G'_{init} = 10 ± 1.9 Pa and G''_{init} = 3.9 ± 0.8 Pa (n=9). The large standard deviations reflect rapid initial changes, making the observed moduli sensitive to the precise time from dissection to loading. Smaller standard deviations for porcine samples were achieved by using a consistent loading time of approximately 1 minute from removal of the dissected globe to inception of measurement. The average steady-state moduli for bovine vitreous were G'_{fin} = 7.0 ± 2.0 Pa and G''_{fin} = 2.2 ± 0.6 Pa; and for porcine vitreous G'_{fin} = 2.8 ± 0.9 Pa and G''_{fin} = 0.7 ± 0.4 Pa.

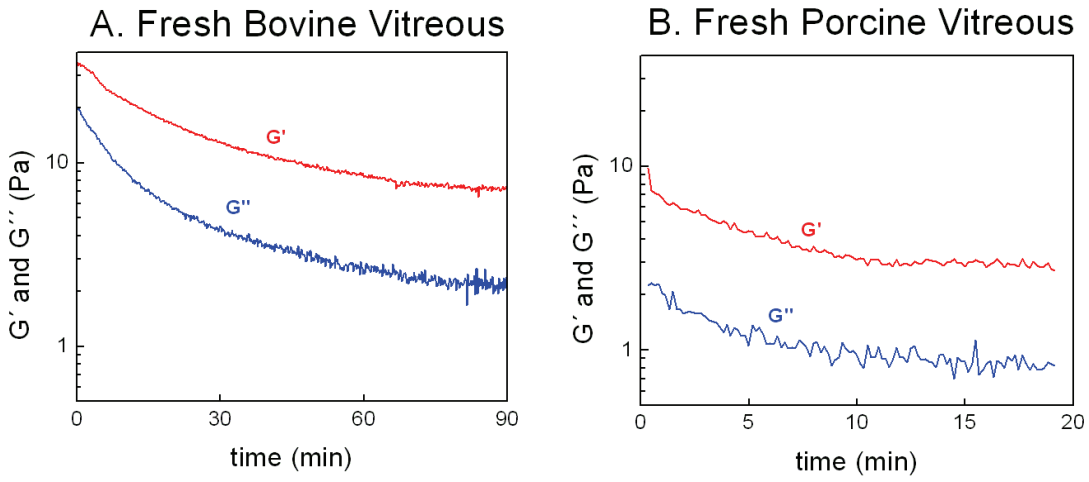

Figure 3. Typical time sweep of fresh bovine (A) and porcine (B) vitreous samples showing the rapid modulus decay to a steady-state after removal from the eye (γ = 3%, ω = 10 rad/s).The loss tangent reached steady-state more rapidly, often in as little as 20 minutes in bovine (tan δ = 0.31 ± 0.03) and 2 minutes in porcine (tan δ = 0.24 ± 0.09) specimens.

The drastic drop in shear modulus indicates a significant molecular-level change from a relatively rigid *in-oculo* state, which is not stable outside of the constraints of the eye, to a measurably softer state *ex-oculo*. Therefore, the initial moduli may be closer to the moduli

of the vitreous *in vivo* and the steady-state moduli represent a lower bound on the *in vivo* moduli, perhaps as much as five times lower. Nevertheless, these steady-state moduli are significantly *greater* than previously reported values,[4, 6, 9, 10] by orders of magnitude in some cases (Figure 4). Additionally, time-dependent modulus changes have not previously been reported. An interpretation of the time-dependent modulus changes as well as structural differences between the initial and steady states will be examined in the next section.

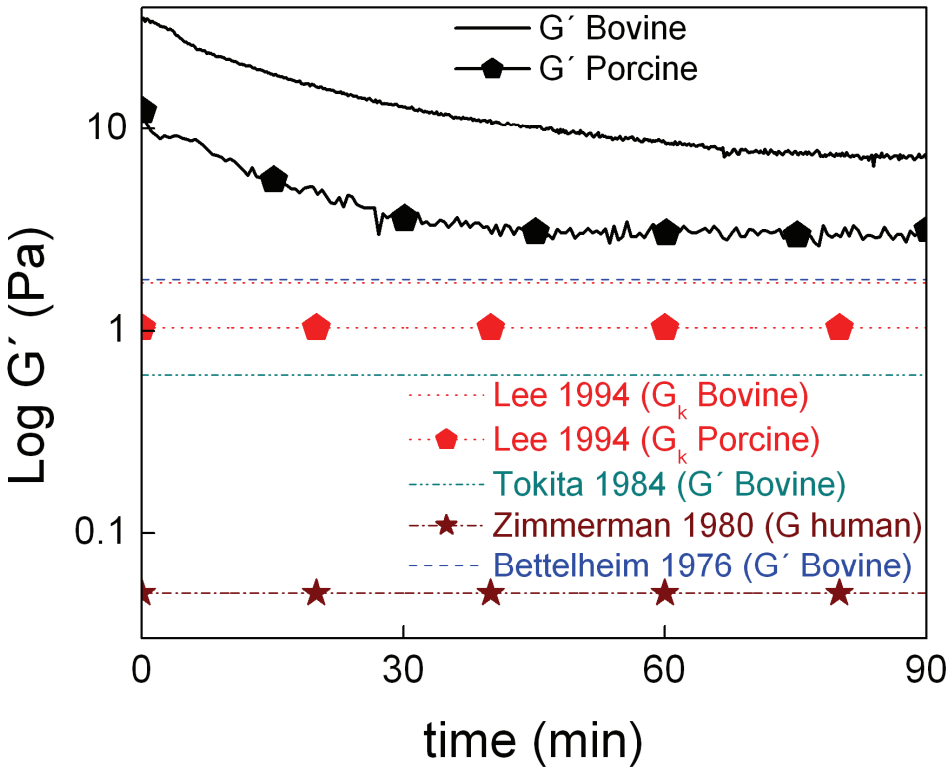

Figure 4. Typical time-dependent behavior of G' at fixed strain amplitude (3%) and frequency (10 rad/s) for bovine and porcine vitreous. Estimates of the modulus based on prior literature are indicated for reference.

The strain amplitude (3%) and frequency (10 rad/s) for vitreous analysis were optimized to allow us to apply gentle deformations close to the linear regime of the gel network. Variable strain experiments conducted at 10 rad/s show that the porcine vitreous is linear just below 3% strain and weakly non-linear thereafter (Figure 5). The "linear" or "strain-independent" regime indicates that the level of strain applied is small enough not to perturb the structure of the material. In biological specimens, the mechanical properties of the linear regime are particularly interesting because it includes normal physiological loads. Thus, linear viscoelastic properties represent the normal response of many tissues *in vivo*. In order to optimize the signal-to-noise ratio for these soft samples, oscillatory shear experiments were conducted near the upper limit of the linear regime at 3% strain.

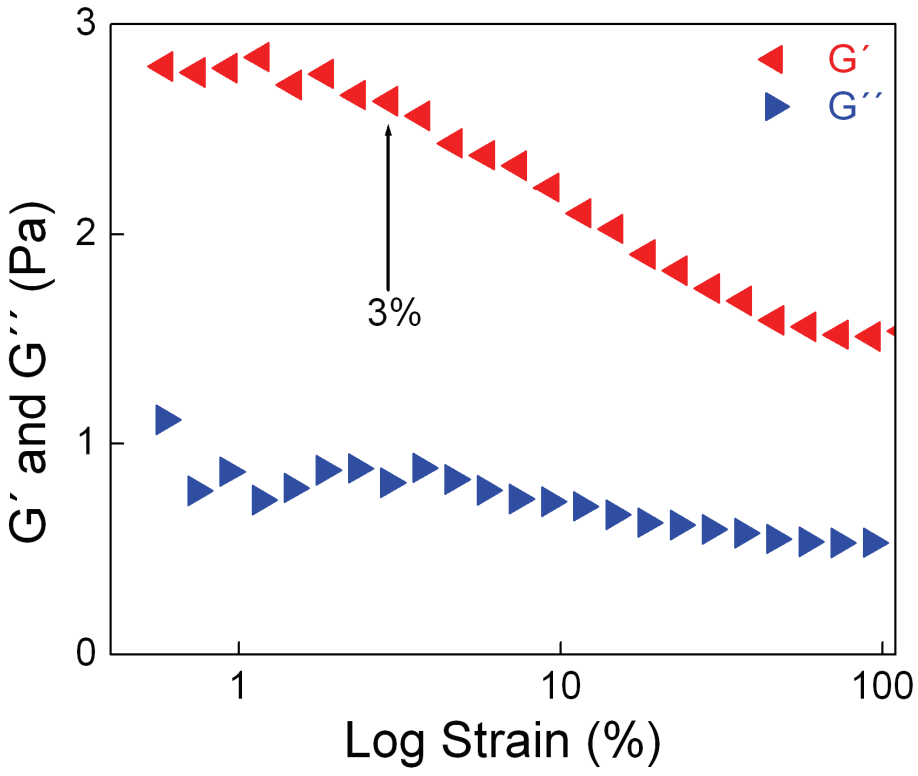

Figure 5. Typical variable strain experiment conducted after the shear modulus of the vitreous had reached steady-state (Porcine

vitreous ~ 20 minutes after loading, frequency=10 rad/s). 3% strain is just above the linear regime but lower strains do not generate sufficient torque for accurate determination of moduli.

Regarding the frequency dependence of the dynamic moduli: the storage modulus of steady-state porcine vitreous varies weakly with frequency up to ~ 5 rad/s and rises significantly thereafter (Figure 6). This frequency dependence is typical of a lightly cross-linked amorphous network of macromolecules[16] – consistent with the accepted model of vitreous structure. The broad plateau modulus region expected for gels appears below ~ 5 rad/s. To generate sufficiently large torques for the instrument specifications while operating at small strain amplitudes, a frequency of 10 rad/s was required. Thus, the moduli we report may be somewhat higher than the gel's steady-state plateau modulus. The strain and frequency dependencies of bovine vitreous are similar to the porcine data shown.

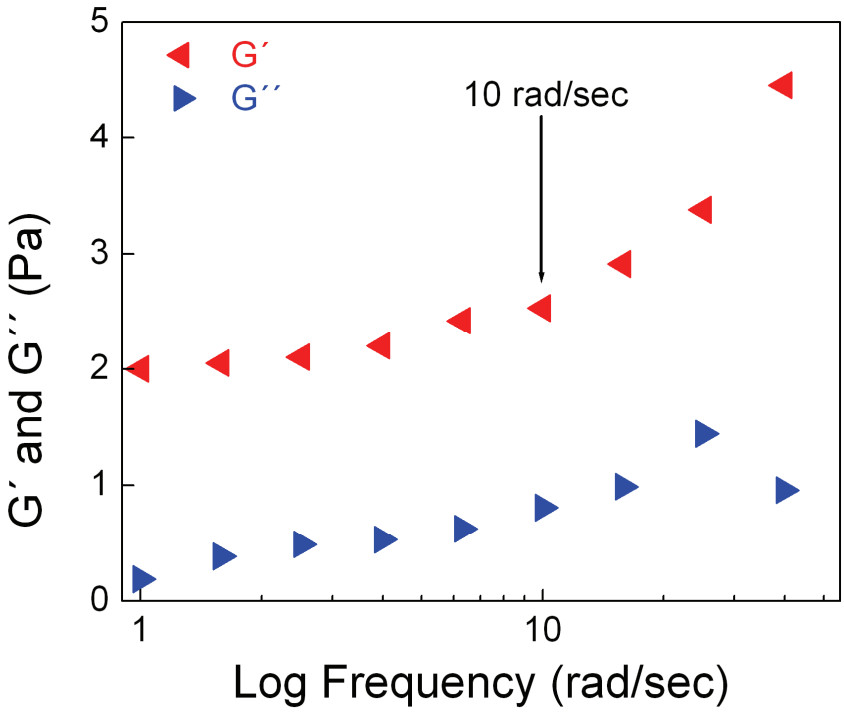

Figure 6. Typical variable frequency experiment conducted after the shear modulus of the vitreous had reached steady-state (porcine vitreous, γ = 3%). 10 rad/s is slightly above the plateau regime, but lower frequencies do not generate sufficient signal for accurate modulus measurements at low strain amplitude.

A limited number of matched pairs of human donor eyes were analyzed using the protocols developed above for porcine and bovine eyes (Figure 7). The mechanical properties of human vitreous appear to be highly variable between individuals. With one exception, however, fellow eyes had very similar properties. This, taken together with the large difference between the two 21 year old donors, suggests that the large standard deviation seen in porcine eyes comes as a result of sample-sample variability and not inconsistencies in the measurement method.

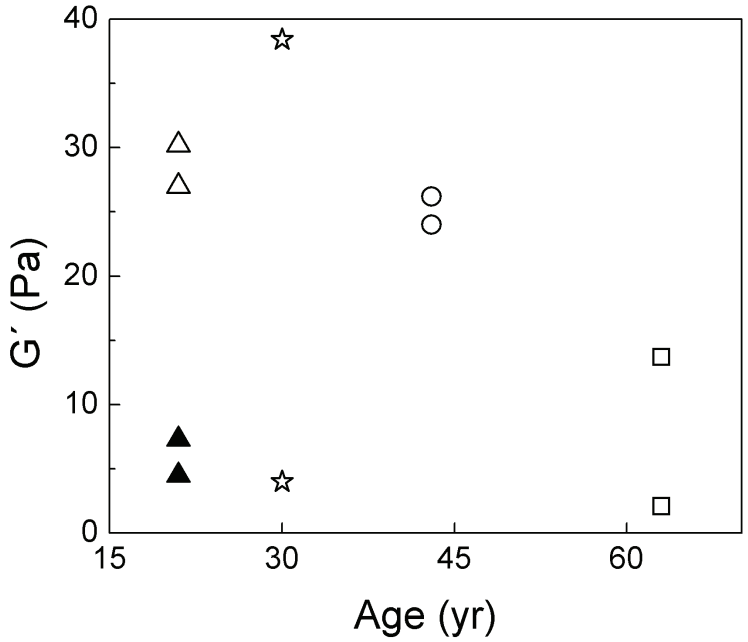

Figure 7. Initial shear moduli of matched human donor vitreous as a function of donor age. Experimental parameters developed for bovine and porcine eyes were used (γ = 3%, ω = 10 rad/s). Matching symbols denotes matched pairs.

In addition to linear viscoelastic properties, tissue failure under high stress is relevant to certain injuries and surgical procedures. During severe head trauma, the vitreous gel can be torn and cause retinal tears. Also, during vitrectomy procedures performed to treat diabetic retinopathy, among other major eye diseases, surgeons need to destroy the vitreous in order to remove it from the eye. However, to our knowledge, there have been no published studies that demonstrate the maximum stress load the vitreous can bear, nor have studies demonstrated the response of the tissue when stress exceeds this maximum and the tissue fails. We have addressed this need using steady-shear experiments in which the vitreous specimens are sheared (at a constant rate) to the point of failure.

The failure patterns of the vitreous demonstrate a natural protective effect against head trauma and provide new considerations for vitreous surgery. Shear stress rises sharply at the onset of strain, rapidly reaches a rate-dependent maximum (failure stress and strain increase with shear rate), and then gradually declines (Figure 8). Thus, the vitreous is relatively soft when deformed slowly; however, it stiffens considerably against rapid deformations—possibly a protective mechanism for the retina during head trauma. In the context of vitreous surgery, this failure pattern suggests that removing the vitreous quickly puts unnecessary stress on the retina. The need for slow vitreous removal appears even more important in light of the gradual decline in stress that occurs even after failure; the vitreous can continue to transfer stress to the retina even after it has failed.

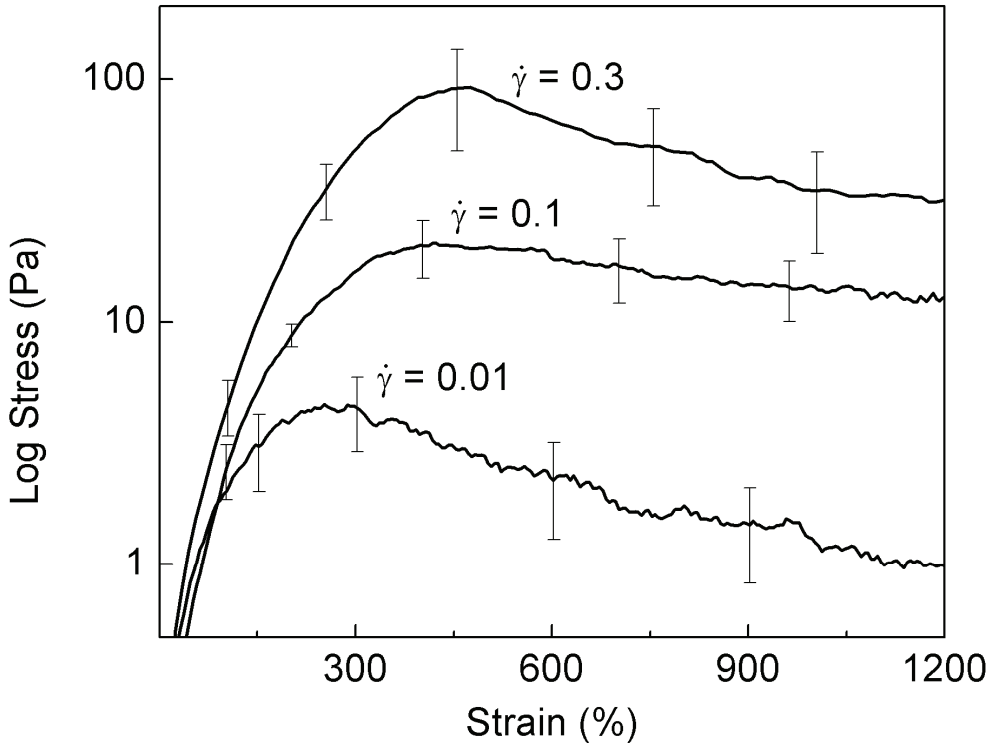

Figure 8. Average failure behavior of porcine vitreous strained under steady shear at three different shear rates (0.01, 0.1, and 0.3 s^{-1}; $n \geq 3$).

Shearing at lower rates appears to allow the network to relax, thereby reducing the stress at any given strain. Based on the frequency dependence of the storage modulus in oscillatory tests, a shear rate of $\dot{\gamma} = 0.1\ s^{-1}$ is sufficiently slow to allow the high frequency relaxation processes evident at $\omega > 5$ rad/s to relax. However, slower relaxation mechanisms are apparently active under high strains because a lower shear rate ($\dot{\gamma} = 0.01\ s^{-1}$) decreases the failure stress from $\sigma_{max} = 24 \pm 3$ Pa ($\dot{\gamma} = 0.1\ s^{-1}$) to $\sigma_{max} = 5.7 \pm 0.9$ Pa ($\dot{\gamma} = 0.01\ s^{-1}$) and failure strain from $\gamma_{fail} = 418 \pm 51$ Pa ($\dot{\gamma} = 0.1\ s^{-1}$) to $\gamma_{fail} = 259 \pm 35$ Pa ($\dot{\gamma} = 0.01\ s^{-1}$). The distribution of relaxation times and gradual failure also indicate significant heterogeneity in

the network; short, thin collagen fibrils break under small strains, while larger and longer filaments last longer, breaking only after large deformations (beyond the peak stress).

3.4 Mass Loss Associated with Post-Dissection Softening

Upon removal of the test samples from the rheometer, two obvious changes in the tissue confirm that the steady-state moduli are lower than the moduli of the vitreous *in vivo*. First, the post-rheology vitreous appears to sag, elongating far more when lifted with forceps. The reason for the softening may be found in the second major observation: a small puddle of liquid is left behind on the instrument where aqueous material has seeped out of the vitreous.

To explore the possible connection between the loss of aqueous material and rheological changes in freshly extracted vitreous, we observed changes in mechanical integrity and mass as a function of time (Figure 9). Immediately following dissection, the vitreous partially retains the native shape of the vitreous cavity. After being placed in a sealed Petri dish for 10 minutes, the vitreous has visibly lost fluid and elongates upon lifting. This trend continues until 90 minutes after dissection, when the specimen reaches its post-dissection steady state. Morphological changes coincide with mass loss, which was rapid immediately after removal from the eye but stabilized within 2 hours.

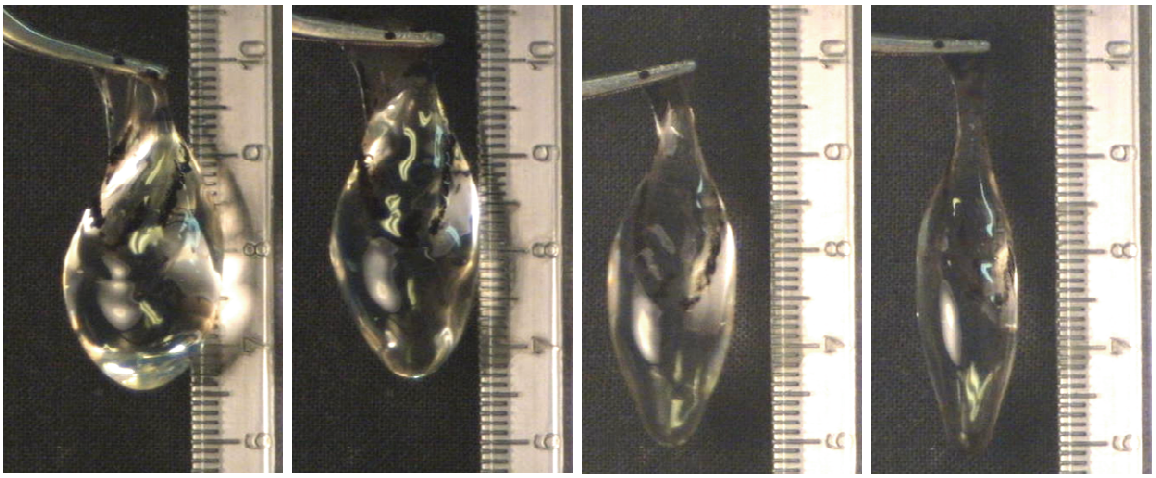

Figure 9. This sequence of photographs illustrates the state of a whole vitreous gently removed from a fresh porcine eye 1, 10, 30, and 90 minutes after dissection. The vitreous was kept in a dry, covered Petri dish during the course of the experiment.

The ejected fluid was rich in hyaluronan and soluble protein (presumably albumin), but contained no detectable helical collagen. In condition C, more than 10% of the vitreous HA was ejected after 120 minute, as determined by enzyme-linked hyaluronic acid binding protein assay. The loss of protein was not as great; ≤ 10% of the total protein was ejected, as measured by the ninhydrin amino acid assay. The circular dichroism spectrum of the ejected fluid is characteristic of albumin, but not collagen (Figure 10). Because slightly more than 10% of the total vitreous mass (volume) was also lost, it appears that the ejected fluid contained the soluble components of the vitreous in roughly the same proportions as the vitreous itself. Fluid loss was very similar in bovine and porcine vitreous.

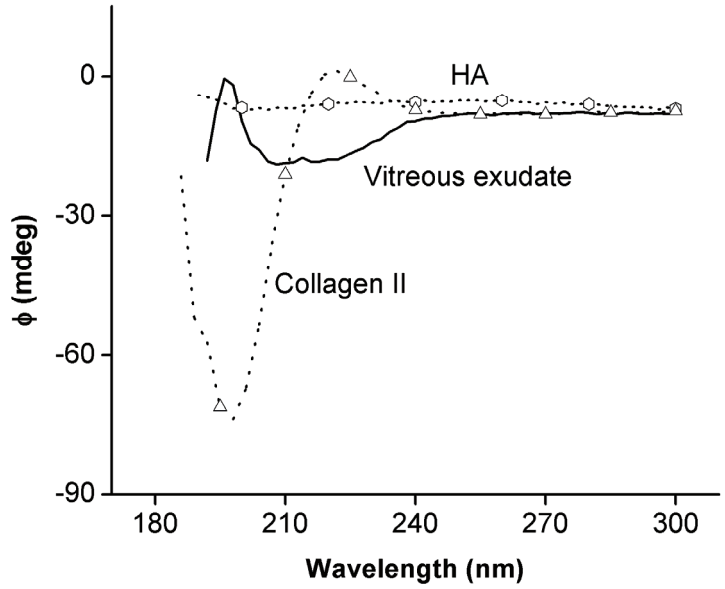

Figure 10. Circular dichroism spectrum of conition C exudate compared with spectra of collagen type II and HA standards at room temperature.

To quantify the liquid-loss observations, we extracted fresh vitreous specimens and placed them under the four conditions listed in the methods section (A—Whole vitreous placed in covered Petri dish, B, C, and D—Disc shaped vitreous sample placed in covered Petri dish either dry [B], filled with isotonic saline [C], or filled with liquefied vitreous [D]). The mass-decay period started immediately after the vitreous body was removed from the eye. Regardless of the conditions under which the vitreous was placed, the mass dropped 5 to 10% within the first 5 minutes. Thereafter the mass of A and B dropped monotonically, with A continuing to drop below 50% of its initial mass and B reaching a near-equilibrium value near 75% within 1 hour (Figure 11). The masses of C and D dropped only slightly between 10 and 120 min. to ~90% of their initial mass. The masses of A and B continued to drop monotonically after 10 min., and fluid continued to seep out of the vitreous body.

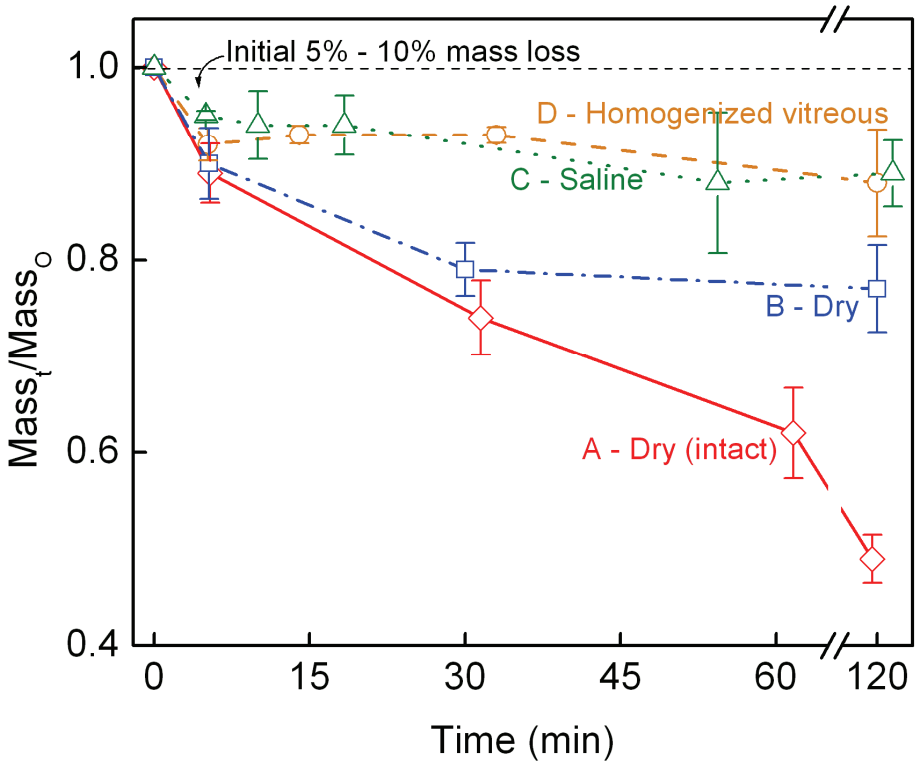

Figure 11. Changes in porcine vitreous sample weight monitored over time under the following conditions: whole vitreous placed in covered Petri dish (A), central section of vitreous placed in covered Petri dish that is dry (B), contains isotonic saline (C), contains mechanically liquefied vitreous (D) (n = 4).

The differing magnitudes of mass loss under conditions A – D provide insight into the mechanisms that drive mass loss. In A there is a significant and continuing driving force for expulsion of fluid. Two obvious driving forces are gravity (the globe collapsing under its own weight) and wetting/diffusion (fluid diffuses out of the tissue along the concentration gradient). The same diffusion forces are present in both A and B, however, the disk shape of B has less gravitational potential energy. Because all other factors are equal, B appears

to retain a greater fraction of its mass due to the smaller gravitational driving force for fluid loss. It was surprising that cutting sample B did not increase the mass loss as compared with A but actually had the opposite effect.

Conditions C and D are significantly different from A and B because the two obvious fluid-loss driving forces (gravitational collapse and concentration gradient-driven diffusion) have been eliminated. In C, the saline bath allows the vitreous to float at neutral buoyancy in a solution that is isotonic with the primary soluble component of the vitreous – NaCl. In D, the vitreous is completely surrounded by other vitreous material – thereby completely eliminating the concentration gradient for all components, including hyaluronic acid. Despite these changes there is still a mass loss on the order of 7% in the first 5 – 10 minutes. This rapid initial weight loss appears to be driven by an internal force that becomes imbalanced when the *in-vivo* constraints on the vitreous are removed. It is also coincident with the sharp initial drop in shear modulus (Figure 2). We will present a novel hypothesis that links these two phenomena and suggest two possible underlying mechanisms.

3.5 Network Tension – the Contribution of Hyaluronic Acid

The loss of hyaluronan-rich fluid from the vitreous was unexpected and provides several clues to the mechanism driving fluid loss and modulus drop. The observations regarding potential mechanisms of fluid loss reported in Section 3.4, that a significant portion of the fluid loss is neither driven by diffusion down a gradient nor by gravity, and that the rate and magnitude of fluid loss are independent of sample surface area, combine to suggest that

hyaluronan is not simply diffusing out of the vitreous but, rather, that it is driven out. Furthermore, the driving force must be present throughout the volume of the vitreous. Based upon these observations and the correlation between fluid loss and modulus decrease, we suggest that the driving force for this fluid expulsion is tension in the collagen network induced by hyaluronan.

It is well accepted that hyaluronan draws water into the fibril network to achieve Donnan equilibrium, adds chemical stability to the collagen, and separates the fibrils.[1, 3, 12] Polyelectrolytes such as HA are swollen by the hydration spheres of their associated counter ions.[17] Counter ions also increase the entropic cost of overlap because a single overlap event between two polymers results in the doubling of the local concentration of many counter ions. The expanded configuration of HA, combined with its resistance to overlap, make it ideal for accomplishing the functions listed above. The literature, however, makes no firm assertions concerning contributions of hyaluronan to the elasticity of the gel.[1, 3, 12] Using the cleat geometry we have been able to monitor the evolution of the moduli after dissection and, thereby, gain new clues that suggest that hyaluronan does stiffen the gel. We propose that hyaluronan increases the moduli of the vitreous by placing the collagen network under internal tension as it swells to find a Donnan equilibrium hydration state (Figure 1A vs. 1B). Tension on individual collagen fibrils would reduce their ability to deform and, thereby, increase the modulus. If the vitreous is approximated as a contracting, isotropic sphere, the average measured mass reduction in C and D in the first 5 minutes (7%) corresponds to a 7% volume contraction and ~ 2% radial contraction.

Two possible mechanisms by which hyaluronan could induce network tension through a small stretch (~ 2%) are consistent with the fact that hyaluronan is essentially retained in the vitreous. The vitreous is enveloped in a semipermeable membrane. One possible source of network tension is the hydrostatic pressure (due to hyaluronan-induced Donnan swelling), which exerts an outward force on the semipermeable periphery of the vitreous network until the collagen fibrils are pulled taut. Semiflexible polymers exert an entropically driven elastic force when their end-to-end distance is increased beyond its equilibrium value.[18] Thus, in a taut state, fibrils are loosely analogous to long elastic ropes that are stretched by the swollen HA. Upon release of the boundary constraints, the HA is driven out of the network as the stretched ropes contract to a tension-free length. However, physical entanglements due to the high molecular weight (~ 5 million) of HA prevent it from exiting immediately. There is also evidence to suggest that HA is anchored to the collagen network and not just physically entangled, which would further slow the loss of HA.[19] There is a modest HA concentration gradient in the vitreous, with the highest concentration located in the posterior of the eye.[2] If HA were completely free to diffuse through the vitreous, even if motion were slowed by entanglements one would anticipate that HA would distribute itself homogeneously throughout the eye eventually.

A second possible tension mechanism arises if the hyaluronan is indeed bound to the network strands, be it directly or through binding mediators. As explained previously, each hyaluronan molecule must retain its hydration volume. If the HA molecules are bound to fibrils, crowding between two neighboring hydration spheres would effectively drive the attachment points of the two HA molecules to separate. The fibril would extend either

until the chemical potential of swelling was balanced by the fibril's conformational entropic loss or to the limit of full extension. Just as in the first case, HA swelling would induce internal tension that would be distributed throughout the collagen network. These two mechanisms are not mutually exclusive, so both may contribute. And in both cases, removal from the eye would provide a thermodynamic driving force for an efflux of hyaluronan-rich fluid.

Both scenarios are similar and consistent with all of our observations. In both cases, any portion of the network should behave the same as the intact vitreous. The accuracy of this "homogeneous properties" prediction can be verified by comparing the weight-loss behavior of conditions A and B of the previous section. Biochemical assays also demonstrated that the ejected fluid was rich in HA. In both cases, loss of fluid should cause the vitreous to soften even though the concentration of collagen in the shrunken network is higher than in the swollen state. Both internal tension mechanisms are also in accord with Bos's microscopic observation that the collagen network appears to "relax" after the removal of hyaluronan.[3]

To envision the feasibility of crowding of hyaluronan in the vitreous – a key feature of both models – we calculated the maximum volume available to each hyaluronan molecule and compared it with the volume that an isolated hyaluronan polymer of the same molecular weight would occupy under physiological conditions. We calculated the volume available per hyaluronan molecule in the vitreous using literature hyaluronan concentration and molecular weight values to evaluate the following expression:[1]

$$Volume = \frac{1}{\left[HA\ concentration\left(\mu g/ml\right)\right] \times \left(1/molecular\ weight\right) \times N_A}$$

We estimated the volume that a hyaluronan molecule of the species-appropriate molecular weight occupies at 37° C and 150 mM NaCl based upon radius-of-gyration (R_g) values given by Mendichi.[20] These calculations were performed for human ([HA] = 65 – 400 μg / ml, MW = 3.5 x 10^6 g / mol, R_g = 260 nm) and bovine ([HA] = 560 μg / ml, MW = 2.36 x 10^5 g / mol, R_g = 90 nm) vitreous. The bovine molecular weight value was chosen from within the range listed[1] because of available R_g data.[20] Based upon $4/3 \times \pi \times R_g^3$, in humans a typical molecule of vitreous hyaluronan would occupy 7.4 x 10^{-14} ml, fully filling the 1.4 x 10^{-14} to 8.9 x 10^{-14} ml space available. In the bovine case, one vitreous hyaluronan molecule would occupy 7.0 x 10^{-16} ml, while 6.9 x 10^{-16} ml per hyaluronan molecule is available *in vivo*. The values are approximate since hyaluronan is not evenly distributed through the vitreous. However, the close match between average space available in the vitreous and average single chain volume suggests that there are not large void volumes between hyaluronan molecules *in vivo*.

While this is the first evidence that network tension stiffens the vitreous, the concept of hydrostatic structures, or "hydrostats," is well accepted in the biomechanics literature.[21] One notable example of hydrostatic pressure contributing to mechanical strength is cartilage.[21, 22] Like the vitreous, cartilage consists of a hydrated network of collagen II fibrils filled with highly-charged HA. Cartilage has a much higher modulus due to its higher protein content, but the underlying mechanism is the same – Donnan swelling due to

the high fixed charge density stiffens the tissue by extending the collagen fibrils of the network.

Our internal tension model suggests that the initial value of the modulus, measured within minutes of dissection, may resemble the mechanical properties of tissue *in vivo*, where the collagen fibrils are stretched. Steady-state moduli represent essentially the same collagen network, with the same degree of connectivity but with a reduced presence of HA and no net tension. While it appears that our steady-state moduli are systematically lower than *in vivo*, they are also useful for several reasons. First, while they represent minimum values for the native moduli, they are higher than any previous estimates found in the literature. Second, they provide useful target values for those striving to create synthetic vitreous replacements.[23-25] Third, the steady-state network properties are quantitative and reproducible, suitable for quantifying the effects of pharmacological vitrectomy agents, examining natural and pathologic vitreous liquefaction, and also understanding the molecular architectures that produce the structure of the healthy vitreous. Equipped with an understanding of the primary structure of the vitreous and the tools to quantify changes in its mechanical properties, we are prepared to take a rational-design approach to vitreous engineering.

BIBLIOGRAPHY

1. Bishop PN. Structural macromolecules and supramolecular organisation of the vitreous gel. *Progress in Retinal and Eye Research.* May 2000;19(3):323-344.

2. Sebag J. *The Vitreous - Structure, Function, and Pathobiology*. New York: Springer-Verlag Inc.; 1989.

3. Bos KJ, Holmes DF, Meadows RS, Kadler KE, McLeod D, Bishop PN. Collagen fibril organisation in mammalian vitreous by freeze etch/rotary shadowing electron microscopy. *Micron.* Apr 2001;32(3):301-306.

4. Tokita M, Fujiya Y, Hikichi K. Dynamic viscoelasticity of bovine vitreous body. *Biorheology.* 1984;21(6):751-756.

5. Pfeiffer HH. Zur analyse der fliess-elastizitaet durch spinnversuche am corpus vitreus. *Biorheology.* 1963;1:111-117.

6. Bettelheim FA, Wang TJY. Dynamic Viscoelastic Properties of Bovine Vitreous. *Experimental Eye Research.* 1976;23(4):435-441.

7. Lee B, Litt M, Buchsbaum G. Rheology of the vitreous body. Part I: Viscoelasticity of human vitreous. *Biorheology.* Sep-Dec 1992;29(5-6):521-533.

8. Lee B, Litt M, Buchsbaum G. Rheology of the vitreous body: part 3. Concentration of electrolytes, collagen and hyaluronic acid. *Biorheology.* Jul-Aug 1994;31(4):339-351.

9. Lee B, Litt M, Buchsbaum G. Rheology of the vitreous body: Part 2. Viscoelasticity of bovine and porcine vitreous. *Biorheology.* Jul-Aug 1994;31(4):327-338.

10. Zimmerman RL. In Vivo Measurements of the Viscoelasticity of the Human Vitreous-Humor. *Biophysical Journal.* 1980;29(3):539-544.

11. Walton KA, Meyer CH, Harkrider CJ, Cox TA, Toth CA. Age-related changes in vitreous mobility as measured by video B scan ultrasound. *Experimental Eye Research.* Feb 2002;74(2):173-180.

12. Sebag J, Balazs E. Morphology and ultrastructure of human vitreous fibers. *Investigative Ophthalmology and Visual Science.* 1989;30:1867-1871.

13. Nickerson CS, Kornfield JA. A "cleat" geometry for suppressing wall slip. *Journal of Rheology.* 2005;49(4):865-874.

14. Weber H, Landwehr G, Kilp H, Neubauer H. The Mechanical-Properties of the Vitreous of Pig and Human Donor Eyes. *Ophthalmic Research.* 1982;14(5):335-343.

15. Fatt I, Weissman BA. *Physiology of the Eye.* Second ed. Boston: Butterworth-Heinemann; 1992.

16. Ferry JD. *Viscoelastic Properties of Polymers.* 3rd ed. New York: John Wiley & Sons; 1980.

17. Flory PJ. *Principles of Polymer Chemistry*. Ithaca, NY: Cornell University Press; 1953.

18. Rubinstein M, Colby RH. *Polymer Physics*. New York: Oxford University Press; 2003.

19. Scott JE. Structure and function in extracellular matrices depend on interactions between anionic glycosaminoglycans. *Pathologie Biologie.* May 2001;49(4):284-289.

20. Mendichi R, Soltes L, Schieroni AG. Evaluation of radius of gyration and intrinsic viscosity molar mass dependence and stiffness of hyaluronan. *Biomacromolecules.* Nov-Dec 2003;4(6):1805-1810.

21. Vogel S. *Comparative biomechanics: life's physical world.* Princeton, NJ: Princeton University Press; 2003.

22. Hasler EM, Herzog W, Wu JZ, Muller W, Wyss U. Articular cartilage biomechanics: Theoretical models, material properties, and biosynthetic response. *Critical Reviews In Biomedical Engineering.* 1999;27(6):415-488.

23. Dalton PD, Chirila TV, Hong Y, Jefferson A. Oscillatory shear experiments as criteria for potential vitreous substitutes. *Polymer Gels And Networks.* 1995;3(4):429-444.

24. Chirila TV, Hong Y, Dalton PD, Constable IJ, Refojo MF. The use of hydrophilic polymers as artificial vitreous. *Progress In Polymer Science.* 1998;23(3):475-508.

25. Soman N, Banerjee R. Artificial vitreous replacements. *Bio-Medical Materials and Engineering.* 2003;13(1):59-74.

C h a p t e r 4

ENGINEERING THE VITREOUS HUMOR

4.1 Introduction

Having defined the mechanical properties of the vitreous and the functions of its two primary components in Chapter 3, we are now prepared to examine the nanoscale architecture of the network in search of points of attack for pharmacological vitreolysis. We will show that enzymatically cleaving the peptide bonds of collagen fibrils will destroy the network and liquefy the vitreous. However, this is not clinically relevant because of the toxicity of collagenase. Hyaluronidase has advanced to clinical trials for clearing blood clots in the vitreous.[1] Is it possible to induce liquefaction by cleaving the glycosidic linkages in HA? Better yet, is it possible to gently weaken or dissolve the vitreous by disrupting key noncovalent interactions within the network, such as hydrogen bonds? These questions are of significant fundamental and therapeutic interest – if answered, they will reveal the chemistry that binds the components of the vitreous together and thereby provide a road map for the rational design of pharmacological vitrectomy agents.

The ideal pharmacological vitrectomy agent would rapidly eliminate vitreoretinal adhesion and then liquefy the vitreous without harming the sensitive cells of the retina.[1] There are two possible chemical routes to these objectives: destroying components of the network (e.g., using collagenase) or causing the intact components to dissociate (e.g., using a denaturant). The wood-framed house metaphor is again useful in this context: a house can be leveled either by cutting the beams or by simply removing the nails. Most of the prior literature has focused on the former, while we will show that the latter is safer and also promising.

Proteases (most notably plasmin[2, 3], dispase[4], and collagenase[5]) have been proposed for vitreolysis, but none have proven to be clinically viable because many of the structural proteins of the vitreous (collagens, fibronectin, etc.) also support adjacent tissues, including the retina.[1] Proteases pose too great a danger because they diffuse to the edge of the vitreous during treatment and damage the retina irreversibly.[6] Hyaluronidase enzyme has also been proposed for pharmacological vitrectomy;[7] however, it has been proven unacceptable because it causes the vitreous network to shrink without inducing posterior vitreous detachment (PVD).[8] At points of vitreoretinal adhesion, shrinkage of the vitreous exerts traction on the retina. Traction at adhesion foci may induce macular holes, macular edema, vitreous hemorrhage, retinal tears, or even retinal detachment.[9] These dangers motivate the search for gentle pharmacological vitrectomy agents that denature network components rather than cleaving peptides. The possibility for retinal toxicity exists with gentle approaches as well, but *in vivo* rabbit and porcine studies and human clinical trials indicate that the effects of urea, for example, are minimal and transient.

Recent work by Oliveira, et al. has shown that posterior vitreous detachment can be induced in donor eyes by administration of RGD peptide.[10] Their supposition is that vitreoretinal adhesion is dominated by the noncovalent interactions of the RGD binding domain and that their short RGD fragment induces separation by competing for binding sites. Also, Vitreoretinal Technologies, Inc. has demonstrated that urea is a useful adjunct to surgical vitrectomy, improving surgical outcomes and reducing surgical time in a masked, double-blind human study.[11] Urea is a common biochemical reagent that does not cleave proteins; therefore, the beneficial effect is thought to come from its ability to disrupt hydrogen bonds. Both the RGD and the urea studies indicate that noncovalent interactions play a significant role in stabilizing the vitreous and vitreoretinal adhesion.

We present a systematic approach to examining the stability of the vitreous against an array of treatments designed to disrupt distinct types of molecular interactions: covalent bonds, hydrogen bonds, electrostatic effects, and hydrophobic attractions. We show that hydrogen bonds play a key role in stabilizing the vitreous and then proceed by examining the impact of injecting urea into an *in vitro* porcine eye model. Encouraging results from these *in vitro* studies and from clinical work by Vitreoretinal Technologies, Inc. prompted us to then administer small doses of urea to an *in vivo* porcine eye model to quantify its impact.

4.2 Materials and Methods

Chemical Stability of the Vitreous – Fresh porcine eyes (< 36 hours *post mortem*, stored at 5° C in physiological saline prior to arrival) were acquired through Sierra for Medical Science (Santa Fe Springs, CA). All pigs were 3 – 6 month old Chester Whites, weighing

50 – 100 kg and in good health at the time of slaughter. Eyes were gently dissected to remove the vitreous with minimal disruption. The intact vitreous specimens were then weighed (initial mass, typically M_o ~ 3 g) and place immediately in 10 ml of one of the treatment solutions listed below (Table 1) for 1 or 24 hours at 37° C. Treatments were chosen to probe the importance of specific types of intermolecular interactions (urea to disrupt hydrogen bonds, NaCl and $MgCl_2$ to screen electrostatic attractions/repulsion, etc.). After incubation, each vitreous specimen was removed from its treatment bath and weighed a second time (M_f) (Figure 1).

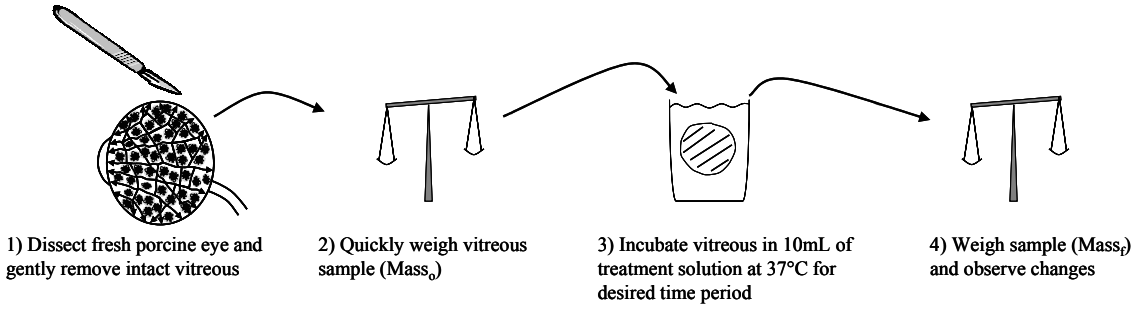

Figure 1. For chemical stability experiments each vitreous was: 1) gently removed from a fresh porcine eye (< 36 hours *post mortem*, stored at 5° C in physiological saline prior to dissection), 2) weighed (M_o), 3) placed in 10 ml of the appropriate treatment solution at 37° C for 1 to 24 hours, and 4) weighed again (M_f).

Treatment	Concentrations Examined [M] or pH	Targeted Intermolecular Interaction	Typical Lab Concentrations [M] or pH	Solubility Limit [M]
Enzymatic Cleavage	Hyaluronidase, Collagenase	Covalent bonds	N/A	N/A
Urea	0.5, 1, 2, 4, 5, 6, 8	Hydrogen bonding	4 – 8 for denaturation	8
Guanidinium HCl	6	Hydrogen bonding	4 – 6 for denaturation	6
Mid – high pH 10 mM phosphate buffer	(pH) = 7.4, 9.8, 12.0	Electrostatics and H-bond scheme (deprotonation)	7.45	N/A
Mid – low pH 10 mM citrate buffer	(pH) = 2.0, 2.6, 4.5, 6.0, 7.5, 8.1	Electrostatics and H-bond scheme (protonation)	7.45	N/A
NaCl	0, 0.05, 0.075, 0.1, 0.15, 0.25, 0.5, 1, 2, 5	Electrostatics (monovalent cation)	0.150 (physiologic)	5
$MgCl_2$	0.1, 0.02, 0.3, 0.4, 0.5, 0.6, 1	Electrostatics (divalent cation)	~ 0.001 (physiologic)	1
Triton® X–100	0.01, 0.016, 0.05, 0.1, 0.3	Hydrophobic Interactions	0.016 (1%)	None

Table 1. List of bath solutions in which vitreous specimens were placed for chemical stability tests. Each treatment was designed to probe the importance of a specific interaction: covalent, hydrogen bond, electrostatic, or hydrophobic.

Quantitative Analysis of the Mechanical Impact of Urea and pH – Urea and extreme pH changes were the only treatments capable of causing complete vitreous collapse; therefore their effects were studied further. Vitreous specimens were removed from fresh porcine eyes by gentle dissection and given 100 μl injections of one of the following urea treatment solutions: variable concentration (0, 3, 6, or 24% in 0.9% saline; pH = 6) or variable pH (2, 6, 8, or 12; concentration = 24%). Following injection, each specimen was placed in 10 ml of 0.9% saline for 24 hours at 37° C. After the incubation period, a central section of each vitreous was removed and its modulus was measured immediately on an ARES-RFS rheometer from TA Instruments, Inc. (New Castle, DE) using the same "cleat geometry" method (ω = 10 rad / sec, γ = 3%, T = 22° C) described in Chapter 2. After reaching a stable plateau modulus, a few treated and control specimens were subject to the "failure-stress" tests described in Chapter 3.

In Vivo Exploration of Vitreous Mechanics – Live animals used for this study were housed, treated, and examined by our collaborators in Professor Hugo Quiroz-Mercado's lab at the Hospital "Dr. Luis Sánchez Bulnes" de la Asociación Para Evitar la Ceguera (APEC) in Mexico City, in accordance with Association for Research in Vision and Ophthalmology (ARVO) standards for the ethical treatment of animals.[12] Landras mini pigs age 2-3 months were anesthetized, then 100 μl of 0.9% saline containing 0, 12, or 24% urea were injected into the vitreous of 11 of the 13 pigs. In each case, the left eye was injected with either 12 or 24% urea and the fellow (right) eye was injected with pure saline as a control. In the remaining 2 pigs, no injections were made in order to document differences between saline-treated "control" eyes and untreated eyes. Each solution was injected either 1 or 14

days prior to the animals being tested as outlined in Appendix B. On the assigned test day the animals were again anesthetized, and then the intraocular pressure (IOP) of each eye was measured. After IOP measurements, the animals were sacrificed by lethal injection with sodium pentobarbital and the eyes were examined for general health, retinal inflammation, and vitreous changes indicative of liquefaction, using an ophthalmoscope. After examinations were completed the eyes were enucleated, placed individually in physiological saline, and transported (~ 1 hour on wet ice) to Professor Alberto Tecante's lab at the National Autonomous University of Mexico (UNAM) for physical analysis. Within minutes after dissection, each vitreous was carefully weighed and loaded on a 15 mm diameter cleat tool on an ARES-RFS rheometer that was identical to the instrument used for *in vitro* analyses. The dynamic modulus (ω = 10 rad/s, γ = 3%, T = 22° C) was monitored until it reached steady state (~ 10 minutes). Thus, approximately 15 minutes elapsed between successive dissections and analyses. Results did not show any trend with elapsed time *post mortem.*

4.3 The Chemical Stability of the Vitreous

From a therapeutic perspective, though it is valuable to know the chemistry of the intermolecular interactions that are most significant for the mechanical stability of the vitreous network and to know the identity of the species involved, knowledge of either is sufficient for designing therapeutics to disrupt connectivity. For example, if a specific protein is identified as a critical crosslink, then a therapeutic that targets the binding sites of that peptide would be appropriate. Alternatively, if a particular type of bonding (e.g.,

hydrogen bonding) is critical for network stability, then a therapeutic designed to disrupt that interaction is appropriate, regardless of the identity of the particular proteins involved.

There are dozens of components of the vitreous, and the functions of many remain unknown (Chapter 1). A number of these components have been proposed as potential network stabilizers or crosslinks (Chapter 1) but, to our knowledge, there is no literature regarding how such a crosslink might be joined to collagen or HA. Incomplete information on the many potentially-significant species makes a "bottom-up" approach prohibitive, because it requires isolating and fully identifying all of the network components first, and then determining their functions within the network. For identifying a pharmacological vitrectomy agent, the bottom-up approach is inefficient because many of the components may not play significant structural roles.

We present a "top-down" approach to vitrectomy agent discovery organized by the main types of interactions that stabilize the nanostructure of biological tissues. We first determine the relative importance of specific covalent bonds (within collagen and HA), hydrogen bonds, electrostatic interactions, and hydrophobic interactions. These experiments yield direct suggestions for pharmacological vitrectomy agents by revealing the nature of the chemistry that must be disrupted. The most promising therapeutic approach identified in these experiments is explored further *in vitro* and *in vivo* in the following sections.

Covalent Bonding – Hyaluronidase cleaves the native high molecular-weight HA chains into smaller fragments that diffuse out of the vitreous more readily, causing up to a 60% reduction in vitreous mass (~ 10% reduction occurs without treatment) (Figure 2). This level of mass reduction is not seen after one hour because it takes several hours for the enzyme to cleave a significant portion of the chains into small pieces. The hyaluronidase effect is saturated with 100 units of enzyme: 1,000 units provided no additional mass loss. Thus, no quantity of hyaluronidase will cause global network collapse. As previously mentioned, hyaluronidase does not weaken vitreoretinal adhesion; therefore, HA-induced contraction could endanger the retina.

Collagenase enzyme treatment had a much more dramatic effect (data not shown): 1000 units of collagenase enzyme fully liquefied the vitreous, leaving no detectable residual solid in the bath solution. Collagenase was the only treatment to completely liquefy the vitreous. This result was anticipated based upon the structure of the vitreous and the literature cited above. As stated previously, however, enzymatic digestion of collagen is not a satisfactory pharmacological vitrectomy approach because it attacks all collagen-rich tissues and membranes.

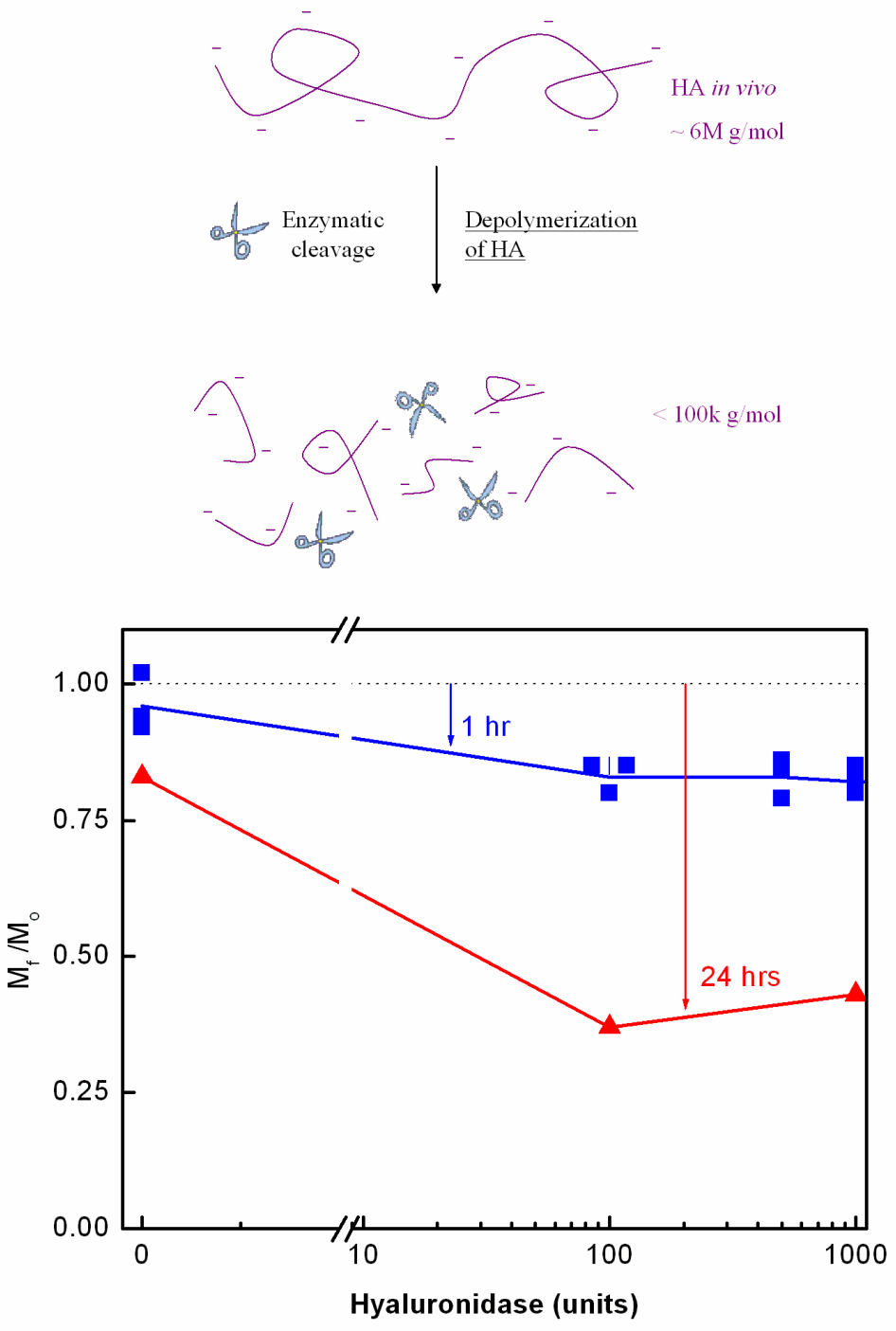

Figure 2. Hyaluronidase enzyme reduces the molecular weight of hyaluronic acid by random chain scission, which causes the vitreous to shrink but not collapse

Hydrogen Bonding (Urea and Guanidinium HCl) – Moderate concentrations of urea (1 – 4 M) cause the vitreous to lose ~ 50% of its mass after 24 hour but a sharp transition occurs at concentrations ≥ 5 M urea. At or above 5 M concentrations the vitreous totally and irreversibly collapses to a small opaque pellet of protein (> 98% of mass is lost). 6 M Guanidinium HCl yielded the same result as high concentrations of urea (data not shown).

We propose that in the vitreous the most important aspect of these well-known chaotropic agents is their ability to disrupt intermolecular hydrogen bonds. Specifically, intermolecular hydrogen bonds between network components and intrafibrillar hydrogen bonds within collagen type II. Hirano, et al. have also shown that urea is capable of disrupting hydrogen bonds that form between HA molecules in solution,[13] although the question of whether or not hydrogen bonds link HA molecules *in vivo* is still a topic of active debate.[14] Our emphasis on hydrogen bonds is generally consistent with the accepted view of chaotropic agents;[15] however, the precise mechanism by which they denature proteins remains unclear[15, 16] and appears to also involve hydrophobic effects.[17, 18] We have examined the effects of hydrophobic interactions separately using surfactant solutions (see *Hydrophobic Interactions* below). Contrast between the effects of the chaotropics and the effects of the surfactant allow us to distinguish between hydrophobic attractions and hydrogen bonding. Disrupting hydrophobic interactions may contribute to the effects of urea; however, we will demonstrate that they do not play a dominant role.

Regarding the kinetics of the effect: one hour is not sufficient time for urea or guanidinium to totally collapse the vitreous even at high concentrations, although significant size reduction was obvious after just a few hours. Given that urea and guanidinium are both small molecules capable of rapid diffusion and that H-bond disruption also proceeds rapidly (within minutes), the rate-limiting step in vitreous collapse appears to be the diffusion of large molecules out of the collagen network. This is consistent with the concept that H-bond disruption frees bound structural components but does not destroy them.

The proteinacious pellet that remains after vitreous collapse is composed primarily of collagen fibrils: they are stable against the chemical treatments listed in Table 1 hyaluronidase digestion but easily dissolved with collagenase. Collagen fibrils swell in high concentrations of urea due to the fact that the fibrils assemble initially by H-bonding.[19] However, the fibrils are reinforced with covalent crosslinks, and it is these crosslinks that maintain fibril integrity in high concentrations of urea.

An interesting qualitative observation is that the pellet retains the shape of the vitreous, but in miniature form. Analogous to a tiny balloon that has been deflated the vitreous pellet can, like a balloon, easily be stretched with forceps. Unlike a balloon, however, once the vitreous collapses it cannot be inflated again. Even when placed in saline or pure water over night, the pellet does not expand. Collapse appears to be total ejection of hydrophilic species; therefore, when the tissue is immersed in aqueous solutions, there is no longer a driving force for water to enter. To our knowledge, this is the first direct evidence that H-bonding is crucial to the architecture of the vitreous (Figure 3).

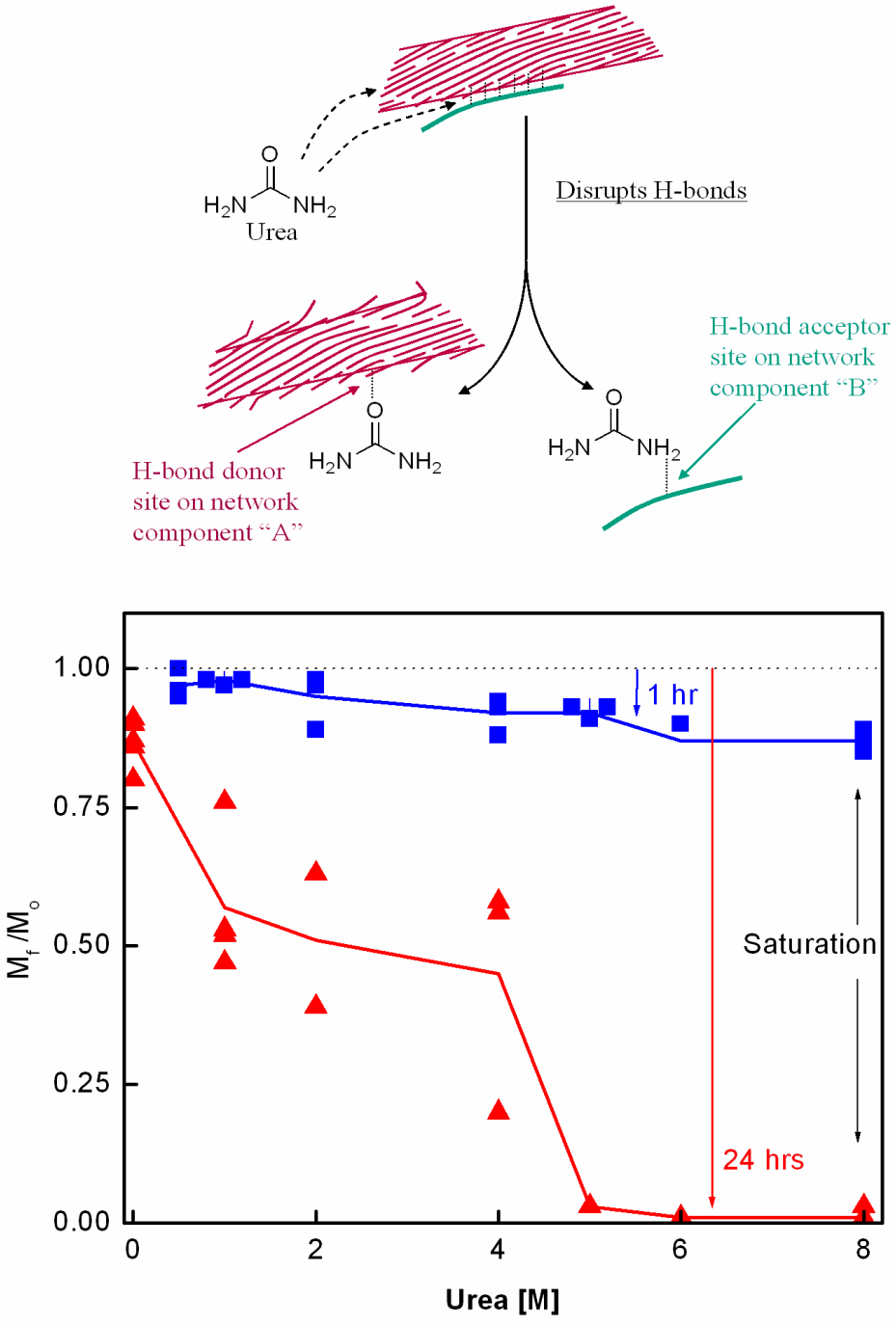

Figure 3. Incubation in high concentrations of urea causes totall vitreous collapse at long times but have little effect after one hour. There is also an intermediate concentration range [1 - 4 M] which causes a 50% collapse, while concentrations below 1 M have little effect even after 24 hours.

Electrostatics and H-bonding (effects of pH) – 10 mM citrate buffer rapidly causes catastrophic collapse of the vitreous below pH 4, such that after 1 hour 60% of the mass has been lost and after 24 hours only a small, opaque pellet of protein is left (> 97% mass loss). At neutral pH the structure of the vitreous is stable in 10 mM citrate and 10 mM phosphate buffers, but at very high pH (phosphate buffer) the structure of the vitreous is again destabilized.

It is unlikely that covalent bond scission is responsible for the monotonic, nearly-linear mass loss trend observed under moderately acidic conditions (pH 6.0 and 4.5). Harshly acidic solutions are capable of hydrolyzing glycosidic and peptide bonds;[20, 21] however proteins are normally heated in 6 N HCl to achieve peptide bond cleavage.[15] Hyaluronic acid has recently been shown to degrade in acidic buffer solutions,[14] but our hyaluronidase experiments show that glycosidic bond cleavage cannot cause total vitreous collapse. We attribute the impact of mildly acidic buffers to the protonation of the carboxylic acid moieties of aspartic acid, glutamic acid, and hyaluronic acid.

Protonating the carboxylic acid moieties listed above will impact the network by changing the charge profile of HA (pKa = 3.2) and some peptide residues and altering the hydrogen bonding scheme of the newly protonated species.[22] As pH falls, HA approaches its isoelectric point of 2.5 at which the number of negatively charged acid groups matches the number of positively charged amines. Very near the isoelectric point, HA has an attractive intramolecular potential corresponding well with the sharp drop in mass seen for the 1 hour incubations.[14, 22] Our observation of total vitreous collapse in this pH range is consistent with a view of HA contracting (Figure 4, schematic).

In addition to the drastic changes in HA, changes in pH may also induce significant changes in protein-protein binding. Specific interactions between collagen fibrils and other proteins and proteoglycans presumably rely on a combination of hydrogen bonding, hydrophobic effects, and electrostatics. As the amino acids that mediate these interactions become protonated, binding sites may lose functionality. One likely example is the carboxylic acid moiety of Asp and Glu: when these residues are protonated, the hydroxyl oxygen becomes a potential H-bond donor, loses its capacity for electrostatic interactions, and the amino acid becomes less hydrophilic.

Unlike acidic solutions, alkaline solutions have little effect on the vitreous until the pH is so high that peptide bond cleavage by deamidation[21] may be significant (Figure 4). Although HA does not undergo rapid chain scission at pH 12.5, solutions of HA show chain contraction and a drop in viscosity at such high pH.[14, 22] Therefore, a combination of protein degradation and HA conformational change may contribute to vitreous collapse under strongly alkaline conditions.

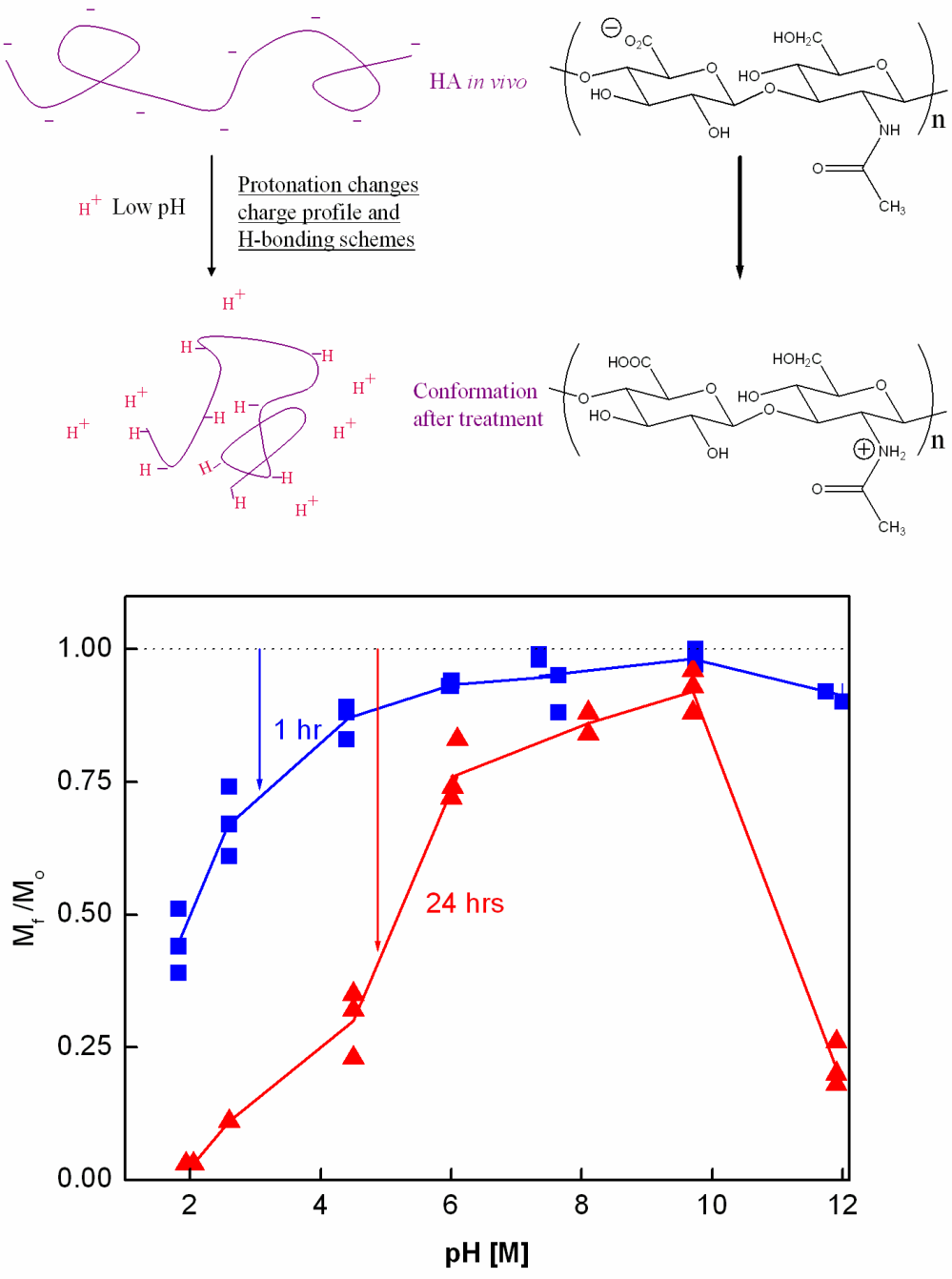

Figure 4. The stability of the vitreous is very sensitive to pH. The vitreous has maximum stability at physiological pH, as expected, but degenerates quickly below pH 6 and above 10.

Electrostatic Interactions Isolated (*NaCl and $MgCl_2$)* – Increasing salt concentration screens electrostatic interactions and shifts the Donnan equilibrium of polyelectrolytes toward higher polymer concentration. Addition of a monovalent salt, here sodium chloride, produces a moderate, dose-dependent mass loss for 24 hour incubations, but essentially no effect after 1 hour (Figure 5). The effect of added salt is relatively mild: even at the solubility limit of NaCl (~ 5 M at pH ~ 7), the vitreous retains half its weight after 24 hours. Protein-protein interactions may not be significantly disrupted, since the polyelectrolyte effect of HA can explain the observed mass loss.

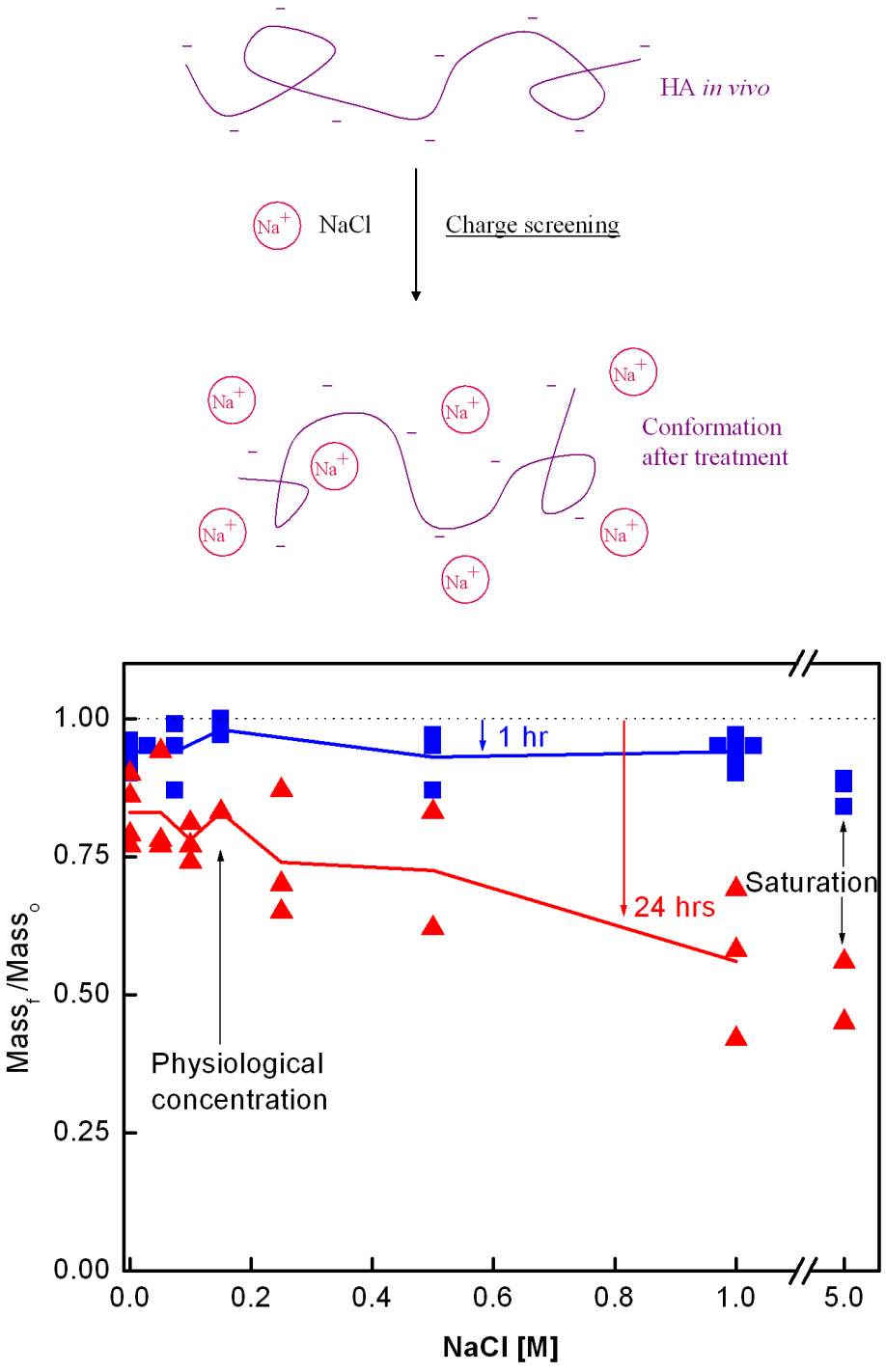

Figure 5. Vitreous soaked in NaCl loses mass in a dose- and time-dependent fashion. Salts screen bound charge, decreasing electrostatic repulsion and attractions.

It is well known that divalent cations cause polyanions to contract. In the case of the vitreous, adding $MgCl_2$ does produce a greater mass loss than NaCl, consistent with the hypothesis that HA contraction plays a major role (Figure 6).

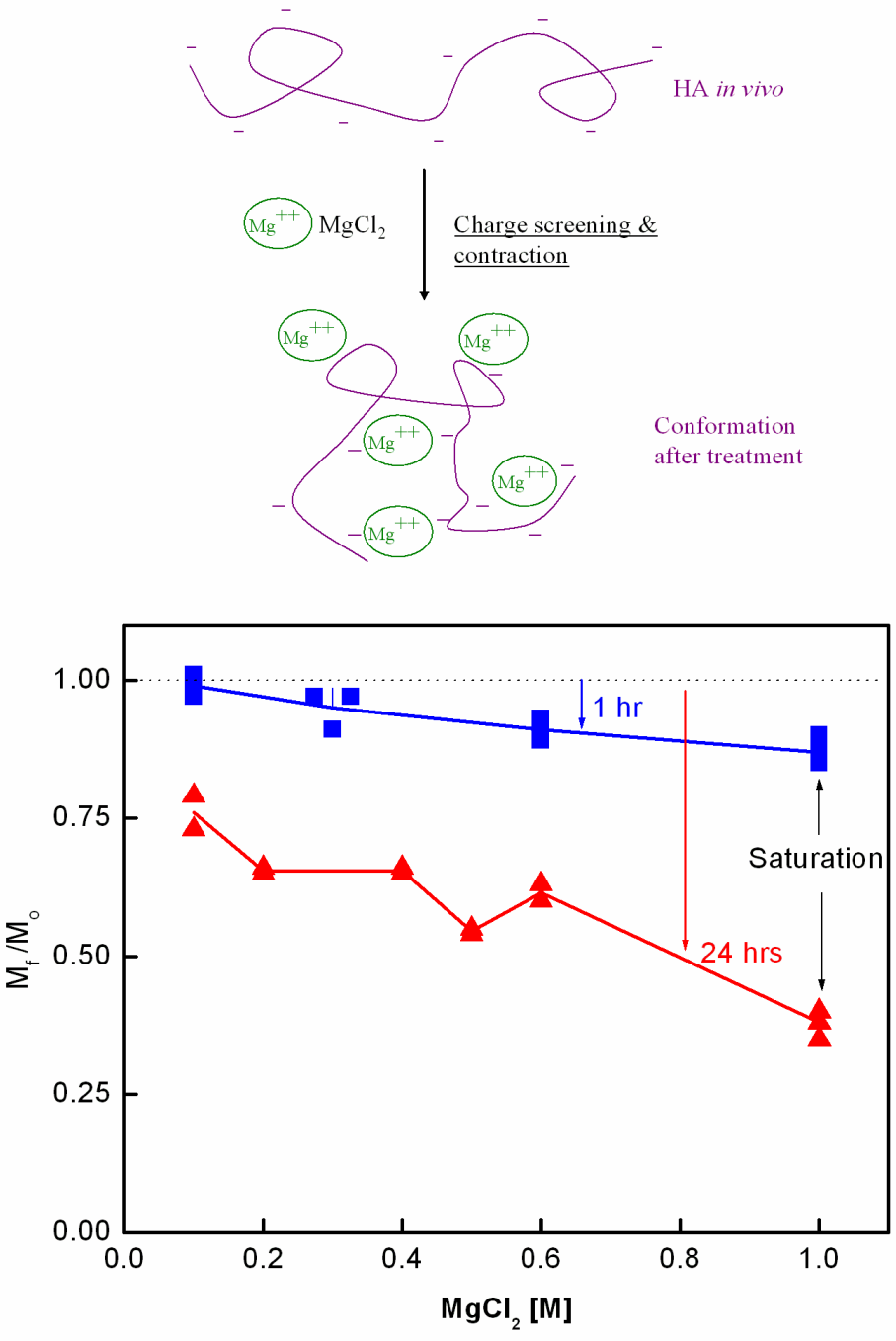

Figure 6. Vitreous soaked in $MgCl_2$ loses mass in a dose- and time-dependent fashion. The mass loss is significantly more than for NaCl solutions of much higher concentrations, apparently an effect of higher valency of the cation on HA.

Hydrophobic Interactions (*Triton® X-100)* – Triton® X-100 induces moderate weight loss at very high concentrations, but the effect is the smallest of all the treatments measured. Triton® X-100 is a non-ionic surfactant typically used to solubilize membrane proteins at 1-5 mM concentrations. We see that, while very large concentrations of Triton® tend to destabilize the network, standard concentrations have only a moderate effect even after 24 hours (Figure 7). Hydrophobic interactions apparently do little to stabilize the structure of the vitreous.

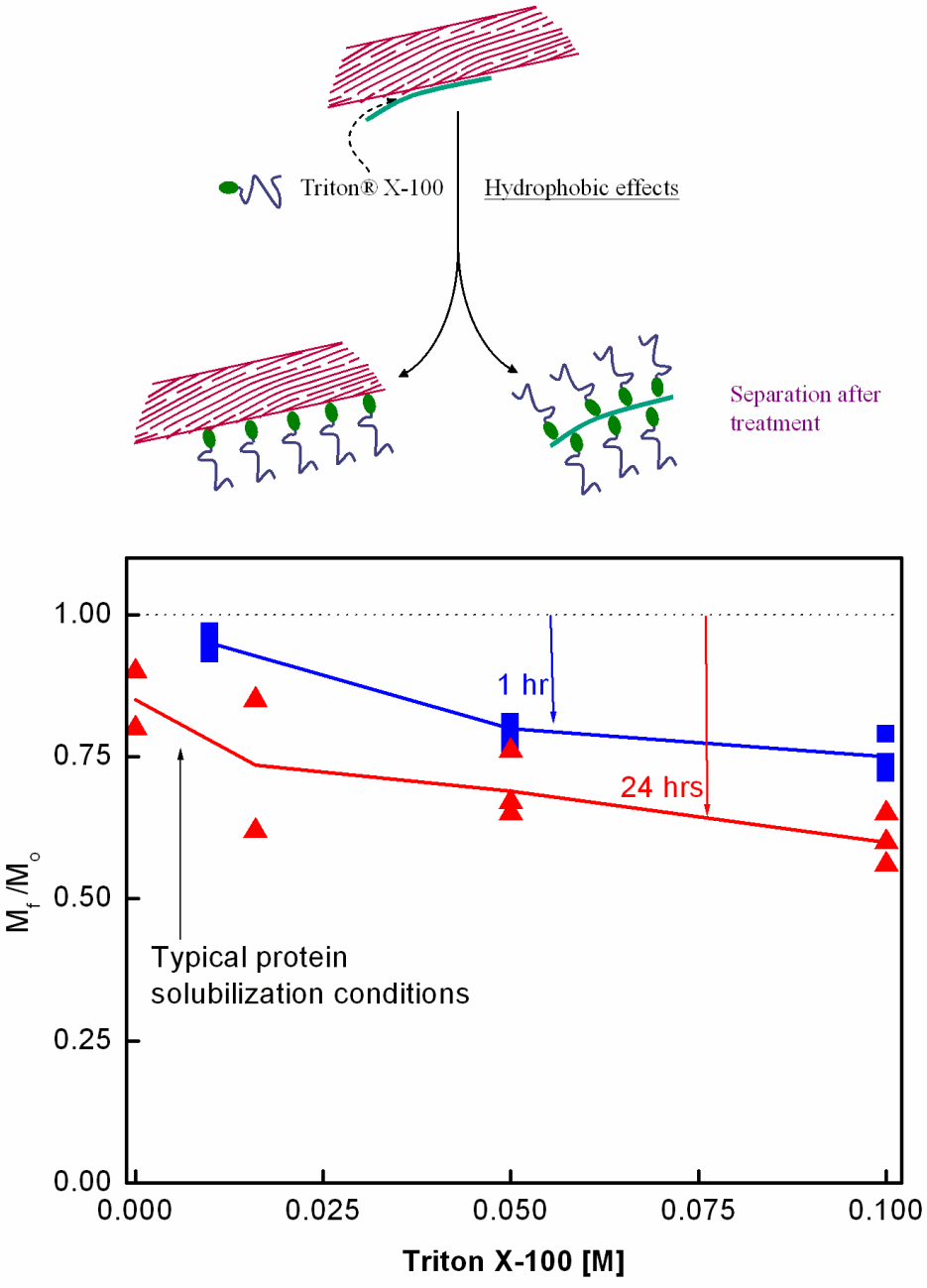

Figure 7. Concentrations of Triton® X-100 normally used in laboratory settings had almost no effect on the stability of the vitreous. Moderate, dose-dependence mass loss is apparent at higher concentrations.

4.4 Targeted Vitreous Engineering and Rheology

Urea and low pH were the only nonenzymatic bath treatments to fully collapse the vitreous; therefore, we proceeded by exploring the therapeutic potential of low-pH urea solutions in an *in vitro* porcine eye model. As mentioned previously, Vitreoretinal Technologies, Inc. has observed a clinical benefit to intravitreal urea injections prior to vitrectomy in the form of reduced surgical time and improved retinal reattachment.[11, 23, 24] In safety studies conducted prior to clinical trials, they observed that injecting 100 μl of up to 12% urea into the vitreous of rabbit eyes showed no adverse reactions and that urea concentrations up to 24% elicited only mild, transient retinal inflammation. In collaboration with Vitreoretinal Technologies, we have found that injections of 24% urea elicited no adverse response in porcine eyes. Using these findings as guidelines for therapeutic doses, we have examined experimental injections to a maximum of 100 μl of 24% urea, although it is likely that higher concentrations would be safe for clinical use. Adult human eyes have an internal volume of ~ 5 ml;[25] therefore, a 100 μl bolus of urea is rapidly diluted ~ 1/50. The volume of a human vitreous is approximately x1.5 larger than porcine and x3 larger than rabbit vitreous. Thus, the effective retinal exposure in an adult human (~ 0.5% for a 24% injection) is significantly lower than that of a rabbit (~ 1.5% for the same injection).

When we injected porcine vitreous specimens with 100 μl of 6% urea or less (pH 5 - 6), and incubated in a 10ml saline bath at 37˚ C for 24 hours, no softening was observed (Figure 8). However, increasing the concentration to 24% caused a discernible drop in modulus and narrowing of the relative standard deviation. The decrease in deviation is not symmetric: the relatively-consistent minimum modulus remains unchanged, while the

maximum moduli are significantly reduced. The change in *average* modulus is ~ 35% (from 9.3 to 6.1 Pa); in contrast, the relative modulus above the base line (G'_{bl}) decreases ~ 60%, from G'_{avg} - G'_{bl} = 3.8 to 1.6 Pa, based on G'_{bl} = 4.5 Pa computed from minimum modulus values in Figures 8 and 9.

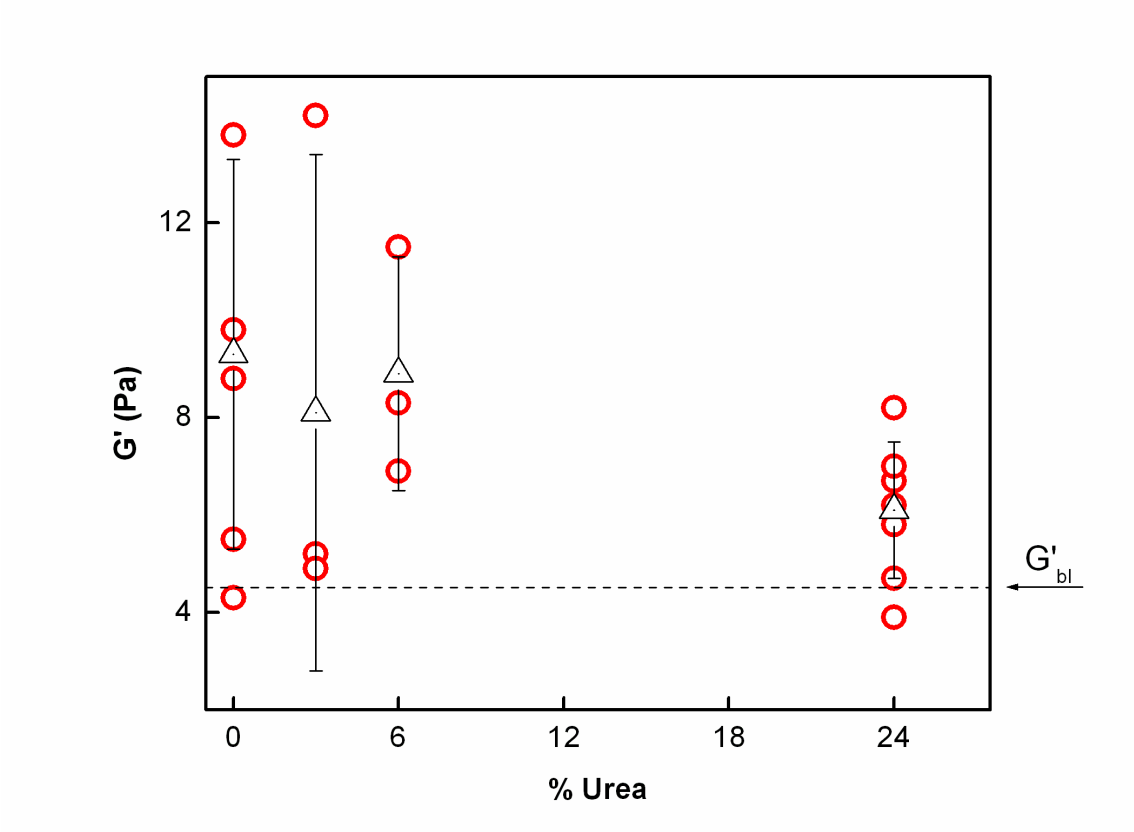

Figure 8. Fresh porcine vitreous specimens were injected with 100 µl of a urea solution (0, 3, 6, or 24% urea in 0.9% saline) and placed in 10 ml of saline to incubate at 37° C. Each circle represents the initial storage modulus of a porcine vitreous immediately after it was removed from the incubator. G'_{bl} (dashed line) indicates the apparent minimum or baseline modulus of porcine vitreous.

The high relative standard deviation (~ 50% for saline-treated controls) appears to be due to sample-to-sample variability. Porcine eyes are not delivered as matched pairs and sample-

sample difference are some times obvious even under visual inspection. Due to the delicate nature of the network, the age of the animal (3 – 6 months), previous head trauma, dietary factors, and even genetic differences may alter its structure. These effects would be compounded by any additional variability in handling (enucleation, transportation, and dissection).

We speculate that G'_{bl} represents the properties of a vitreous network in which only covalent network junctions are intact, i.e., the underlying, crosslinked collagen network. Higher modulus values may reflect added structure and connectivity due to physical associations among proteins that may increase the rigidity of the collagen network or noncovalent interactions that link the network to HA. In that case, the variability in modulus would reflect the differing degrees of residual noncollagenous structure in each particular sample. This interpretation of sample variability is consistent with rheological measurements of human vitreous that showed great consistency between matched pairs but drastic differences between individuals (see Chapter 3).

Decreasing the pH of the urea solution below neutral also has a marked softening effect (Figure 9). In these experiments the treatment solution pH was varied (2, 6, 8, and 12) at a fixed concentration of 24%. Due to the dilution of the injected solution and the buffering capacity of the vitreous, these changes in the pH of the injected solution only mildly alter the pH of the vitreous (Figure 9, top axis). Vitreous has a powerful buffering effect due to the buffering capacity of the proteins and the carboxylic acid moieties of HA. Thus, it is surprising to find even a moderate pH dependence. Nevertheless, high pH urea solutions are less effective than neutral or acidic ones in reducing the mean modulus and sample-to-

sample variability. One possible explanation is the influence of acids on urea. Urea has been show to sequester protons from acid solutions by forming a cation.[26, 27] It has been argued that the added proton prevents urea degradation and dimerization in aqueous solutions, which may influence the treatment.

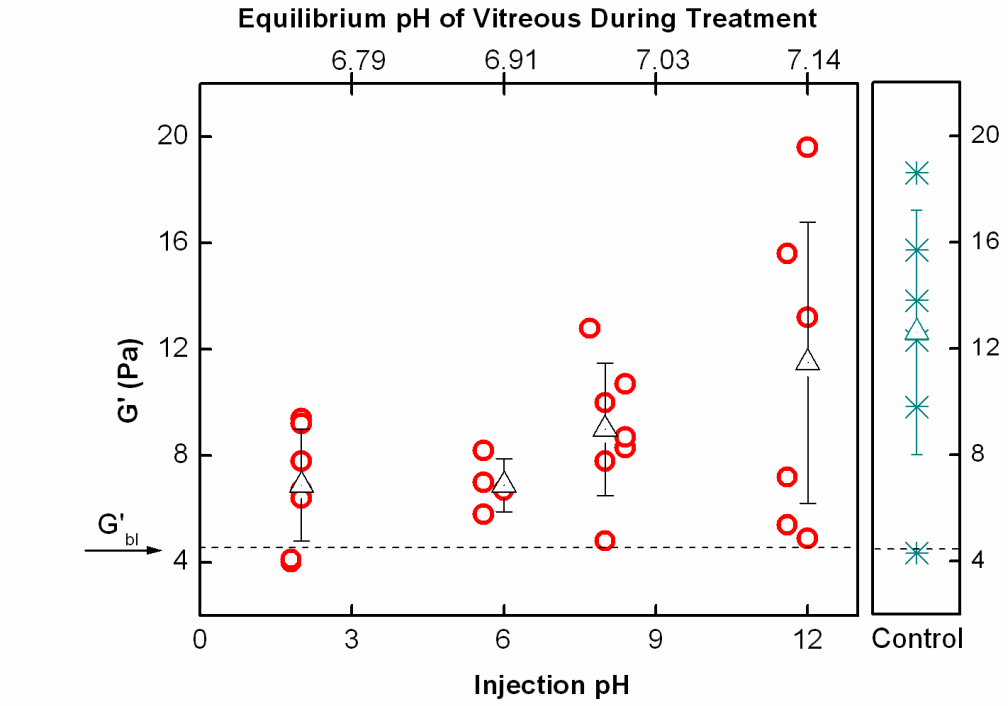

Figure 9. Fresh porcine vitreous specimens were injected with 100 µl of 24% urea solution (pH 2, 6, 8, or 12) and placed in 10 ml of saline to incubate at 37° C. Open circles represent the initial storage modulus of individual porcine vitreous immediately after it is removed from the incubator. Stars represent the modulus of controls injected with 100 µl of isotonic saline at neutral pH. G'_{bl} (dashed line) indicates the apparent minimum or baseline modulus of porcine vitreous. Top axis indicates the actual pH of the vitreous measured after incubation. Note that the pH of the tissue (top axis here) varies over a narrow range relative to the soak tests described in Section 4.2.

While the pH and concentration effects are significant, the modulus reduction in both cases was less dramatic than expected based upon the documented clinical benefits.[23, 24] There are several possible explanations for this discrepancy. First, it is possible that the primary clinical benefit of urea is the induction of PVD rather than a drastic effect on bulk mechanics (this will be discussed further in Section 4.5). A second possibility is that urea destabilizes the vitreous indirectly by increasing the susceptibility of network components to enzymatic degradation. In most vitrectomy cases, the barrier protecting the vitreous from blood and proteases has been compromised. Urea is known to affect the structure of collagen fibrils and permanently alter the ultrastructure of collagenous tissues.[28-30] The structural changes may occur equally *in vivo* and *in vitro*, however *in vivo* proteolytic degradation of the weakened network may have a significant influence over time. It is also possible that the moderate softening effects observed in the lab do reflect the *in vivo* changes in treated vitreous that lead to clinical benefits.

To explore this final possibility, failure stress and strain values from urea-treated vitreous were compared with saline controls and with values from fresh tissues presented in Chapter 3 (Figure 10). As stated in Chapter 3, high stresses are relevant because they develop during vitrectomy as the vitreous is aspirated through the vitrectomy tool tip (an aperture the size of a 22-gauge needle, I.D. ~ 0.4 mm). The failure of vitreous under high stress was measured by shearing the vitreous between cleated plates for 150 seconds at a rate of $\dot{\gamma}$ = 0.1 s^{-1}. Urea treatment did not affect the average failure stress or strain (~ 25 Pa and 450%, respectively). This is consistent with our inference that urea removes network reinforcements but does not have a strong effect on the underlying network; bulk failure

involves straining the network to such an extent that the majority of the bonds are broken. High-strain tests push past the loss of noncovalent interactions and on to a regime dominated by covalent bonds.

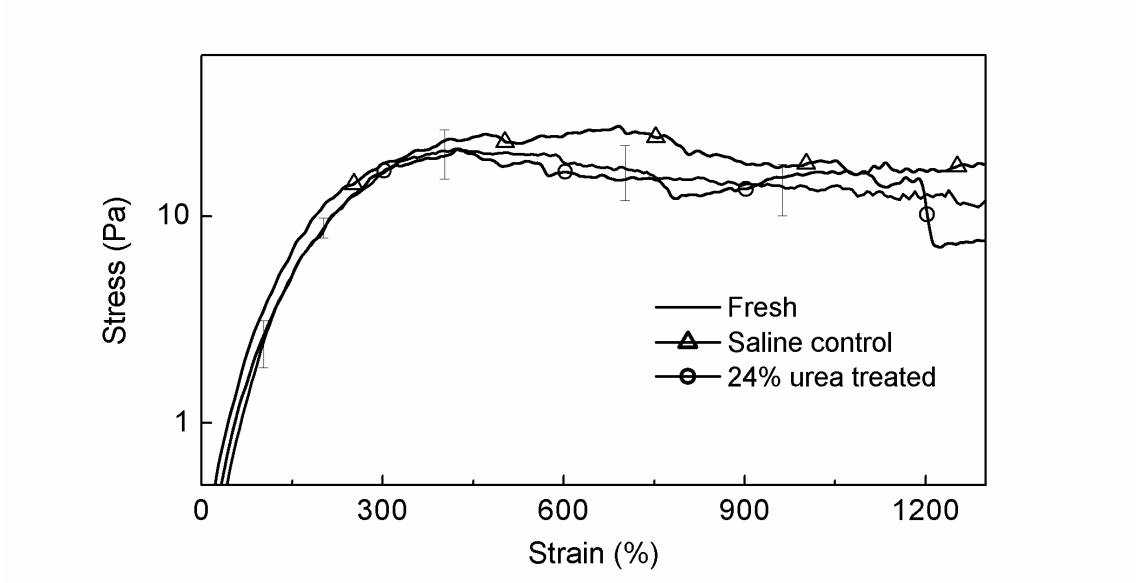

Figure 10. Vitreous treated with 24% urea and incubated for 24 hours fails with the same average stress and strain as saline controls and fresh vitreous ($\dot{\gamma}$ = 0.1 s^{-1}).

4.5 *In Vivo* Exploration of Vitreous Mechanics

Based on the effects of urea treatment *in vitro*, rheological methods were applied to an *in vivo* porcine study with five objectives:

- To quantify vitreous "liquefaction" observations reported by surgeons by measuring the fraction of the vitreous body that is liquid vs. gel and the storage modulus changes induced by treatment with urea

- To have one observer monitor every stage of the therapeutic process, from live medical evaluation through dissection and rheological analysis, to correlate qualitative clinical indicators of liquefaction with rheological measurements
- To reconcile retinal surgeon's reports of vitreous liquefaction *in vivo* with the modest rheological changes observed *in vitro*
- To look for potential intraocular pressure (IOP) changes resulting from treatment
- To look for inflammation or adverse effects on the retina that might accompany treatment with 24% urea

The *in vivo* study clearly demonstrates that 100 μl injections of 12% and 24% urea do not liquefy young, healthy porcine vitreous (Figure 11). Nevertheless, the surgeons *reported* seeing liquefaction in these same eyes. By performing observations side-by-side with surgeons, we learned that the clinical evaluation of liquefaction consists of visualizing the motion of the posterior aspect of vitreous (*post mortem*) using a slit lamp microscope. A vitreous was considered "liquefied" if oscillations of the visible irregularities in the posterior vitreous were out of phase with an oscillatory perturbation induced by shaking the eye with forceps. While out-of-phase motion does indicate inhomogeneity in the vitreous, it also suggests that the vitreous retains elastic character; liquids flow and do not return to their initial positions like the points on the vitreous used by the surgeons to indicate "liquefaction." Therefore, the *in vivo* study reconciled the *in vitro* results with clinical observations and fundamentally changed the way the therapeutic effect of urea is viewed.

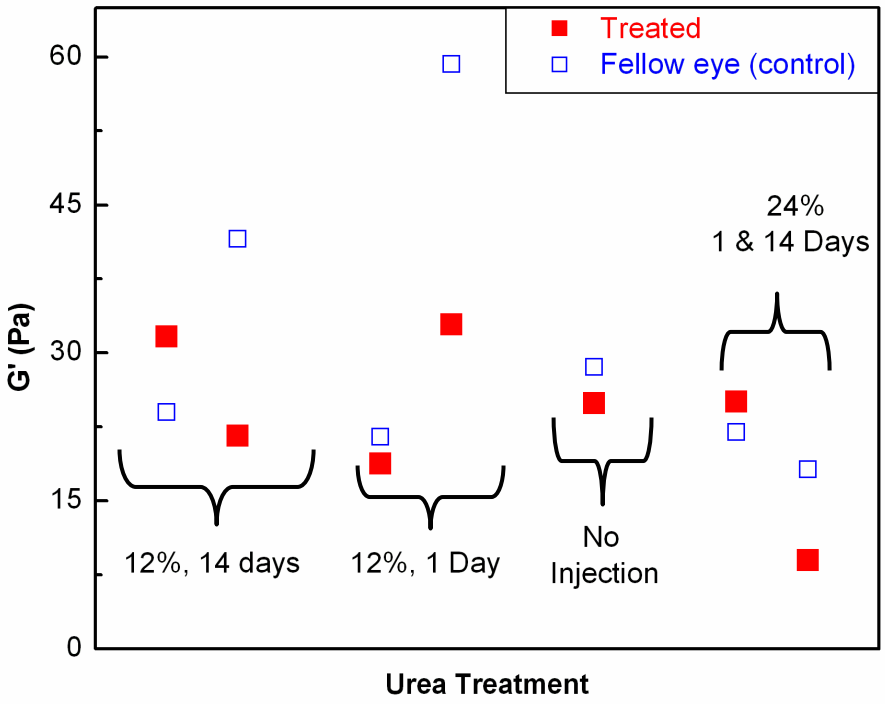

Figure 11. The initial storage modulus of fresh vitreous samples from matched pairs of treated and control eyes is not affected regardless of the treatment. All experiments were conducted at 10 rad/s with 3% strain to avoid damaging the tissue.

Using the slit lamp method described above, out of phase vitreous motion was not observed in either of the eyes treated with 24% urea when examined immediately *post mortem*. It was, however, observed in the vitreous of 2 of the 12%, 14 day treated eyes and 2 of the saline control eyes. The surgeons confirmed that the "vitreous motion" we observed in these specimens was the same as had previously been observed and that these vitreous specimens were liquefied. The eyes were then enucleated and transported individually in phosphate buffered saline (PBS) on ice to the rheological lab of our collaborator, Professor Alberto Tecante at the UNAM, where I performed the mechanical characterization.

The vitreous is not significantly softened *in vivo* by any of the treatments (Figure 11), including eyes that appeared to have "liquefied" by visual examination. Among the four eyes (two treated/fellow pairs) in the 12% urea/14 day group, the standard deviation was 65%, so the observation that the average modulus of the treated eyes was 18% lower than that of the fellow eyes is not significant. Indeed, the modulus of one of the eyes treated with 24% urea for 14 days had a modulus 13% greater than its fellow eye (again, not statistically significant). The 1-day data points in Figure 11 represent measurements on posterior vitreous only, while the full vitreous body was measured in the 14-day experiments. Even analyzing cortical vs. basal vitreous had no apparent effect on modulus.

Further evidence that treatment did not liquefy the vitreous is that treatment did not reduce the gel mass of the vitreous (Figure 12). If any degree of liquefaction had occurred at the vitreoretinal interface, the mass of urea-treated vitreous specimens should have been consistently and measurably reduced compared with their fellow eyes. No such mass reduction was seen regardless of treatment concentration or time. The average mass difference between vitreous bodies of treated and fellow eyes (1 ± 93 mg, n = 10; mass difference ± standard deviation, sample size) was much smaller than the standard deviation of the weight difference.

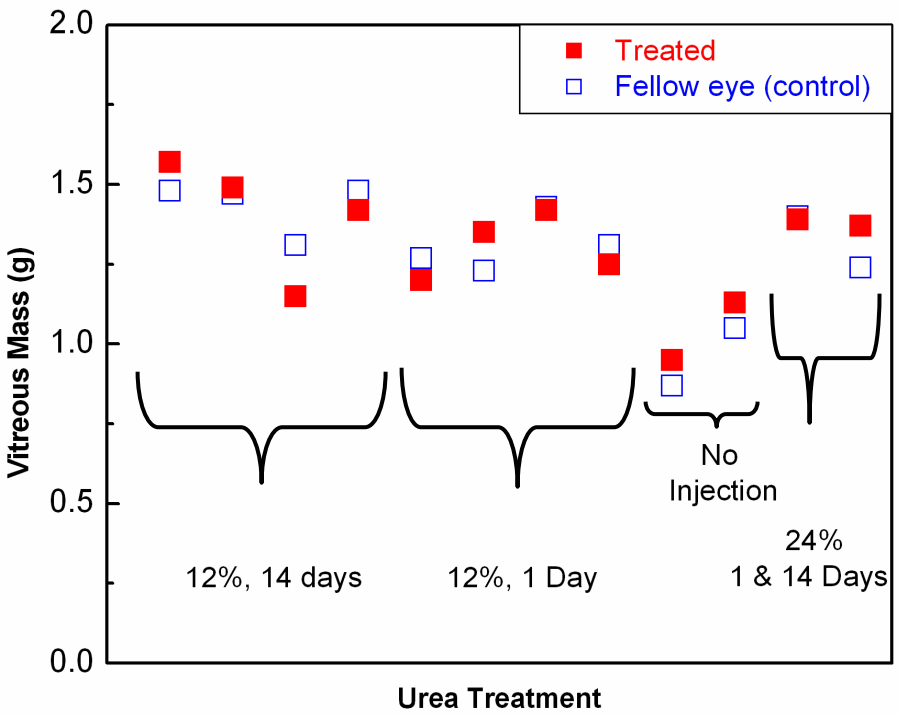

Figure 12. The vitreous of treated eyes do not weigh less than their fellow (control) eye, regardless of the treatment solution or treatment time. This clearly indicates that treatment does not induce vitreous liquefaction.

Apparently, the clinical definition of "liquefaction," prior to quantitative mechanical analysis, actually referred to posterior vitreous detachment rather than significant changes to the bulk properties of the gel. The "specs" visualized at the posterior aspect of the vitreous are probably portions of the peripheral vitreous; release of the posterior vitreous from the retina via detachment allows the protein fibrils to collapse locally and form scattering centers, the same process that produces "floaters" that interfere with human vision. Indeed, we observed during dissection that vitreous was more easily separated from

the retina in urea-treated eyes. The most difficult aspect of vitrectomy is separating the vitreous from the retina. This may explain why surgeons find urea treatment to be helpful and report the perception of liquefaction. We propose that the primary clinical advantage gained from urea treatment is posterior vitreous detachment rather than significant vitreous liquefaction.

In addition to liquefaction studies, the impact of treatment on the general health of the eyes was evaluated by retinal surgeons. Prior to sacrifice, the animals were anesthetized and the IOP of each eye was measured using a Schiotz tonometer. The IOPs of all eyes were normal (Figure 13). The average IOP of treated and control eyes were 15.6 ± 2.0 mm Hg (n=10) and 16.1 ± 2.0 mm Hg (n=10), respectively. Pair wise analysis also shows no significant effect of urea on IOP. The average pair wise IOP difference between treated and control eyes is 4% ± 16%.

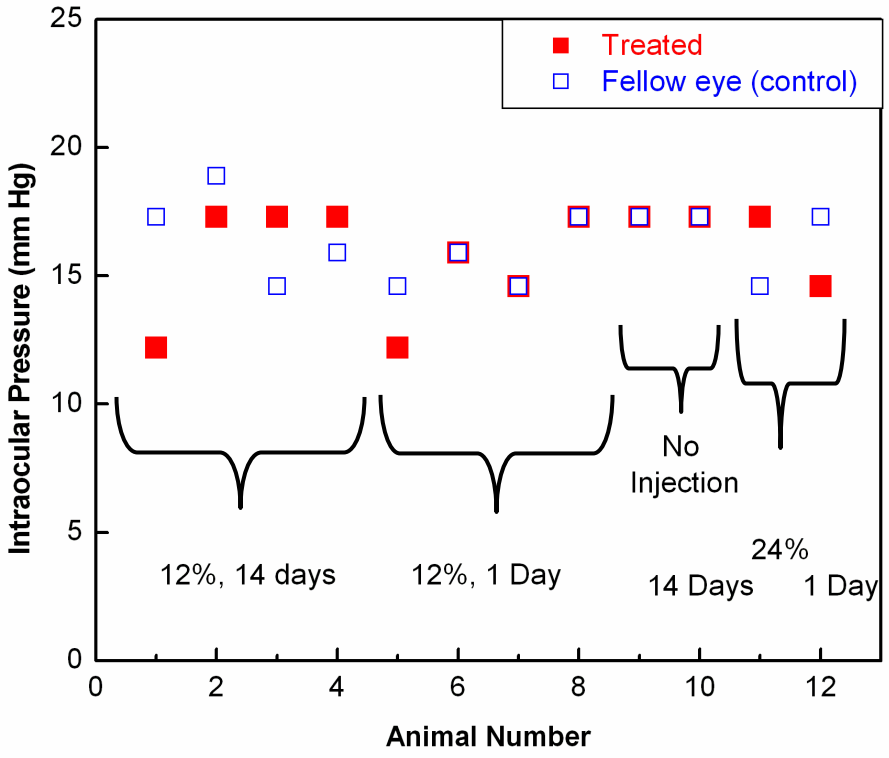

Figure 13. Intraocular pressure, measured with a Schiotz tonometer using a 5.5 g weight, appears to be independent of treatment solution or time. Similar results are obtained with the same instrument and a 10 g weight.

Evaluation by ophthalmoscope demonstrated no adverse reaction or inflammation of the retinas. The tolerance of porcine eyes to an increased dose of urea, relative to rabbit eyes, may be a result of the larger intraocular volume. Cataracts were observed in 3 eyes (2 in treated eyes, 1 in an untreated eye) but they appeared to be unrelated to treatment; the type of cataract observed is common in this species. All eyes were otherwise in good health.

In summary, we have shown that high concentrations of urea and low pH can cause total vitreous collapse *in vitro*. In the case of urea, this is apparently achieved without breaking covalent bonds. Low levels of urea appear to disrupt some component(s) of the vitreous

network without having a significant impact on the strength of the underlying collagen framework. In the course of investigating the therapeutic potential of urea *in vivo* and *in vitro*, we have shown that the clinical benefits of urea for vitrectomy do not rely on changes in bulk mechanical properties and have found evidence that urea destabilizes vitreoretinal adhesion, which could explain its surgical benefit in vitrectomy. We have also shown that therapeutic doses of urea do not negatively impact the health of the porcine retina.

BIBLIOGRAPHY

1. Sebag J. Is pharmacologic vitreolysis brewing? *Retina*. Feb 2002;22(1):1-3.

2. Verstraeten TC, Chapman C, Hartzer M, Winkler BS, Trese MT, Williams GA. Pharmacological Induction Of Posterior Vitreous Detachment In The Rabbit. *Archives Of Ophthalmology*. Jun 1993;111(6):849-854.

3. Hikichi T, Yanagiya N, Kado M, Akiba J, Yoshida A. Posterior vitreous detachment induced by injection of plasmin and sulfur hexafluoride in the rabbit vitreous. *Retina-The Journal Of Retinal And Vitreous Diseases*. 1999;19(1):55-58.

4. Tezel TH, Del Priore LV, Kaplan HJ. Posterior vitreous detachment with dispase. *Retina-The Journal Of Retinal And Vitreous Diseases*. 1998;18(1):7-15.

5. Oneill R, Shea M. Effects Of Bacterial Collagenase In Rabbit Vitreous. *Canadian Journal Of Ophthalmology-Journal Canadien D Ophtalmologie*. 1973;8(2):366-370.

6. Wang FH, Wang ZL, Sun XD, Wang F, Xu X, Zhang X. Safety and efficacy of dispase and plasmin in pharmacologic vitreolysis. *Investigative Ophthalmology & Visual Science*. Sep 2004;45(9):3286-3290.

7. Pirie A. The Effect Of Hyaluronidase Injection On The Vitreous Humour Of The Rabbit. *British Journal Of Ophthalmology*. 1949;33(11):678-684.

8. Sasaki M, Hikichi T, Kado M, Yoshida A. Intravitreal injection of hyaluronidase cannot induce posterior vitreous detachment in the rabbit. *Investigative Ophthalmology & Visual Science*. Mar 15 2000;41(4):S345-S345.

9. Sebag J. *The Vitreous - Structure, Function, and Pathobiology*. New York: Springer-Verlag Inc.; 1989.

10. Oliveira LB, Meyer CH, Kumar J, et al. RGD peptide-assisted vitrectomy to facilitate induction of a posterior vitreous detachment: A new principle in pharmacological vitreolysis. *Current Eye Research*. Dec 2002;25(6):333-340.

11. Personal communication: Vitreoretinal Technologies, Inc.; 2004.

12. Association for Research in Vision and Ophthalmology. http://www.arvo.org/AboutArvo/animalst.asp.

13. Hirano S, Kondo S. Molecular Conformational Transition Of Hyaluronic-Acid In Solution. *Journal Of Biochemistry*. 1973;74(4):861-862.

14. Gatej L, Popa M, Rinaudo M. Role of the pH on hyaluronan behavior in aqueous solution. *Biomacromolecules*. Jan-Feb 2005;6(1):61-67.

15. Stryer L. *Biochemistry*. 4th ed. New York: W. H. Freeman and Co.; 2000.

16. Moelbert S, De Los Rios P. Chaotropic effect and preferential binding in a hydrophobic interaction model. *Journal Of Chemical Physics*. Oct 15 2003;119(15):7988-8001.

17. Bruning W, Holtzer A. Effect Of Urea On Hydrophobic Bonds - Critical Micelle Concentration Of N-Dodecyltrimethylammonium Bromide In Aqueous Solutions Of Urea. *Journal Of The American Chemical Society*. 1961;83(23):4865-&.

18. Kauzmann W. Some Factors In The Interpretation Of Protein Denaturation. *Advances In Protein Chemistry.* 1959;14:1-63.

19. Scott JE, Thomlinson AM. The structure of interfibrillar proteoglycan bridges ('shape modules') in extracellular matrix of fibrous connective tissues and their stability in various chemical environments. *Journal of Anatomy.* Apr 1998;192:391-405.

20. Carey FA. *Organic Chemistry*. 3rd ed. New York: McGraw-Hill; 1996.

21. Tylercross R, Schirch V. Effects Of Amino-Acid-Sequence, Buffers, And Ionic-Strength On The Rate And Mechanism Of Deamidation Of Asparagine Residues In Small Peptides. *Journal Of Biological Chemistry.* Nov 25 1991;266(33):22549-22556.

22. Cowman MK, Matsuoka S. Experimental approaches to hyaluronan structure. *Carbohydrate Research.* Apr 11 2005;340(5):791-809.

23. Karageozian HL. Determine the safety and efficacy of Vitreosolve administered intravitreally to induce a complete posterior vitreous detachment (PVD) in non proliferative diabetic retinopathy human subjects. *Investigative Ophthalmology & Visual Science.* 2005;46.

24. Ochoa-Contreras D, Romero-Castro RM, Rivera-Sempertegui JO, Karageozian V, Karageozian H, Quiroz-Mercado H. Anatomical and visual outcome of retinal detachment surgery in children with intravitreal carbamide previous a vitrectomy surgical procedure. *Investigative Ophthalmology & Visual Science.* May 2003;44:U94-U94.

25. Oyster CW. *The Human Eye: Structure and Function*. Sunderland, MA: Sinauer Associates, Inc.; 1999.

26. Dasgupta PK, Moulik SP. Interaction Of Urea With Weak Acids And Water. *Journal Of Physical Chemistry.* Oct 22 1987;91(22):5826-5832.

27. Shaw WHR, Bordeaux JJ. The Decomposition Of Urea In Aqueous Media. *Journal Of The American Chemical Society.* 1955;77(18):4729-4733.

28. Bittorf SV, Williams EC, Mosher DF. Alteration Of Vitronectin - Characterization Of Changes Induced By Treatment With Urea. *Journal Of Biological Chemistry.* Nov 25 1993;268(33):24838-24846.

29. Kischer CW, Droegemueller W, Shetlar M, Chvapil M, Vining J. Ultrastructural-Changes In The Architecture Of Collagen In The Human Cervix Treated With Urea. *American Journal Of Pathology.* 1980;99(3):525-537.

30. Neumark T, Toth G, Marot I. Alterations Of Collagen Structure After Urea Treatment. *Acta Histochemica.* 1967;28(1):1-&.

C h a p t e r 5

STIFFENING THE CORNEA: THE THERAPEUTIC POTENTIAL OF GLYCATION

5.1 Introduction

Whereas the goal of our vitreous efforts was liquefaction, our therapeutic objective in the cornea is fortification. The primary purpose of fortification is the treatment of keratoconus, a disease in which the cornea softens and subsequently bows under the influence of intraocular pressure (as explained in Chapter 1). Here, we present the biochemical modifications and concomitant mechanical reinforcement that result from treating corneal tissue with glyceraldehyde (GA), a reducing sugar known to crosslink proteins through a complex series of reactions known as the Maillard reaction.[1]

The Maillard reaction, initially characterized as the browning of proteins treated with reducing sugars, results in the non-enzymatic glycosylation (glycation) of amino acids with primary amine groups, particularly lysine and arginine. Over the past two decades, some intermediates and advanced glycation end products (AGEs) of these reactions have been

characterized,[2-14] including cross-linking structures[2-6, 13, 14] that may be responsible for the increased tissue stiffness and decreased protein solubility also characteristic of glycation.[15-18]

While glycation has primarily been explored because of its apparent connection with health problems[19-23] associated with diabetes[16, 24] and aging,[25, 26] if properly harnessed this nonenzymatic crosslinking method has potential therapeutic and tissue engineering applications.[27-29] By imparting strength to weakened connective tissue such as diseased corneas, glycation may provide an alternative to tissue transplants in diseases such as keratoconus. Glycation may also be a helpful tool for adding mechanical strength to protein-based and polyamide synthetic tissues.

Understanding glycation-induced stiffening and quantitative indicators thereof is necessary for understanding the pathology of natural glycation and for utilizing its positive potential. However, a quantitative correlation between the formation of specific AGEs and physiologically-significant tissue stiffening has not previously been established. Furthermore, previous studies on the biomechanical influences of glycation have employed methods based upon tissue failure, which do not demonstrate whether the stiffening effects of glycation are significant under physiological stresses.[26]

In the present work, rotational rheometry has been used in combination with analytical biochemistry to explore the therapeutic potential of GA for treating keratoconus. GA is an appealing glycating agent for tissue engineering because of its relatively high reactivity and low toxicity.[30] Small amplitude oscillatory shear stresses have been applied to probe the

mechanical response of porcine corneas to physiologically relevant stresses, which do not destroy the nanostructure of the tissue. We have correlated the rise in shear modulus of porcine corneas with the levels of one non-cross-linking and two cross-linking AGEs (Figure 1).[9, 14] We have also examined the stabilizing effect of glycation against enzymatic degradation. Finally, solid-state NMR of the treated corneas and solution NMR of their lysates are compared to investigate the merits of enzymatic digestion versus acid hydrolysis for AGE isolation.

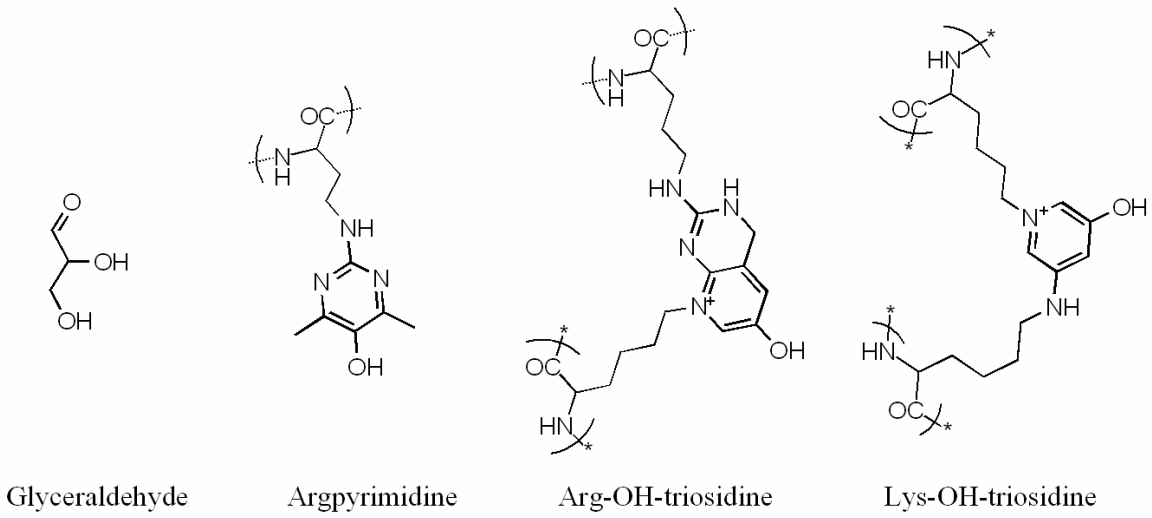

Figure 1. The structure of glyceraldehyde and three of its AGEs

5.2 Materials and Methods

Materials – Fresh porcine eyes (< 36 hours *post mortem*, stored at 5° C in physiological saline prior to arrival) were acquired through Sierra for Medical Science (Santa Fe Springs, CA). All pigs were 3 – 6 month old Chester Whites, weighing 50 – 100 kg and in good

health at the time of slaughter. 99% [U-^{13}C]glyceraldehyde was obtained from Cambridge Isotope Laboratories Inc. (Andover, MA). Argpyrimidine, Arg-hydroxy-triosidine, and Lys-hydroxy-triosidine were synthesized and purified as described previously.[14] All other enzymes and reagents were purchased from Sigma Chemical Co. (St. Louis, MO).

Cornea sample preparation – Corneas were excised from fresh porcine eyes. An 8.0 mm circular section was cut from the center of each using a trephine from Jedmed Instrument Co. (St. Louis, MO), washed in metal-free 200 mM phosphate buffer solution pH 7.4 (PBS), and weighed (typical wet weight = 60 mg). The epithelium of each sample was removed and corneas were either characterized directly to obtain "native" rheological and biochemical properties or treated according to the following regimen: 30 μl of either PBS, 1% (weight of dry GA / weight of solution) GA in PBS (0.3 mg GA), or 2% GA in PBS (0.6 mg GA) was applied topically. In all cases, 1 μl each of toluene and chloroform were added per ml treatment solution to prevent bacterial growth. Corneas were incubated in sealed tubes at 37° C for 2 or 6 days and rheological and/or biochemical measurements were made immediately thereafter; at least 6 repetitions of each treatment were made.

Rheology – Oscillatory shear modulus measurements under controlled stress were made using AR2000 and SR5000 stress-controlled rheometers from TA Instruments (New Castle, DE). The anterior and posterior surfaces of corneas were gently dried by contact with an absorbent pad (< 3% weight change as noted in Chapter 2) and immediately loaded on 8 mm parallel disc fixtures at 25° C. The dynamic moduli were found to be highly sensitive to hydration levels; therefore, a solvent trap and well were used to prevent

evaporation and hydrate the air within the sample chamber. To obtain mechanical properties representative of physiologically relevant stresses, measurements were performed using small oscillatory shear stresses (σ = 5 Pa). After the rheological data were collected, the corneas were used either for solid-state ^{13}C-NMR, digested for HPLC, protein content analyses, fluorescence spectroscopy, and solution state ^{13}C-NMR, or acid hydrolyzed for HPLC.

Solid-state NMR – Digestion was not necessary to prepare samples for solid-state NMR. To remove ^{13}C-bearing compounds not covalently bound, corneas were washed in 200 mM phosphate buffer solution pH 7.4 and lyophilized for analysis. In each experiment, 6 treated corneas were packed into a 7 mm ZrO_2 rotor and spun (rate = 4.0 kHz) at the magic angle. ^{13}C Solid-state NMR direct polarization (Bloch decay) spectra of lyophilized cornea samples were obtained using a Bruker 200 DSX spectrometer (Brucker BioSpin Corp., MA). The probe was doubly tuned for ^{1}H and ^{13}C observation at frequencies of 200.1 MHz and 50.3 MHz, respectively. 8,000 scans were acquired in each measurement with a 20 second delay time between scans. All solid-state NMR experiments were conducted by Dr. Sonjong Hwang (Caltech SSNMR facility manager) and Dr. Giyoong Tae (former Kornfield group member).

Enzymatic Digestion – The greater the extent of glycation, the more difficult it is to solubilize the cornea. To do so with minimal change to the chemical structures of the pendant adducts and crosslinks, an enzymatic digestion protocol was used rather than acid hydrolysis. Acid hydrolysis completely hydrolyzes peptide bonds.[31] However, it also destroys some amino acids (e.g. tryptophan) and AGEs. To access acid-labile AGEs, we

employ a gentle, enzymatic method for solublizing cornea proteins via sequential incubation in collagenase, pronase E, and proteinase K. Glycated corneas were gently agitated for 24 hours at 37° C in these three complimentary proteinases in succession. 2% (weight dry enzyme / wet weight of cornea) collagenase A in 100 mM HEPES buffer solution, pH 7, and 5 mM calcium chloride was used for the first digestion. 1 μl each of toluene and chloroform were added per ml digestion solution to prevent bacterial growth as with the treatment solutions. After the 24 hour incubation period, the cornea mixture was centrifuged to pellet insoluble cornea fragments and the supernatant was collected for protein content and NMR analyses. The supernatant was replaced with a 2% pronase E solution in 100 mM HEPES buffer, pH 7.5, and 5 mM calcium chloride and again agitated for 24 hours at 37° C. After the pronase E incubation, the cornea mixture was again centrifuged to pellet residual cornea fragments, and the supernatant was collect. A third solution, containing 2% proteinase K in 100 mM Tris buffer, pH 8.0, and 5 mM calcium chloride was added for the final incubation. After 24 hours in the proteinase K solution, the supernatant was collected and the final pellet was rinsed in PBS and then dried for acid hydrolysis. The bovine serum albumin (BSA)-equivalent protein content of each lysate solution was determined by absorbance measurements at 210 nm; the respective enzyme solutions were used as blanks.

No organic buffers (e.g., HEPES or TRIS) were used in the enzymatic digests for solution-state NMR because it was found that the naturally abundant ^{13}C in the buffer mask the adduct signals. Phosphate buffer could not be used because it would chelate calcium ions needed for enzymatic activity. Solution-state NMR digestions were conducted in 0.9%

saline, pH 7.4 – 7.6. To compensate for the likely reduction in enzyme activity due to deviation from optimal pH late in the incubation periods, the concentration of $CaCl_2$ added to collagenase and proteinase K solutions was increase from 5 to 10 mM.

Acid Hydrolysis – Insoluble protein aggregates from the enzymatic digest were dissolved by acid hydrolysis in 0.5 ml of 6 N HCl for 16 hours at 110° C for analysis. Nine untreated corneas and two sets of six glycated corneas were also hydrolyzed under the same conditions in 2 ml of 6 N HCl. After hydrolysis, the acid was evaporated and samples were reconstituted in water. Leucine-equivalent amino acids were measured by the ninhydrin assay to determine protein content.

Glycation Product Identification and Quantification by High Performance Liquid Chromatography (HPLC) – A Waters HPLC system including an in-line degasser, 600 controller, 717 autosampler, 996 photodiode array detector, 474 scanning fluorescence detector (monitored at 380 nm with an excitation wavelength of 325 nm), and Millennium software (Waters corporation, MA) were used. Each sample was filtered with a Costar Spin-X 0.45 μm cellulose acetate filter (Corning Incorporated, NY) prior to injection into the HPLC system. Separations were made on a 250 x 4.6 mm Discovery C18 column, 3 μm (Supelco, PA), protected by a 20 x 4.0 mm Supelguard Discovery C18 column, 5 μm. Peak collection was performed using a FRAC-100 fraction collector (Amersham Pharmacia Biotech, Sweden). Adduct quantification was achieved by method of external standard, where chromatogram peak area by fluorescence detection was used to quantify adducts formed as described in detail by Tessier, et al.[14] HPLC analyses were conducted

with Dr. Tessier (former Kornfield group member) and results appeared in the aforementioned reference.

Solution NMR – After digestion each cornea solution was concentrated using a Speed Vac Plus SC110A (Savant Inc., NY). The concentrated fractions were pooled and dissolved in 700 μl of 99% D_2O for ^{13}C-NMR analysis. The samples were transferred to 5 mm glass NMR tubes (Kontes glass company, NJ). ^{13}C solution NMR spectra of digested cornea solutions were taken on a Varian 500 MHz spectrometer at 25° C (Varian Inc., CA). For quantitative analysis, the proton decoupling was turned off during excitation and a 20-second delay time was used. Acetonitrile was added to each NMR sample as a standard.

Spectrometry – Fluorescence spectra of the protein digest solutions of each cornea were recorded with a Photon Technology International spectrofluorometer (Photon Technology International, NJ). Individual adducts were prepared for fluorescence measurements by purifying, concentrating, and redissolving each in pure water as described by Tessier, et al.[14] UV-Visible absorbance measurements for ninhydrin protein content analyses were recorded with a Beckman DU 640 spectrophotometer (Beckman Instruments Inc., CA).

5.3 Mechanical Properties of Glycated Corneas

The shear modulus of corneal tissue increased upon treatment with GA in a dose-dependent fashion (Figure 2). Relative to the mean modulus of corneal buttons incubated in phosphate buffer (457 ± 142 Pa, n = 7), the mean modulus of corneas treated with 1% GA (1359 ± 372 Pa, n = 6) and 2% GA (2862 ± 467 Pa, n = 8) increased by 300% ($P < 0.0001$) and

600% ($P < 0.0001$), respectively, after 2 days. Rheological properties at day 6 of incubation (2904 ± 349 Pa, n = 5) did not change significantly from day 2.

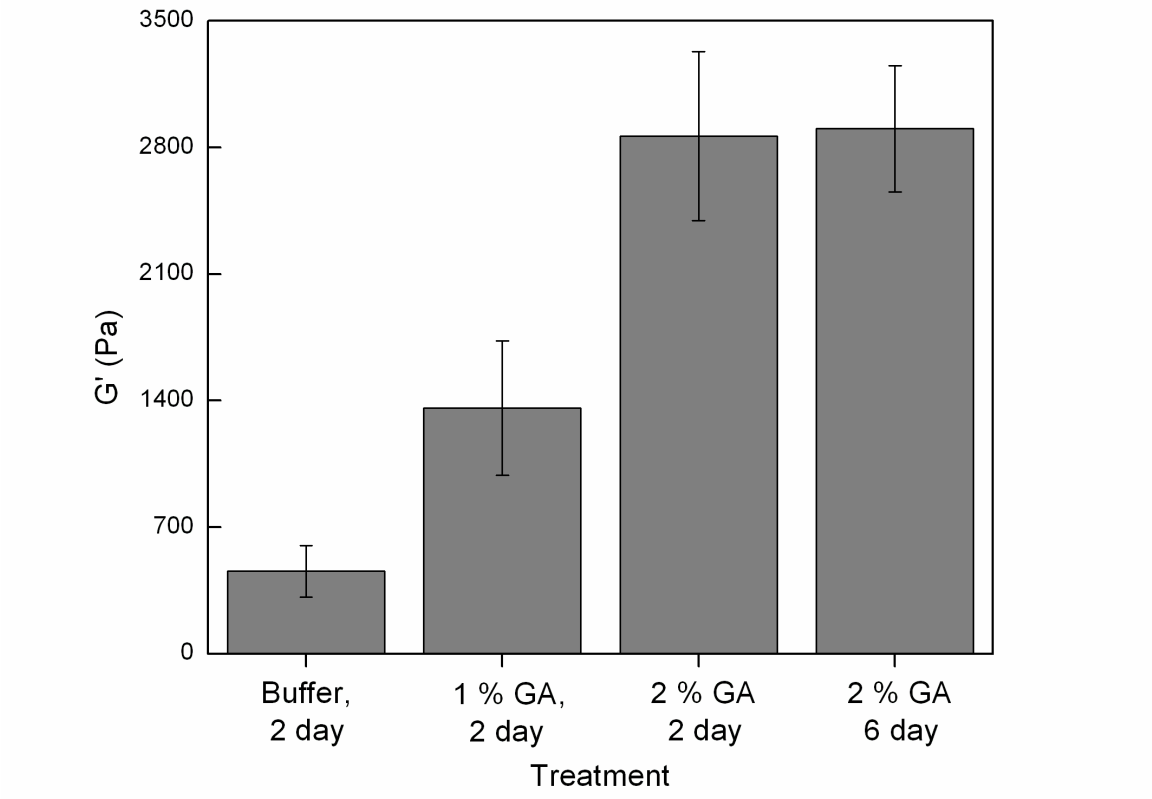

Figure 2. Modulus increases with treatment. Stiffening goes to completion within 2 days; additional incubation time yields no change.

Prior literature indicates that the level of mechanical reinforcement obtained with application of 2% GA is more than sufficient to stabilize the keratoconus cornea. Using a protein crosslinking strategy that involves topical application of riboflavin and UV irradiation, Wollensak et al. showed that stiffening keratoconus corneas by ~ 350% was sufficient to stop coning for at least three years.[32, 33] They also showed that porcine corneas,

which are x1.5 thicker (850 μm vs. 550 μm), stiffened by only 80% when subject to the same level of treatment. Using this ratio (80% stiffening in porcine cornea is equivalent to 350% stiffening in human tissue) as a guide, we anticipate that treating human corneas with significantly less than 1% GA, which stiffened *porcine* corneas by 300%, would be sufficient to stop the progression of keratoconus.

GA treatment may offer advantages over riboflavin treatment: UV irradiation is not required, reducing the likelihood of keratocyte apoptosis[34] and cataracts[35], and we observed that GA-treated corneas yellow much less than corneas treated with riboflavin/UV irradiation. Having demonstrated that glycation with GA can produce therapeutically significant improvement in the mechanical properties of the cornea, we proceed to analyze its biochemical impact.

5.4 Resistance to Proteolytic Degradation

The most significant biochemical benefit to treating keratoconus by glycation may be the increased resistance to enzymatic digestion. The cornea is composed of 78% water, 15% collagen type I fibrils, 5% other proteins, 0.7% keratin sulfates, 0.3% chondroitin sulfates, and 1% salts.[36] It has been proposed that the softening associated with keratoconus is the result of abnormally high protease activity against collagen.[37-40] A number of enzymes are over expressed in keratoconus corneas, including acid esterase, acid phosphatase, and matrix metalloproteinases 2 and 9.[40-42] Glycation decreases the susceptibility of collagenous tissues to proteolytic degradation.[43] Thus, in addition to its mechanical

benefits, the proposed GA treatment may also arrest the pathologic mechanism behind mechanical destabilization.

Our results confirm that glycation of the cornea with therapeutic doses of GA has a protective effect against collagenase. Corneas glycated with 2% GA are approximately 1/10 as susceptible to collagenase solubilization as buffer-treated controls, though pronase appears to work relatively efficiently even after treatment (Figure 3). Glycation reduces the total fraction of protein solubilized after exposure to all three enzymes from > 90% to ~ 50%, but by far the bulk of that reduction is in the collagenase incubation. This suggests that the unglycated collagen helices in treated corneas are preferentially solubilized, which would leave the insoluble fragments with a disproportionately high fraction of AGEs. HPLC analysis corroborates this conclusion: only trace amounts of the AGEs triosidine and argpyrimidine were detected in the soluble portion of the enzymatic lysates, whereas HPLC analysis of the precipitate (solubilized by subsequent acid hydrolysis) showed substantial amounts of these acid-stable adducts. The inability to solubilize heavily-glycated proteins using gentle methods that preserve acid-labile AGEs was the primary motivation for analyzing native samples using solid-state NMR.

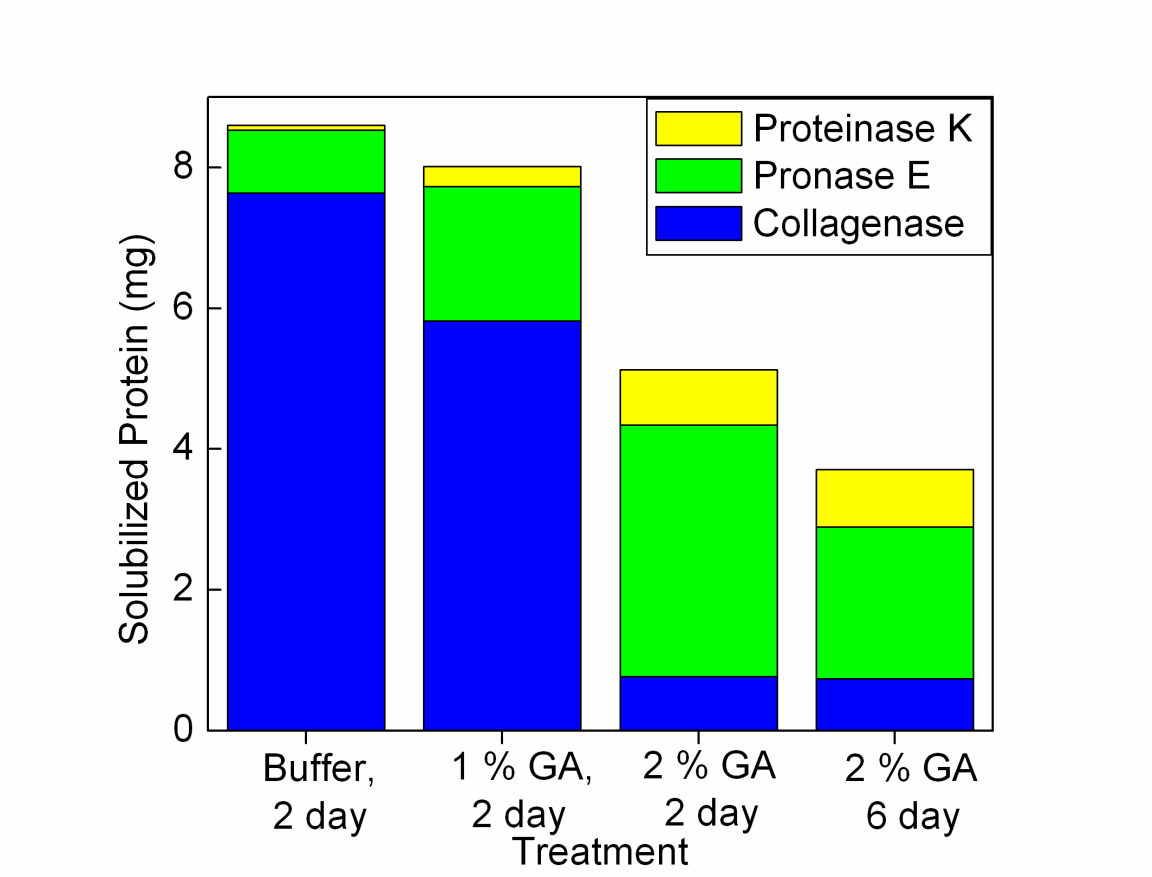

Figure 3. Glycated corneas resist enzymatic digestion. AGEs are likely to partition with the insoluble fraction; thus, concentrations of AGEs in enzymatic lysates do not necessarily represent concentrations in the intact tissue.

5.5 Quantification of Specific AGEs

As mentioned above, HPLC analysis of cornea lysates allowed us to isolate and quantify three known, acid-stable glyceraldehyde AGEs. Because enzymatic digestion proved ineffective for quantitative solubilization of cornea AGEs, acid hydrolysates were used. The total protein contents of all cornea hydrolysates were measured using the Ninhydrin method. Acid-labile AGEs are lost in this process, but arg-hydroxy-tiosidine, lys-hydroxy-triosidine, and argpyrimidine are quantitative markers of the extent of glycation: the level

of all three adducts increased upon treatment with GA (Figure 4). Neither arg-hydroxy-triosidine nor argpyrimidine were found in the acid hydrolysate solutions of the control corneas, and less than 400 pmol / mg total protein (358 ± 273 pmol / mg protein, n = 5) of lys-hydroxy-triosidine were found. The 2-day rise in all three adducts was dose-dependent (lys-OH-triosidine: 1% GA – 1427 ± 89, 2% – 2515 ± 575; arg-OH-triosidine: 1% GA – 129 ± 31, 2% – 206 ± 45; argpyrimidine: 1% GA – 2547 ± 236, 2% – 6011 ± 1085, n = 5 in all cases) but, like rheological properties, adduct levels did not change significantly from day 2 to day 6 (for 2% GA – lys-OH-triosidine, day 6: 2189 ± 98; arg-OH-triosidine, day 6: 312 ± 42; argpyrimidine, day 6: 5779 ± 631). Previous biochemical analyses in our labs have shown that additional AGEs will form with application of additional GA;[14] therefore, the lack of additional AGE formation from day 2 to day 6 indicates that all available GA reacts within two days— not that the cornea is saturated with AGEs.

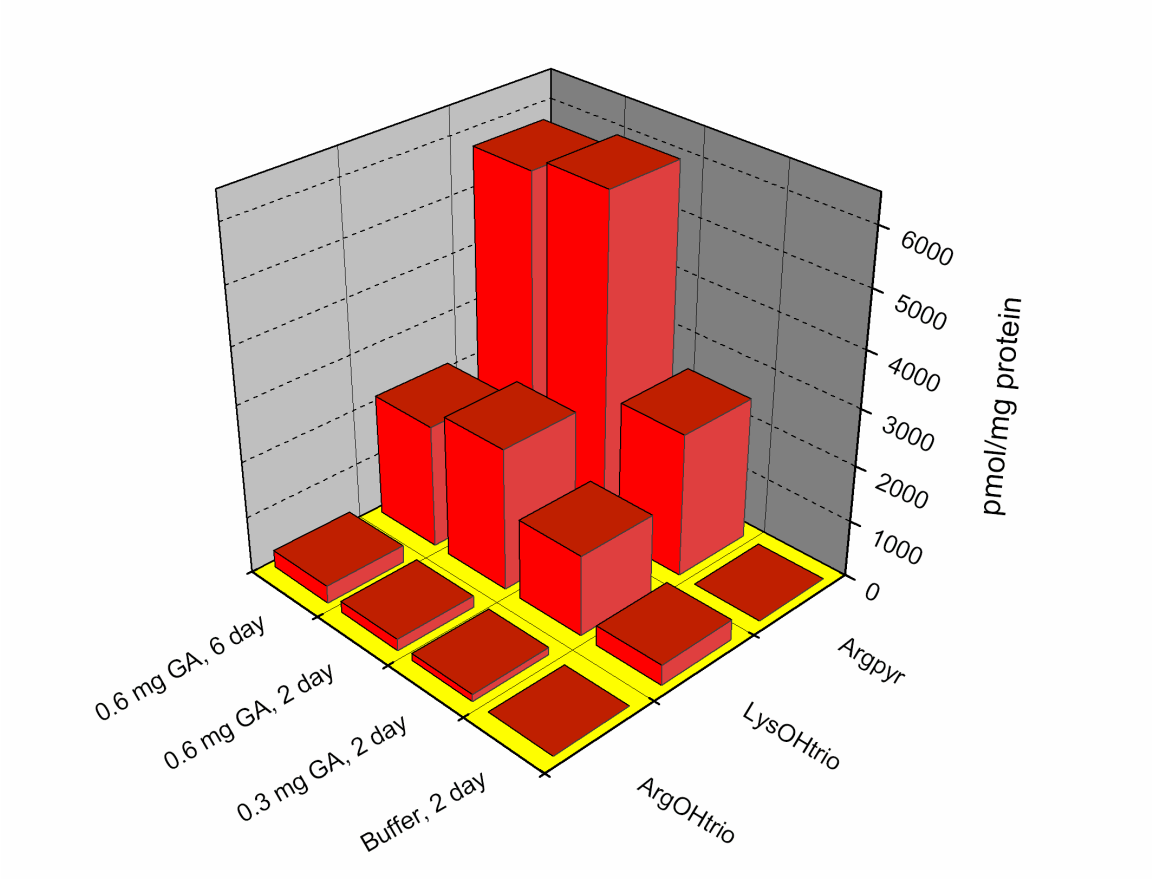

Figure 4. Three known glyceraldehyde AGEs were found in treated corneas. Levels of all three adducts rose in a dose-dependent fashion, with argpyrimidine rising fastest, followed by lys-OH-triosidine and arg-OH-triosidine. Glycation appears to be complete after 2 days; additional incubation did not increase the levels of any of the three AGEs treated with 0.6 mg of GA.

Additionally, a strong linear relationship between AGE formation and shear modulus is apparent (Figure 5). Note that the intercept of the lys-OH-triosidine fit is different from the other two because it was the only AGE detected in control corneas. The diagnostic significance of this correlation will be explored in Section 5.7, where we will show that global tissue fluorescence can also be directly correlated with AGE formation and mechanical property changes.

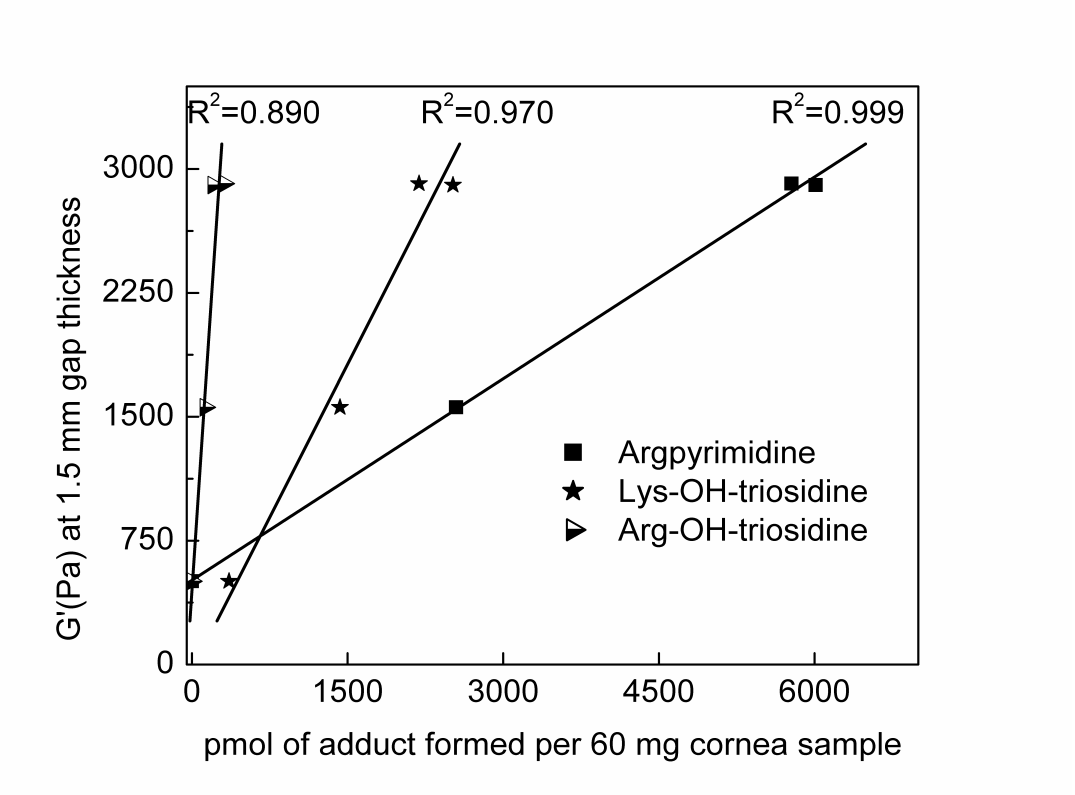

Figure 5. Shear modulus (G') of 60 mg cornea samples as a function of the quantity of three AGEs. After treatment and mechanical analysis, argpyrimidine, lys-hydroxy-triosidine, and arg-hydroxy-triosidine were quantified after 2 days in the control cornea, after 2 days using the 1% and 2% solutions, and after 6 days using the 2% solution. Modulus values and AGE content are nearly identical at 2 and 6 days, indicating that the tissue had been stabilized by glycation in two days or less. The R^2 values for the best-fit lines of each adduct showed a high degree of linearity.

5.6 Solution and Solid-State NMR of Glycated Corneas

To investigate acid-labile AGEs in treated corneas, we have employed NMR analysis of tissue treated with isotopically labeled glyceraldehyde. Quantitative solid-state ^{13}C-NMR was used to investigate *in situ* the nature of the major non-native resonances detectable in glycated corneal tissue and to compare with solution NMR difference spectra of enzymatically digested and acid hydrolyzed tissue; control spectra have been subtracted from all three (Figure 6). The signals from ~ 75 - 85 ppm and from ~ 185 – 200 ppm

disappeared upon acid hydrolysis, but have counterparts in the solution-state ^{13}C NMR of the enzymatic lysate, suggesting they represent acid labile compounds.

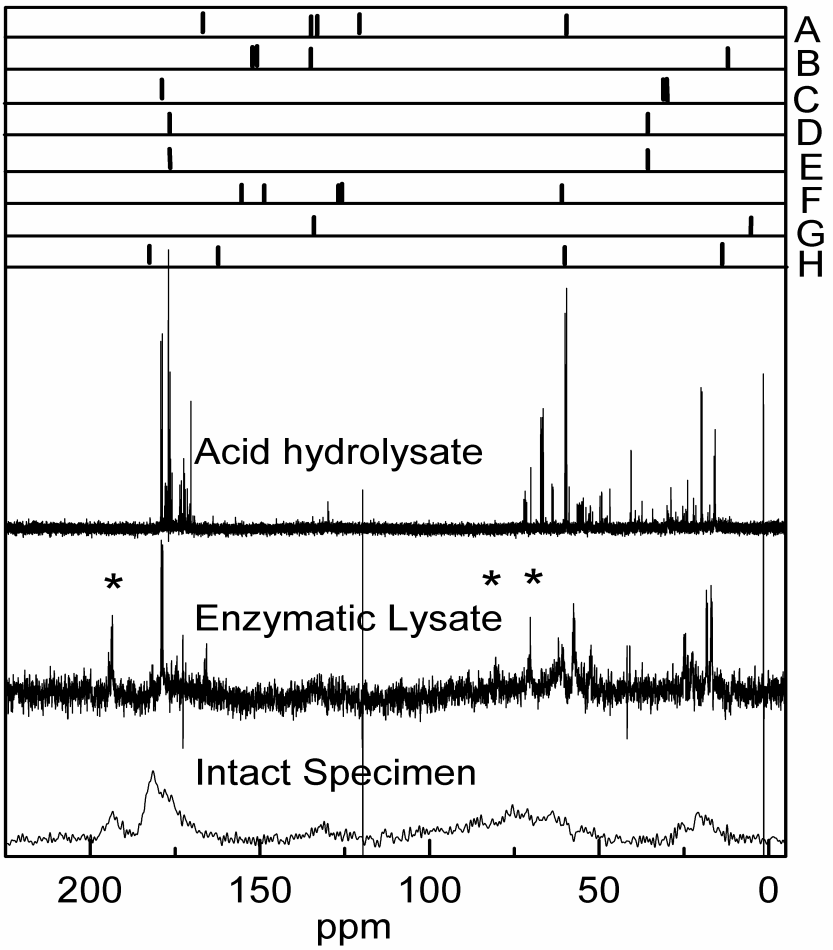

Figure 6. The solid-state 200 MHz 13C NMR spectrum of lyophilized, glycated porcine corneas ("intact specimen") compared with the 500 MHz solution NMR spectrum of equivalent corneas that have been dissolved by enzymatic digestion and by acid hydrolysis. Acetonitrile was used as a reference (120 ppm and 1.5 pmm). For reference, literature values of the chemical shifts of the known GA mediated AGEs are indicated above the spectra: A = arg-OH-triosidine, B = argpyrimidine, C = carboxy-ethyl-lysine (CEL), D = carboxy-methyl-arginine (CMA), E = carboxy-methyl-lysine (CML), F =lys-OH-triosidine, G = methylglyoxal-lysine dimer (MOLD), H = methylglyoxal-derived-imidazoline-cross-link (MODIC). Novel signals not attributable to known AGEs are indicated with asterisks (*).

Resonances in Figure 6 are consistent with the published chemical shifts of CML, CEL, MOLD, CMA, and arg-OH-triosidine.[3, 7, 8, 11, 14] Resonances consistent with MODIC appear in solid-state and enzymatic-lysate spectra, but not in the acid hydrolysate.[13] Argpyrimidine and lys-OH-triosidine appear to be less significant.[9, 14] Because HPLC data showed that arg-OH-triosidine is present at lower concentrations than either argpyrimidine or lys-OH-triosidine (Figure 4), the lack of strong resonances from these two species suggests that resonances consistent with arg-OH-triosidine actually come from other species.

In addition to all expected AGEs, including acid labile adducts, the spectrum of the enzymatic lysate shows new, currently unexplained signals at 70, 81, and 193 – 195 ppm, as indicated by asterisks (Figure 6). These appear to be unsolved AGE structures that are inaccessible when using acid hydrolysis. As explained above, enzymatic lysates contain low concentrations of AGEs and additional losses due to precipitation were observed when lysate solutions were resuspended in D_2O. Thus, the signal:noise ratio is too low to provide reliable data alone. However, similarities in the enzymatic lysate and solid-state spectra indicate that enzymatic digestion is a high-fidelity, albeit low yield method of sampling AGEs from tissue.

Finally, despite decades of AGE research, this experimental approach, combining NMR techniques and HPLC, is the first to gain a perspective on the fraction of all the glycation-induced modifications that are represented by specific AGEs in tissue specimens. Agrpyrimidine illustrates the utility of this perspective. The symmetric ring carbons to which methyl groups are attached have a chemical shift of 150.3 ppm.[9] They originate in

GA and are ^{13}C labeled; however, the 150.3 ppm peak is indistinguishable from the baseline in all three NMR spectra (Figure 6). Thus, the most abundant of the three adducts quantified in the present work contributes almost nothing to the observed NMR spectra. Comparing the chemical shifts of other known AGEs to the observed spectra reveals that known adducts can only account for a small fraction all AGEs. The AGE literature continues to expand rapidly and we hope that this accounting technique will be a useful tool for measuring our progress toward a more complete understanding of glycation. As we find ways to selectively inhibit or induce specific cross-links and examine the resulting tissue properties, solution and solid-state NMR used in tandem with rheology may also be invaluable for exploring the molecular basis of glycation-induced tissue stiffening.

5.7 Fluorescence – Noninvasive Indicator of Glycation

The contribution of these three AGE fluorophores to the total fluorescence of the glycated corneas was found to account for at least 75% (90%, with 15% uncertainty) of the fluorescence at the global fluorescence emission maximum of the lysate solution (Figure 7). The global fluorescence excitation and emission maxima of enzymatically digested corneas treated with 2% GA for 2 days were 334 nm and 399 nm respectively. The "observed" spectrum shown is the difference spectrum of a treated cornea lysate minus the spectrum of a control cornea lysate (Figure 7). To estimate the fluorescence contribution due to the known AGEs, each of the three pure AGE solutions was excited at 334 nm and the emission spectrum was recorded, scaled to the mean concentration at which that adduct was found in the cornea, and added ("estimated" spectrum, Figure 7). Some discrepancy between the estimated and observed spectra is not surprising; we only account for the

contribution of three AGEs. Parallel experiments conducted using acid hydrolyzed corneas rather than enzymatically digested tissue yielded similar results (data not shown).

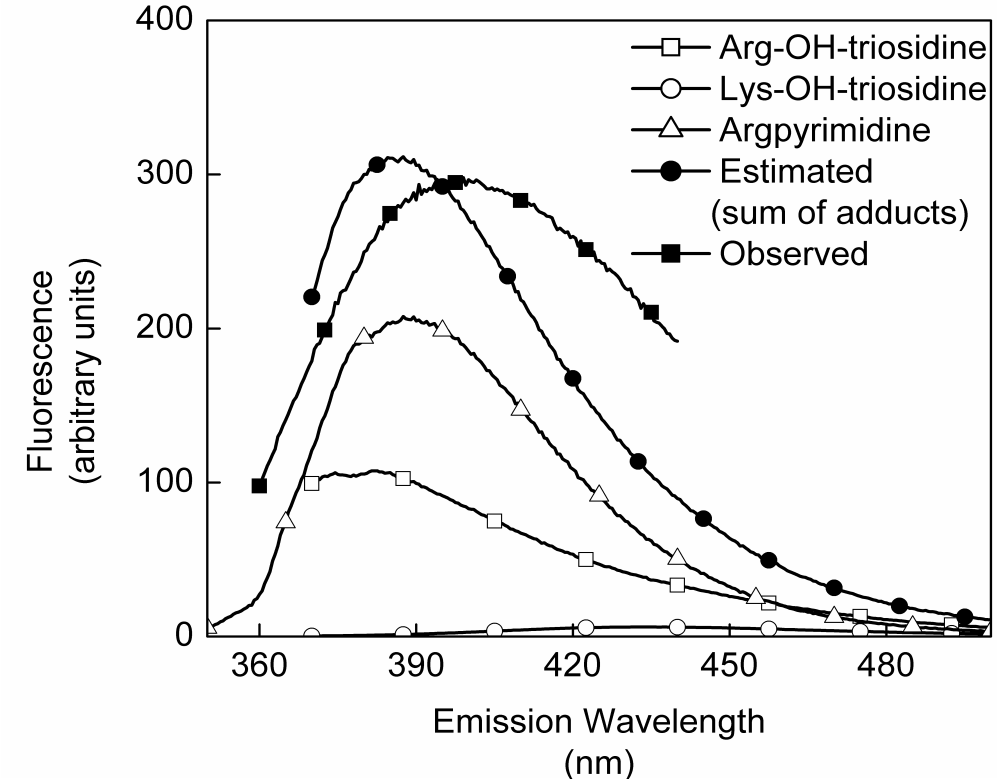

Figure 7. Fluorescence emission spectra (λex = 334 nm) of the cornea that was incubated for 6 days with 2% glyceraldehyde and solubilized by proteolytic digestion ("observed") and of pure solutions of arg-OH-triosidine, lys-OH-triosidine and argpyrimidine. The known adduct spectra are scaled to the mean concentration at which each adduct was found in the cornea. The estimated spectrum is the sum of these three spectra ("estimated").

It is significant that the rise of all three AGEs examined (including the non-cross-linking AGE argpyrimidine) correlate with stiffening, without regard to whether they are responsible for cross-linking. Because fluorescence can be quantitatively correlated with

the concentration of the fluorophores, the linear relation between fluorescent AGEs and shear modulus (Figure 5) also applies to fluorescence in the absence of quenching. Because linearity holds even in the highly-glycated cornea samples analyzed here, quenching is an unlikely problem for the much lower level of AGE accumulation expected in age and diabetes-related glycation. Indeed, fluorescence has recently been shown to be an accurate, noninvasive measure of AGE accumulation.[44] Thus, it should also be possible to indirectly measure the stiffness of collagenous tissues *in vivo* using an empirical relation between fluorescence and shear modulus.

The significant stiffening we have demonstrated with glyceraldehyde suggests that glycation is a promising engineering tool for soft collagenous tissues. We envision two areas of particular interest: bioadhesives and modulating the stiffness of implants. Glyceraldehyde crosslinks form between primary amines; therefore, if amines on adjacent tissues or a tissue and a synthetic implant are bound in the process, then they will be "glued" together. Collagen-based synthetic tissue replacements also have exposed lysine and arginine residues. Glycation may provide a relatively-biocompatible method for engineering the strength and modulus of synthetic biomaterials to match those of the target material.

Determining the chemical nature and location of the cross-links responsible for tissue stiffening and the reasons why they are correlated with the rise of the predominant AGEs will be an important area for future research. Our working hypothesis is that the kinetically favored cross-links are those that link amino acid side chains that are located in close proximity to each other within collagen fibrils. With the known sequence and alignment of

the three stands of the collagen I triple helix,[45] we have identified all 116 potential sites for the formation of crosslinks within collagen I triple helices based upon the number of Arg and Lys residues in proximity to each other. Due to the regularity of corneal collagen fibril diameter (30 nm)[46] and triple helix diameter (1.5 nm)[31], we are also able to determine that there are ~ 400 helices / fibril and 46,545 potential crosslinking sites per 300 nm section of fibril (the approximate length of one triple helix). There are also 26 specific binding sites along corneal collagen fibrils per 300 nm section of fibril, where the protein cores of proteoglycans associate and could potentially be crosslinked, although the precise amino acids involved are not yet known.[47] If all potential crosslinking sites were occupied, there would be a maximum of 26 fibril-proteoglycan crosslinks vs. 46,545 intrafibrillar crosslinks per 300 nm fibril section (i.e., 1 fibril-proteoglycan crosslink per 2,327 intrafibrillar crosslinks). Since collagen fibrils represent 75% of the protein present in the stroma,[36] intrafibrillar AGEs are likely to dominate the NMR and fluorescence spectra. However, they may have little bearing on the mechanical modifications with which we are concerned.

Scott asserts that the mechanical properties of the bulk tissue are dominated by the fibril-proteoglycan interactions.[48] Thus, the adducts responsible for corneal stiffening may predominantly be those that covalently link proteoglycans to their binding sites. This implies that the mechanically-significant crosslinks are vastly outnumbered by *mechanically insignificant* intrafibrillar crosslinks. We will explore this hypothesis in greater depth in Chapter 6.

BIBLIOGRAPHY

1. Hodge JE. Dehydrated foods, chemistry of browning reactions in model systems. *J. Agric. Food Chem.* 1953;1:928-943.

2. Sell DR, Monnier VM. Structure elucidation of a senescence cross-link from human extracellular matrix. Implication of pentoses in the aging process. *Journal of Biological Chemistry.* 1989;264:21597-21602.

3. Brinkmann E, Wells-Knecht KJ, Thorpe SR, Baynes JW. Characterization of an imidazolium compound formed by reaction of methylglyoxal and N-alpha-hippuryllysine. *J. Chem. Soc. Perkin. T.1.* 1995;22:2817-2818.

4. Wells-Knecht KJ, Brinkmann E, Baynes JW. Characterization of an imidazolium salt formed from glyoxal and N-alpha-hippuryllysine – A model for Maillard reaction cross-links in proteins. *J. Org. Chem.* 1995;60(1995):6246-6247.

5. Tessier F, Obrenovich M, Monnier VM. Structure and mechanism of formation of human lens fluorophore LM-1 – Relationship to vesperlysine A and the advanced Maillard reaction in aging, diabetes, and cataractogenesis. *Journal of Biological Chemistry.* 1999;274:20796-20804.

6. Nagaraj RH, Portero-Otin M, Monnier VM. Pyrraline ether crosslinks as a basis for protein crosslinking by the advanced Maillard reaction in aging and diabetes. *Arch. Biochem. Biophys.* 1996;325:152-158.

7. Ahmed MU, Thorpe SR, Baynes JW. Identification of N epsilon-carboxymethyllysine as a degradation product of fructoselysine in glycated protein. *Journal of Biological Chemistry.* 1986;261:4889-4894.

8. Ahmed MU, Frye EB, Degenhardt TP, Thorpe SR, Baynes JW. N-epsilon-(carboxyethyl)lysine, a product of the chemical modification of proteins by methylglyoxal, increases with age in human lens proteins. *Biochem. J.* 1997;324:565-570.

9. Shipanova IN, Glomb MA, Nagaraj RH. Protein modification by methylglyoxal: chemical nature and synthetic mechanism of a major fluorescent adduct. *Arch. Biochem. Biophys.* 1997;344:29-36.

10. Lo TW, Westwood ME, McLellan AC, Selwood T, Thornalley PJ. Binding and modification of proteins by methylglyoxal under physiological conditions. A kinetic and mechanistic study with N alpha-acetylarginine, N alpha-acetylcysteine, and N alpha-acetyllysine, and bovine serum albumin. *J Biol Chem.* Dec 23 1994;269(51):32299-32305.

11. Iijima K, Murata M, Takahara H, Irie S, Fujimoto D. Identification of N(omega)-carboxymethylarginine as a novel acid-labileadvanced glycation end product in collagen. *Biochem J.* Apr 1 2000;347 Pt 1:23-27.

12. Glomb MA, Pfahler C. Amides are novel protein modifications formed by physiological sugars. *Journal of Biological Chemistry.* Nov 9 2001;276(45):41638-41647.

13. Lederer MO, Klaiber RG. Cross-linking of proteins by maillard processes: characterization and detection of lysine-arginine cross-links derived from

glyoxal and methylglyoxal. *Bioorganic & Medicinal Chemistry.* 1999/11 1999;7(11):2499-2507.

14. Tessier FJ, Monnier VM, Sayre LA, Kornfield JA. Triosidines: Novel maillard reaction products and crosslinks from the reaction of triose sugars with lysine and arginine residues. *Biochem J.* Oct 14 2002;Pt.

15. Andreassen TT, Oxlund H. Thermal stability of collagen in relation to non-enzymatic glycosylation and browning in vitro. *Diabetologia.* Sep 1985;28(9):687-691.

16. Reiser KM. Nonenzymatic glycation of collagen in aging and diabetes. *Proc Soc Exp Biol Med.* Jan 1991;196(1):17-29.

17. Bruel A, Oxlund H. Changes in biomechanical properties, composition of collagen and elastin, and advanced glycation endproducts of the rat aorta in relation to age. *Atherosclerosis.* Dec 20 1996;127(2):155-165.

18. Sims TJ, Rasmussen LM, Oxlund H, Bailey AJ. The role of glycation cross-links in diabetic vascular stiffening. *Diabetologia.* Aug 1996;39(8):946-951.

19. Sady C, Khosrof S, Nagaraj R. Advanced Maillard reaction and crosslinking of corneal collagen in diabetes. *Biochem Biophys Res Commun.* Sep 25 1995;214(3):793-797.

20. Baynes JW, Monnier VM. *The Maillard Reaction in Ageing, Diabetes and Nutrition.* New York: A. R. Liss; 1989.

21. McCance DR, Dyer DG, Dunn JA, et al. Maillard reaction products and their relation to complications in insulin-dependent diabetes mellitus. *J Clin Invest.* Jun 1993;91(6):2470-2478.

22. Vitek MP, Bhattacharya K, Glendening JM, et al. Advanced glycation end products contribute to amyloidosis in Alzheimer disease. *Proc Natl Acad Sci U S A.* May 24 1994;91(11):4766-4770.

23. Airaksinen KE, Salmela PI, Linnaluoto MK, Ikaheimo MJ, Ahola K, Ryhanen LJ. Diminished arterial elasticity in diabetes: association with fluorescent advanced glycosylation end products in collagen. *Cardiovasc Res.* Jun 1993;27(6):942-945.

24. Vogel HG. Influence of maturation and age on mechanical and biochemical parameters of connective tissue of various organs in the rat. *Connect Tissue Res.* 1978;6(3):161-166.

25. Galeski A, Kastelic J, Baer E, Kohn RR. Mechanical and structural changes in rat tail tendon induced by alloxan diabetes and aging. *J Biomech.* 1977;10(11/12):775-782.

26. Duquette JJ, Grigg P, Hoffman AH. The effect of diabetes on the viscoelastic properties of rat knee ligaments. *J Biomech Eng.* Nov 1996;118(4):557-564.

27. Girton TS, Oegema TR, Tranquillo RT. Exploiting glycation to stiffen and strengthen tissue equivalents for tissue engineering. *J Biomed Mater Res.* Jul 1999;46(1):87-92.

28. Tae G, et al. In preparation.

29. Spoerl E, Seiler T. Techniques for stiffening the cornea. *J Refract Surg.* Nov-Dec 1999;15(6):711-713.

30. Syrovy I. Glycation of albumin: reaction with glucose, fructose, galactose, ribose or glyceraldehyde measured using four methods. *J Biochem Biophys Methods*. Mar 1994;28(2):115-121.

31. Stryer L. *Biochemistry*. 4th ed. New York: W. H. Freeman and Co.; 2000.

32. Wollensak G, Sporl E, Seiler T. Treatment of keratoconus by collagen cross linking. *Ophthalmologe*. Jan 2003;100(1):44-49.

33. Wollensak G, Spoerl E, Seiler T. Stress-strain measurements of human and porcine corneas after riboflavin-ultraviolet-A-induced cross-linking. *Journal Of Cataract And Refractive Surgery*. Sep 2003;29(9):1780-1785.

34. Wollensak G, Spoerl E, Wilsch M, Seiler T. Keratocyte apoptosis after corneal collagen cross-linking using riboflavin/UVA treatment. *Cornea*. Jan 2004;23(1):43-49.

35. Fatt I, Weissman BA. *Physiology of the Eye*. Second ed. Boston: Butterworth-Heinemann; 1992.

36. Davson H. *The Eye*. Vol 1. fifth ed. New York: Academic Press; 1990.

37. Rehany U, Lahav M, Shoshan S. Collagenolytic activity in keratoconus. *Ann Ophthalmol*. 1982 Aug 1982;14(8):751-754.

38. Abalain JH, Dossou H, Colin J, Floch HH. Levels of collagen degradation products (telopeptides) in the tear film of patients with keratoconus. *Cornea*. Jul 2000;19(4):474-476.

39. Kao WWY, Vergnes JP, Ebert J, Sundarraj CV, Brown SI. Increased Collagenase And Gelatinase Activities In Keratoconus. *Biochemical And Biophysical Research Communications*. 1982;107(3):929-936.

40. Smith VA, Easty DL. Matrix metalloproteinase 2: involvement in keratoconus. *European Journal Of Ophthalmology*. Jul-Sep 2000;10(3):215-226.

41. Lema I, Duran JA. Inflammatory molecules in the tears of patients with keratoconus. *Ophthalmology*. Apr 2005;112(4):654-659.

42. Fukuchi T, Yue B, Sugar J, Lam S. Lysosomal-Enzyme Activities In Conjunctival Tissues Of Patients With Keratoconus. *Archives Of Ophthalmology*. Oct 1994;112(10):1368-1374.

43. Kochakian M, Manjula BN, Egan JJ. Chronic dosing with aminoguanidine and novel advanced glycosylation end product-formation inhibitors ameliorates cross-linking of tail tendon collagen in STZ-induced diabetic rats. *Diabetes*. Dec 1996;45(12):1694-1700.

44. Meerwaldt R, Graaff R, Oomen PHN, et al. Simple non-invasive assessment of advanced glycation endproduct accumulation. *Diabetologia*. Jul 2004;47(7):1324-1330.

45. Meek KM, Chapman JA, Hardcastle RA. Staining Pattern Of Collagen Fibrils - Improved Correlation With Sequence Data. *Journal Of Biological Chemistry*. 1979;254(21):710-714.

46. Oyster CW. *The Human Eye: Structure and Function*. Sunderland, MA: Sinauer Associates, Inc.; 1999.

47. Yu L, Cummings C, Sheehan JK, Kadler K, Holmes DF, Chapman JA. *Dermatan Sulphate Proteoglycans: Chemistry, Biology, Chemical Pathology*. Chapel Hill: Portland Press Inc.; 1993.

48. Scott JE. Extracellular matrix, supramolecular organisation and shape. *J Anat.* Oct 1995;187 (Pt 2):259-269.

Chapter 6

UNDERSTANDING THE MICROSTRUCTURAL CHANGES THAT CAUSE CORNEAL STIFFENING

6.1 Introduction

Having established that glycation has significant therapeutic potential for keratoconus, we proceed by investigating the associated microstructural changes. Starting at the anterior surface and moving back, the cornea is composed of the following five layers: the epithelium, Bowman's layer, the stroma, Descemet's membrane, and the endothelium[1]. The major structural element of the cornea (~ 90% of its thickness) is the stroma, which is composed of approximately 200 lamellae that consist mainly of oriented collagen fibrils embedded in a hydrated matrix of proteoglycans (PGs) and glycosaminoglycans (GAGs) (Figure 1).[2] Lamellae run parallel to the surfaces of the cornea and span its full area. There is even indirect evidence that the individual collagen fibrils in a lamella span the entire cornea.[2] Fibrils are composed of collagen type I triple helices that are enzymatically cross-linked during development (Figure 1, A and B).

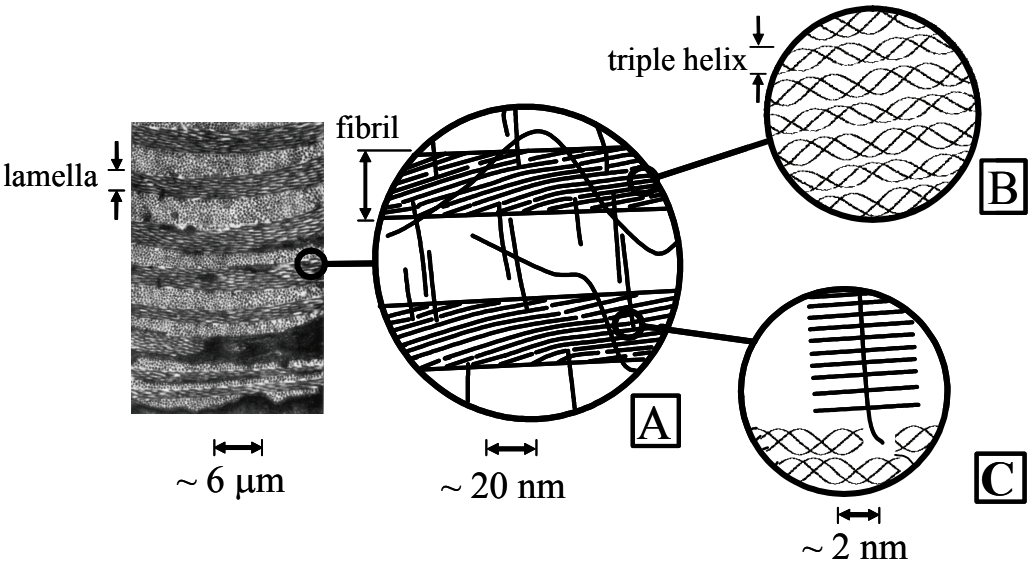

Figure 1. Stroma microstructure. [A] Represents the rigid collagen type I fibrils (D ~ 30 nm) and smaller strands of proteoglycan that compose the lamellae (2 - 3 nm thick) of the corneal stroma. [B] Shows an enlargement of part of one of the fibrils, displaying the collagen triple helices (D ~ 1.5 nm) aligned within a fibril. [C] Depicts the protein core of a proteoglycan non-covalently associated with the surface of a collagen fibril and decorated with polysaccharide chains. Micrograph was used by permission from Prof. K. Kadler, U. Manchester.

The collagen fibrils in adjacent lamellae within the stroma differ in orientation only,[2] but the result is a "stacked sheet" morphology; fibrils within a single layer run parallel to each other and nearly orthogonal to fibrils in adjacent layers. The high tensile-strength fibrils resist axial strains, while the hydrated PG/GAG matrix between layers allows the collagen fibrils to bend and translate relative to each other under off-axis stress. It has been proposed that the regular orientation and spatial distribution of the collagen fibrils is maintained by specific associations with the PGs in the matrix (Figure 1, C).[1, 3]

It is well established, and demonstrated again here, that glycation-induced crosslinks add connectivity to this native morphology within the collagen fibrils and between fibrils and matrix (see Chapter 5). Coordinated biochemical and rheological analyses have allowed us

to correlate tissue stiffening with advanced glycation endproduct (AGE) accumulation. However, it is likely that only a small fraction of the AGEs formed contribute to the mechanical properties of the tissue. Pendant adducts such as argpyrimidine cannot contribute to mechanical strength because they do not add connectivity to the system; only crosslinks contribute to the modulus. The structures of the various AGEs make it obvious which are crosslinks, but it remains unclear *where* (i.e., between which of the macromolecular components) crosslinks have the greatest impact on mechanical properties. The relative importance of contributions from crosslinks 1) within collagen fibrils vs. 2) between fibrils vs. 3) between fibrils and proteoglycans vs. 4) within or between proteoglycans, remains an open question. This is due, in part, to a lack of consensus on the importance of proteoglycans in the mechanical properties of soft collagenous tissues.

The traditional view is that proteoglycans are not mechanically significant. The mechanical strength of ocular tissues and collagenous tissues in general has been attributed solely to the orientation, density, and size of the collagen fibrils.[2, 4-6] In this model, proteoglycans are thought to be a randomly oriented "ground substance" that is distributed throughout the tissue. The primary functions of this amorphous gel are proposed to be the maintenance of tissue hydration and resistance to sudden deformations due to high viscosity.

In the modern view, proteoglycans make significant contributions to mechanical properties through specific interactions with binding sites on the surface of the collagen fibrils.[3, 7-9] In addition to hydrating the tissue, it is proposed that proteoglycans also maintain fibril spacing and orientation and contribute to tissue stiffness by bridging the span between fibrils.

The differences between these two models become particularly relevant in the context of glycating corneal tissue. The predominant view in the literature is that glycation-related tissue stiffening is due to fibril stiffening.[10] We test this hypothesis and attempt to differentiate between the contributions of fibril stiffening and matrix-related changes by comparing the effects of glycation on isolated collagen fibers (from mouse tails) to the effects of glycation on the cornea. Hereafter, "fiber" will be used to denote a coherent, crosslinked subunit of a mouse tendon (typically ~ 100 μm diameter) and "fibril" will generally refer bundles of laterally-associated collagen triple helices (~30 nm diameter) found in the stroma (Figure 1, A and B). Collagen fibers (not found in cornea tissue) are bundles of fibrils.

Previous mechanical analyses of native and engineered cornea focused on the tensile strength of strips of tissue, which does not probe the tissue as a whole. Tensile measurements on cornea strips are dominated by the tensile strength of the collagen fibrils whose axes are coincident with the axis of elongation. We have performed oscillatory shear measurements, which deform the cornea along the axis perpendicular to the planes of the lamellae so that the collagen fibrils are not loaded along their axes. This method of analysis allows us to probe the tissue as a whole and not simply the collagen fibrils.

To determine the relative contribution of changes in the mechanical properties of the collagen fibrils, we have examined glycated mouse tail tendon fibers. Mouse tail tendons are composed almost entirely of bundles of collagen type I fibers and provide a well-studied model system for measuring the mechanical properties of these fibers.[4] The "biomechanics" approach is to measure the stress-strain relation of the fibers directly,

under approximately physiological conditions, by applying a uniaxial load to fibers submersed in a physiological buffer.[4] In these experiments, the stresses that develop as a result of straining fibers at a constant rate are measured. The resulting stress-strain relation reflects the response of native fibers (hydrogen bonds intact) to mechanical loading. Small strains and loads reflect normal physiological conditions, while the failure behavior is relevant to injuries.

Unfortunately, the methods used in the biomechanics literature to characterize fresh tendon[4] are inconsistent with the methods used in the glycation literature to measure the mechanical impact of crosslink accumulation.[11] The metric most commonly used to quantify the mechanical properties of glycated collagen fibers is the tendon breaking time (TBT) test.[11-13] In the TBT procedure, ~ 2 g weights are suspended from mouse tendon fibers submersed in 7 M urea at 40° C. The tendon breaking time begins with hanging the weight on the fibril and submersing it and ends at the time the weight falls to the bottom of the container. While breaking time is well correlated with animal age and the accumulation of covalent crosslinks,[11, 12] it provides little insight into the impact of those crosslinks on the mechanical properties of the fibers *in vivo*. We note that this is a point of confusion in the literature (discussed further in Section 6.5).

Applying this "biomechanics" approach to glycated tissues, we have succeeded in correlating AGE accumulation in glycated mouse-tail collagen fibers with mechanical property changes under nondenaturing conditions. We will show that the mechanical properties of intact collagen fibers are less sensitive to AGE accumulation than those of denatured fibrils. However, we will show that the biomechanics approach, but not the TBT

test, is directly related to the physiologically-relevant impact of glycation on collagen fibrils. With a known, quantitative correlation between AGE formation and the mechanical strength of intact collagen fibrils, we proceed to show that treatment-induced cornea stiffening cannot be explained by changes in the properties of its collagen fibrils. Instead, glycation must also change the way the collagen interacts with the PG/GAG matrix.

6.2 Materials and Methods

Mouse-Tail Collagen Fiber Glycation – Fresh tendons were removed from the tails of 6-week and 6-month old mice and incubated for 24 hours at 37° C in 100 mM phosphate-buffered saline (PBS controls), 0.1 mM methylglyoxal (in PBS), or 0.5 mM methylglyoxal (in PBS). After incubation, tendons were rinsed and placed in PBS at 5° C and either analyzed immediately by GC/MS in Professor Vincent Monnier's lab at Case Western Reserve University (CWRU, Department of Pathology) or shipped overnight to Caltech for mechanical analysis. Mice were bred, sacrificed, and dissected at treated at CWRU (strain C57BL6). Phosphate-buffered saline and methylglyoxal (MGO) were purchased from Sigma Chemical Co. (St. Louis, MO). MGO was distilled prior to use.

HPLC Analysis – A minimum of 3 tendons from each treatment were individually hydrolyzed in 6 N HCl for 18 hours at 110° C. Total lysine and caboxyethyl-lysine (CEL), a surrogate marker for modification of collagen by MGO, were quantified by method of internal standard using GC/MS. These experiments were performed by Christopher Strauch under the supervision of Professor V. Monnier.

Mechanical Analysis – Tendons readily separate into strands ("fibers") when sectioned. If placed in air, fibers dry and shrink rapidly; therefore, fibers were kept in buffer at all times. Precise fiber diameters were measured using optical microscopy with the tendons submersed in physiological saline. Diameters ranged from 75 μm – 200 μm, and lengths were cut to ~ 1.25 cm. It is significant that only fibers in this range were used: fibers less than 75 μm in diameter are easily damaged and above 200 μm results no longer reflect intrinsic properties (e. g., there is a systematic decrease in apparent failure strain and stress with increasing diameter > 200 μm).

Fibers were then loaded on an Instron 5542 Universal Materials Testing Machine (Instron Corp., MA) by gently clamping the ends of the fiber between opposing steel plates and immersing the assembly in a PBS bath at 37° C. Clamping must be done with great care and consistency: excessive clamping force results in the fiber failing prematurely at the edge of the clamp, and insufficient force allows the fiber to slip.[14] Failure strains never exceeded 12%, indicating that fibrils did not slip.[14] Clamps were then gently drawn apart to straighten the fiber. Fibers were considered fully extended when further separation of the clamps induced a measurable normal force. Sample length was then measured as the distance between clamps.

The tensile testing procedure, based on prior literature, consisted of a preconditioning period followed by a linear extension at fixed rate until the fiber failed.[4] Preconditioning was achieved by three successive cycles of extending the fiber to up to 3% strain and back down to 1% at a constant rate of 3%/min (at or below this rate, properties are essentially rate-independent). Precondition was performed as described in the literature to reduce

variability in the high-strain behavior.[4] Apparent tensile stress and strain were recorded throughout the preconditioning period (Figure 2). The linear elastic modulus was calculated from the results before or during preconditioning. After the third return to 1% strain, the sample was extended until it failed, while the apparent tensile stress and strain were recorded. If the breaking point of the fiber was at the edge of the clamp, the result was discarded to eliminate errors due to edge effects.

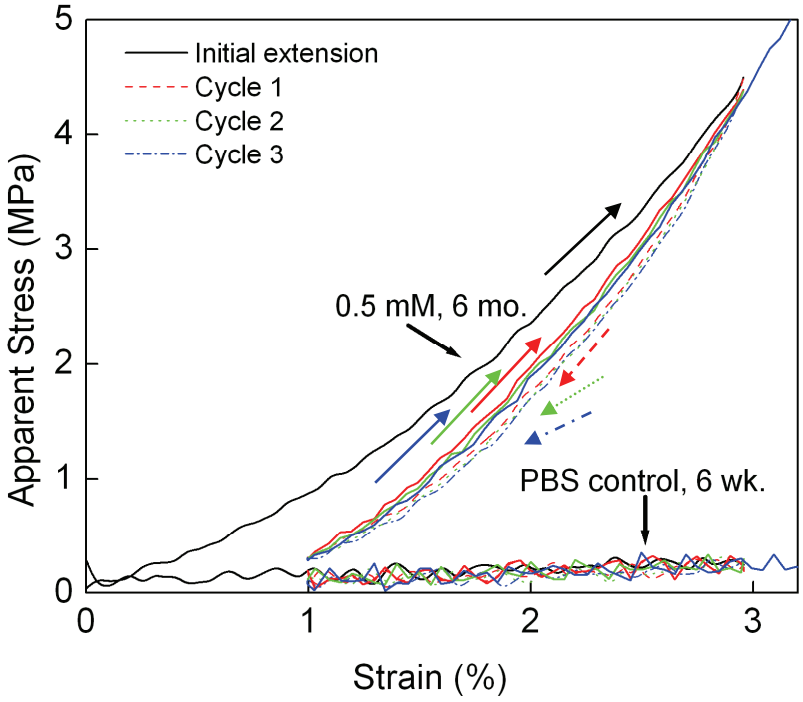

Figure 2. Preconditioning collagen fibrils by cycling from 1 - 3% strain three times provides a common flow history for all samples. Unglycated controls show essentially no hysteresis, whereas tendons glycated with methylglyoxal appear to relax significantly after the first cycle.

6.3 Advanced Glycation Endproducts in Mouse Tail Collagen

Mouse tails were glycated using MGO rather than GA because it glycates tissues more rapidly than GA, while yielding similar AGEs (see Chapter 1).[15, 16] MGO is also physiologically significant; it is a known degradation product of glyceraldehyde-3-phosphate *in vivo*.[17] MGO is formed from GA via a simple dehydration reaction and from GA-3-phosphate via loss of phosphate.[15] Formation of MGO is thought to be a significant mechanism of glycation in the presence of glyceraldehyde, although direct reaction of glyceraldehyde with proteins is prevalent. MGO is useful for examining glycation *in vitro*, however it is unsuitable for tissue engineering due to its high toxicity.

Carboxyelthyl-lysine (CEL) was used as a surrogate marker for glycation levels of mouse tail tendon.[15, 17] CEL is a good surrogate for argpyrimidine because it represents a comparable fraction of the total quantity of AGEs formed with GA and MGO (approximately 1 – 2%).[16, 17]

Collagen fibers taken from 6-week and 6-month old mouse tail tendons incubated with 0.1 mM MGO and 0.5 mM show a dose-dependent rise in AGEs as indicated by levels of CEL (Figure 3). The tendons of 6-month old mice are less susceptible to glycation (μmol CEL / mol lysine = 291 ± 8 for 0.1 mM MGO and 544 ± 100 for 0.5 mM MGO) than 6-week old mice (μmol CEL / mol lysine = 550 ± 9 for 0.1 mM MGO and 1265 ± 68 for 0.5 mM MGO). The maturation of lysyl oxidase-derived crosslinks into trifunctional crosslinks, etc. and the formation of glucosepane crosslinks (the primary AGE thus far identified *in vivo*) appear to block potential glycation sites.[18]

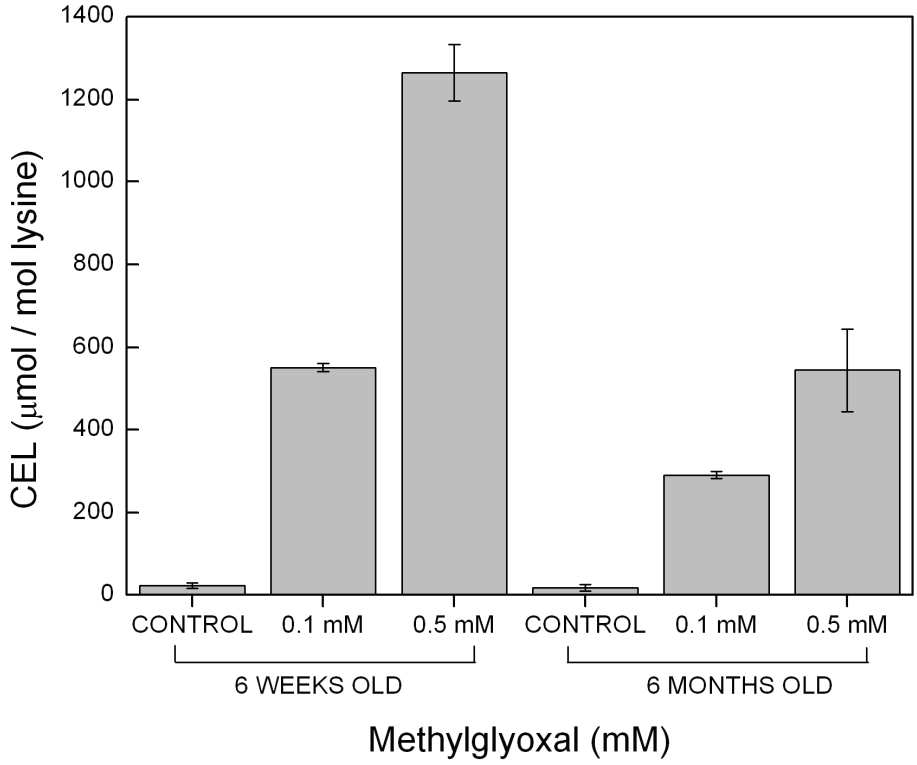

Figure 3. CEL increases with increased exposure to MGO. The effect on young tendon is stronger than the effect on old tendon.

The highest level of glycation achieved (AGEs / mol lysine) in 6-week old tendons is an order of magnitude lower than the glycation achieved in corneas treated with 2% GA. The reason we examine the collagen fibers at a lower level of AGE accumulation is that collagen fibers become stiff and fragile when glycated to the level of the corneas in Chapter 5 (V. Monnier, personal communication). We will return to this observation in the context of quantitative measures of glycation-induced changes in the mechanical properties of collagen fibrils.

6.4 Mechanical Impact of Glycation on Mouse Tail Tendons

The complex stress-strain behavior of collagen fibers under uniaxial extension is well documented, precluding application of a simple viscoelastic model or characterization by a single parameter.[4] Nevertheless, a comparison of the entire stress-strain curve of glycated vs. unglycated fibers, from the strain-free state through failure, does reveal significant mechanical changes that accompany AGE formation (Figure 4). With increasing strain, four regimes may be identified: an initial, linear regime in which the apparent stress increases gradually and proportional to the strain; a transition to nonlinear behavior in which the fibers exhibit strain-hardening; a pseudo-linear regime with an effective modulus much greater than the linear one; and lastly, yield and failure.

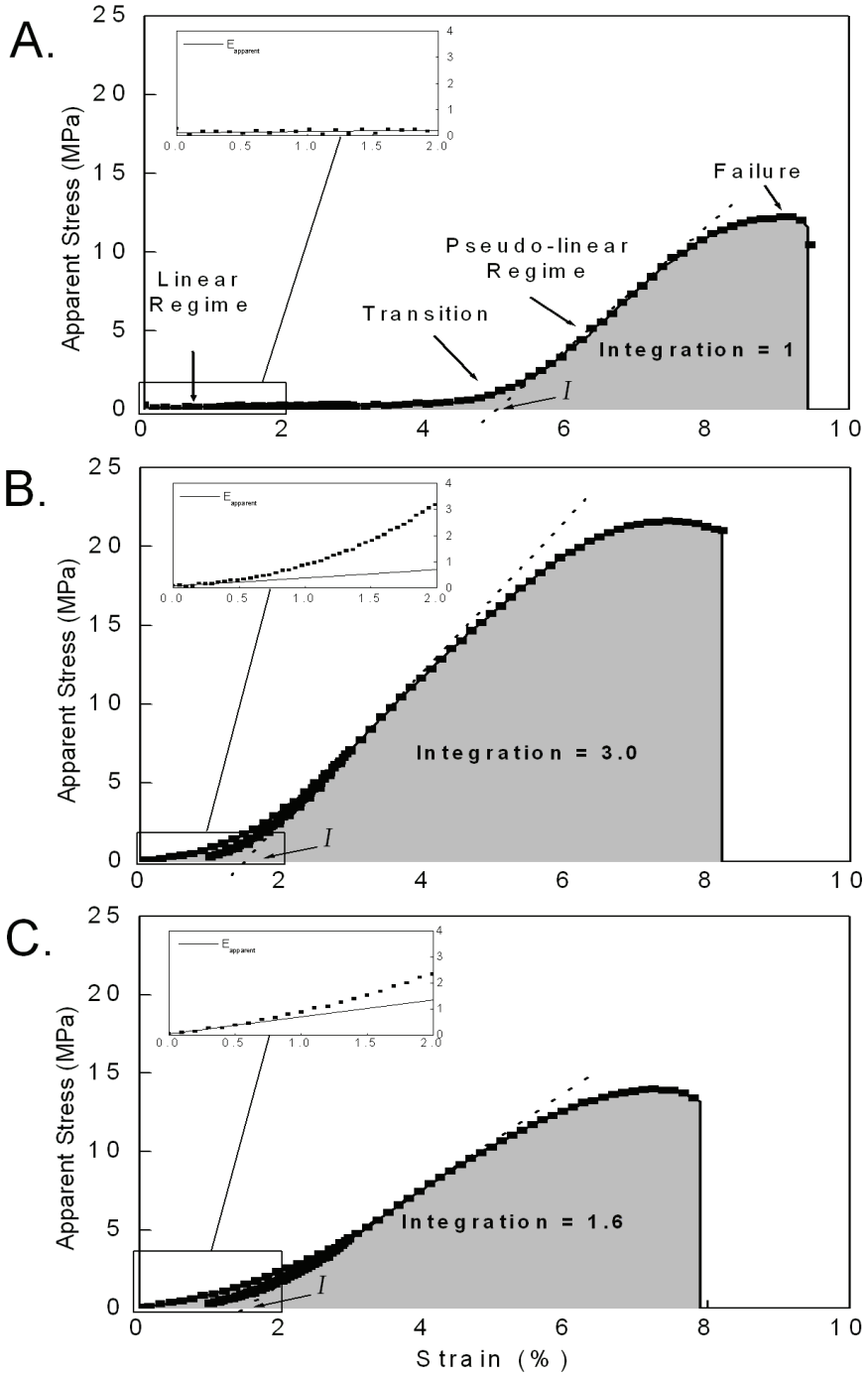

Figure 4. Uniaxial extension stress-strain plots representative of 6 mo. collagen fibrils treated with PBS (A.), 0.1 mM MGO (B.) and 0.5 mM MGO (C.). The four characteristic regimes are: linear, transition, pseudo-linear, and failure. Glycation shortens the linear regime (shifting the x-intercept, "I") and increases the "integration," of the stress-strain relation (toughness). 6 week and 6 month results were similar except where embrittlement became apparent on 6 week tendons treated with 0.5 mM MGO.

The initial linear regime of the stress-strain curve is often lumped together with the transition regime and referred to as the "toe region."[4, 19] Though it is accepted that this toe region is indicative of normal physiological strains, it is not normally analyzed because variability in tissue handling can lead to inconsistent Young's modulus measurements.[20] Instead, most investigations precondition fibers at low strains and focus on the properties of the pseudo-linear regime. Preconditioning is designed to give the fibers a well-defined, reproducible flow history.[4, 19]

We are interested not only in the behavior of the fibers under high loads, but also under physiologically-relevant loads; therefore, we focus on both the linear and the failure regimes. While true moduli cannot be obtained from the linear regime, *relative* differences in this regime can be used to assess the mechanical impact of different levels of AGE accumulation. At the small strains encountered *in vivo*, the treated fibers already show nonlinear, strain-hardening behavior and substantial hysteresis that do not set in until much higher strains for unglycated samples (Figure 2). The most significant glycation-induced changes in mechanical properties appear to be an increase in apparent modulus at low strain amplitude, a loss of extensibility, and an increase in toughness. In the present work we show that all of these parameters are significantly affected by glycation, but that the dependence is nonlinear at high levels of AGE accumulation.

Low-Strain (Young's) Modulus

The apparent modulus, $E_{apparent}$, in the low-strain regime increases significantly with glycation (Figure 5, A). The apparent modulus of fibers increased by ~ 500% for both 6-

week old mice, $E_{apparent}$ = 0.11 ± 0.1 (PBS control) to 0.61 ± 0.04 MPa, and 6-month old mice, $E_{apparent}$ = 0.08 ± 0.02 (PBS control) to 0.58 ± 0.17 MPa, when glycated with 0.5 mM MGO. As mentioned above, this low-strain behavior is particularly significant because it reflects physiological conditions. It has been argued that strain-hardening occurs at the upper limit of the normal physiological range of motion for collagen fibers.[4]

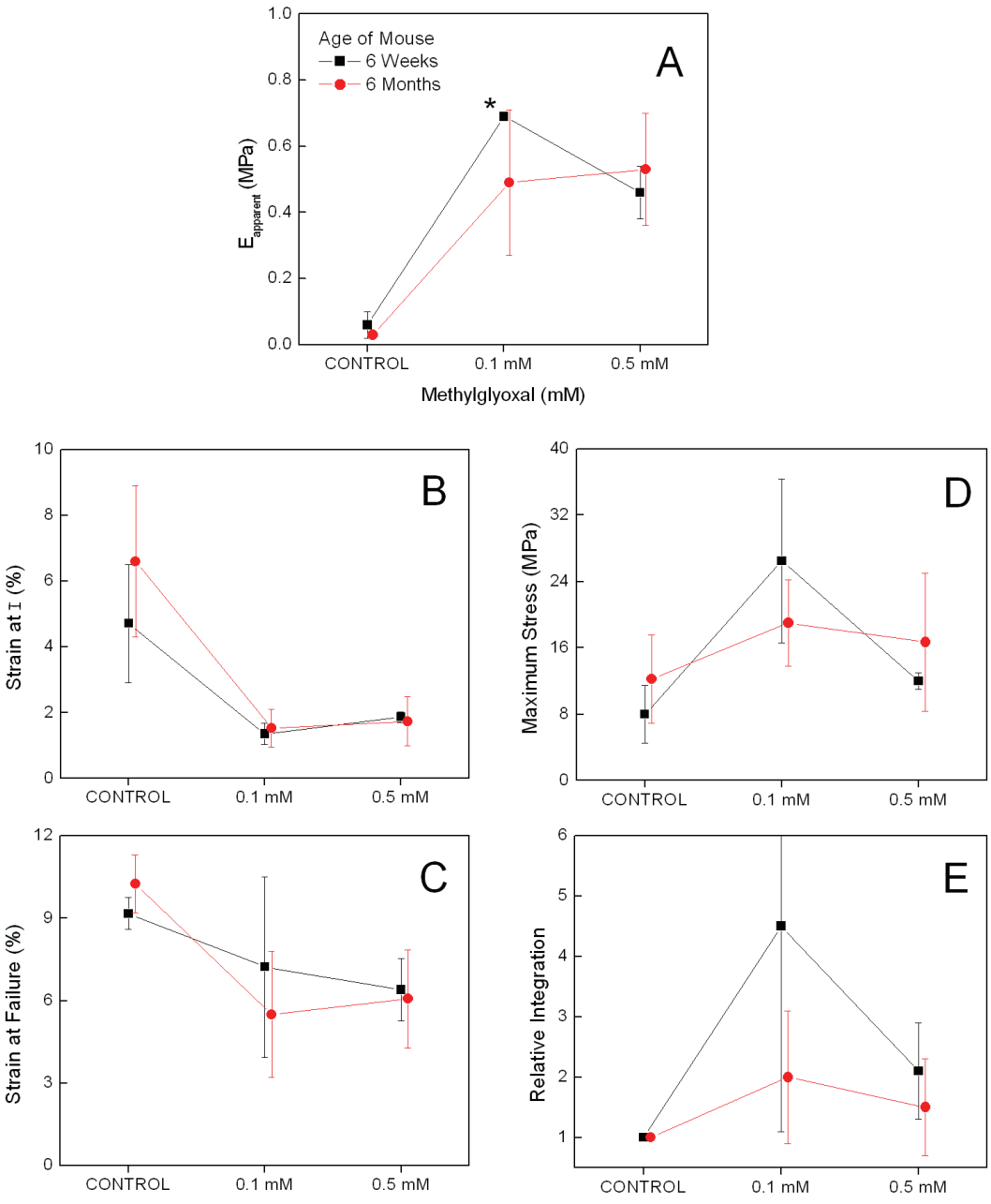

Figure 5. Key changes in the mechanical properties of mouse tail tendon fibers as a function of glycation: (A) Young's modulus increases with moderate glycation (0.1 mM MGO) but does not increase with additional glycation (0.5 mM MGO). (B) The linear regime shrinks, shifting the transition regime to lower strains. (C) Failure strain decreases monotonically with glycation in the 6 week fibers, while the effect saturates at 0.1 mM MGO in 6 month fibers. (D) "Ultimate tensile strength" (UTS), or stress at failure, of 6 mo. fibers increases with glycation but saturates at 0.1 mM MGO, 6 week fibers are strengthened with 0.1 mM MGO but become brittle with additional glycation. (E) Toughness (area under the stress-strain curve) increases with moderate glycation but falls with excessive crosslinking.

Loss of Extensibility

Glycation also correlates with a reduction in extensibility (Figure 5, B and C). The loss of extensibility is accompanied by a narrowing of the low-strain regime as the transition from linear to pseudo-linear behavior broadens and shifts to lower strains (Figure 4). To quantify this shift to lower strain, we extrapolate the line tangent to the high-strain regime down to its x-intercept "*I*" (Figure 4). On average, the maximum slope of the tangent line changes little with treatment condition or mouse age; thus, *I* is a good indicator of extensibility loss. Glycation reduces *I*, however, the effect appears to saturate (Figure 5, B).

Failure Strain and Stress

Loss of extensibility is also manifest in the reduction in the maximum strain attainable before failure (Figure 5, C). When pushed to the point of failure, untreated tendons generally stretch to ~ 10% strain before breaking (consistent with the literature[4, 19]), whereas glycated tendons predominantly break at 6 – 7% strain. Fibers from 6-week old mice showed a monotonic, dose-dependent reduction in failure strain, whereas the effect was saturated in mature fibers with 0.1 mM MGO. It is likely that enzymatic crosslinks and preexisting glycation-related modifications reduce the number of AGEs required to decrease extensibility. Enzymatic crosslinks alone, however, are insufficient to reduce extensibility and may even increase it: in the absence of further glycation, the average extensibility of mature fibers is larger than immature fibers. The increase in failure stress (ultimate tensile strength, or UTS) that accompanies enzymatic crosslinking is also seen for moderate glycation (Figure 5, D).

Collagen fibers from 6 month old mice are capable of bearing significantly higher loads than fibers from 6 week old mice; however, moderate levels of glycation reverse their relative failure stresses. The average failure stress of untreated 6 month fibers is ~ 50% higher than 6 week fibers. Moderate glycation (0.1 mM MGO) causes a much smaller increase in failure stress (60% rather that 230%) in the mature fibers, apparently due to the presence of enzymatic crosslinks. Enzymatic crosslinks (formed primarily on Lys residues[21]) appear to prevent the accumulation of excessive crosslinks, which appear to cause fibers to become brittle. Failure stresses of 0.5 mM MGO-treated mature fibers were not significantly different from 0.1 mM specimens; however, the failure stress of immature fibers decreased by over 50% relative to 0.1 mM treatment. An increase in failure stress with moderate crosslinking followed by a decrease at high levels of crosslinking is also consistent with prior literature.[19]

The combination of changes in failure stress and strain results in changes in the toughness of the fibers. Toughness is characterized by the integration of the area beneath the stress-strain curve and is an indicator of the total strain energy stored in the sample (Figure 4). Variability in the shape of the stress-strain curves from one fiber to another made the failure point difficult to define (some fibers failed with a sharp reduction in stress, while others failed more gracefully). Therefore, the integration was performed up to the strain at the peak stress. The toughness of 6 month fibers increased by an average factor of x2 when treated with 0.1 mM MGO, but only x1.4 when treated with 0.5 mM MGO (Figure 5, E). The effect on 6 week fibers was even more dramatic, increasing the toughness by an average factor of x4.4 with 0.1 mM and x2 with 0.5 mM treatment. Tendons treated with

0.5 mM MGO severed at the edge of the clamps more frequently upon loading and during tensile-strength experiments, further implicating brittleness as the reason for reduced toughness compared with 0.1 mM-treated fibers (Figure 5, D). Graphically, the increase in integration appears to reflect the shortening of the low-strain regime combined with the lengthening of the long, nonlinear high-strain regime. These increases in the magnitude of the stress are sufficient to counter balance the reduction in area that results from the reduced failure strains, even in 0.5 mM specimens. From a physical perspective, this indicates that glycation causes the collagen fibers to resist small deformations with greater force and that the fibers can withstand high stresses over a wider range of strains.

Differences in the mechanical properties of collagen fibers treated with 0.1 mM vs. 0.5 mM MGO are either insignificant (strain at *I*, $E_{apparent}$) or somewhat deleterious (decreasing failure strain, maximum stress, and toughness), in spite of the fact that the concentration of AGEs is much higher for the 0.5 mM treatment (Figure 3). Clearly, the mechanical properties of collagen fibers are not linearly dependent upon the quantity of AGEs. There is likely a dose-dependent regime, but it appears that treatment with 0.5 mM MGO is well beyond that regime. The relative lower amount of CEL incorporated into the 6 month tendons and relative saturation of the physical endpoints at 0.1 mM MGO may not only reflect preexisting blockage of lysine residues at 6 months of age, but also kinetic differences in rates of CEL adduct formation vs. MGO-mediated crosslinks (Figures 3-5). A comprehensive assay of all modifications would be needed to precisely understand the relationship between crosslink formation and changes in modulus, etc; unfortunately, at the present time only a few of the MGO-derived crosslinks are known.

Glycation with 0.5 mM MGO appears to be so extensive that collagen fibers (particularly immature fibers) become somewhat brittle. This may be a result of the way in which stress is distributed in the fiber. Under normal conditions, stress on a fiber is distributed among all of the fibrils and collagen triple helices. When sufficient stress is applied that a triple helix breaks, in the absence of AGEs it does so independent of the other helices. The stress released by the break is then redistributed across the rest of the helices in the fibril. However, if the helix is tightly crosslinked to a neighboring helix, the stress released by the break in the first is transferred directly to its neighbor. Further, the added stress will be localized to the portion of the helix that lies between its crosslinks to the first fibril. The localized stress could then break the second helix, releasing yet more strain energy and allowing the failure to propagate like a crack.

Our findings call into question the oft-repeated assertion that the source of glycation-induced tissue stiffening is intramolecular crosslinking within or between the triple helices of a collagen fibril:[11, 22, 23] at levels of glycation in which the mechanical properties of collagen fibers saturate or decline, the properties of softer collagen-rich tissues (e. g. cornea) continue to increase. The bulk properties of highly-glycated tissues such as cornea do not reflect the brittle state of their constituent fibrils; therefore, stiffening must be more complex than previously assumed.

6.5 Proteoglycans May Play a Role in Tissue Stiffening

Correlations between AGE accumulation, tendon breaking time, and changes in bulk mechanical properties have been used to argue that glycation-induced tissue stiffening is

the direct result of crosslinks that strengthen collagen fibrils;[11, 13, 24] however, we believe this explanation of glycation-induced tissue stiffening to be incomplete. We propose that significant changes in the mechanical properties of soft collagenous tissues such as the cornea must also involve changes in the matrix surrounding the fibrils—most likely via collagen-proteoglycan and proteoglycan-proteoglycan crosslinks.

The Correlation between TBT and Tissue Stiffening is Insufficient to Establish Causality

In the TBT assay, hydrogen bonds and hydrophobic interactions are dissolved in the 7 M urea. This leaves only the covalent crosslinks (enzymatic + AGEs), which are insufficient to keep unglycated fibrils intact under the 2 g load traditionally applied (a 2 g load corresponds to ~ 2.5 MPa for a 100 um fibril).[11] Thus, under denaturing conditions, as AGE crosslinks accumulate, fibril breaking times increase. Under nondenaturing conditions, however, we found that immature fibers (age 6 weeks) with similar diameters to those used in published TBT studies were capable of withstanding loads of no less than 6 g and that mature, unglycated fibers (age 6 months) were capable of withstanding loads up to 20 g in PBS at 37˚ C. Thus, retention of their noncovalent bonds increased the load capacity of the collagen fibrils by a factor of 3 at least. Clearly, noncovalent bonds are responsible for most of the mechanical strength of collagen fibrils *in situ*.

It was assumed that TBT was a good indicator of age-related increases in collagen stiffness *in situ* because of the observed correlations between AGE accumulation and TBT[12, 15, 24] and between AGE accumulation and tissue stiffening.[13, 25, 26] However, we have shown that high levels of AGEs can accumulate (known to increase TBT) without increasing tensile

strength. The assumption that glycation was linearly correlated with increased fiber strength *in situ* resulted in the further assumption that increase in fibril strength was related to the increase in tissue stiffness.[26, 27] In light of our axial extension results, however, it becomes necessary to consider alternative explanations for glycation-induced tissue stiffening at moderate to high levels of glycation.

The Role of Proteoglycans in Glycation-Induced Corneal Stiffening

With knowledge of the relationship between glycation levels and collagen tensile strength, we can estimate the contribution of fibril changes to changes in the cornea as a whole. All mechanical measurements of treated tail tendons indicate that the effect of moderate glycation (treatment with 0.1 mM MGO) is significant; however, glycating with 0.5 mM creates 2 – 3 times more AGEs without a significant increase in mechanical strength. By comparison, corneas treated with 1% GA and 2% GA contain x15 and x30 times more AGEs than the highest levels measured in 0.5 mM MGO-treated collagen fibers, respectively. Thus, if glycation-induced stiffening of cornea were due primarily to stiffening of collagen fibrils, our mouse tail results would predict that 1% GA would already be well into the saturated regime so there would be no further increase in the modulus of corneas treated with 2% vs. 1% GA. This prediction is incorrect: the shear modulus of porcine corneas increased by ~ 300% upon treatment with 1% of GA and by 600% after treatment with 2% GA.

The natural geometry of corneal collagen guides our interpretation of the observed changes in modulus (Figure 1).[3, 28] As stated previously, the major structural element of the cornea

is the stroma, which is composed of lamella of oriented collagen fibrils. We hypothesize that glycation stiffens the cornea and other collagenous tissues primarily by crosslinking fibrils to their associated proteoglycans, which would restrict the translation of collagen fibrils rather than reinforcing/stiffening them. Because the lamellae are believed to compose distinct planes that span the entire cornea,[2] shear modulus measurements on the corneal buttons are analogous to twisting a stack of papers: the resistance to deformation will depend more upon the friction between the sheets of paper than on the moduli of the sheets within the stack. Glycation may "glue the sheets (lamellae) together" in addition to stiffening the fibrils within the sheets.

Using rheometry in combination with biochemistry we have shown that the accumulation of collagen fibril AGEs and increase in TBT at high levels of glycation do not correlate with stronger collagen fibrils. Thus, the simultaneous rise of cornea modulus and accumulation of AGEs on collagen should not be taken to imply causality. Applying the tools of biomechanics to glycated tissue has allowed us to clarify this mechanistic aspect of glycation-induced tissue stiffening.

More generally, our findings suggest that proteoglycans and other apparently nonstructural tissue components may play a more significant role in the biomechanics of healthy and diseased soft collagenous tissues than previously thought. As noted in Chapter 3, the cartilage community is already aware of the importance of proteoglycans in joints; however, other research communities (such as the glycation and ocular biomechanics communities) have yet to explored the biomechanical role of PGs. We hope that this work will help bridge the gap between these fields and bring the tools and understanding of each

to the other. This may be of particular importance in developing novel therapeutics for treating glycation-induced pathologies related to skin[6, 29, 30] and cardiovascular tissues[25, 31, 32] in diabetes and aging.

BIBLIOGRAPHY

1. Fatt I, Weissman BA. *Physiology of the Eye*. Second ed. Boston: Butterworth-Heinemann; 1992.

2. Oyster CW. *The Human Eye: Structure and Function*. Sunderland, MA: Sinauer Associates, Inc.; 1999.

3. Scott JE. Extracellular matrix, supramolecular organisation and shape. *J Anat*. Oct 1995;187 (Pt 2):259-269.

4. Fung YC. *Biomechanics*. Second ed. New York: Springer-Verlag; 1993.

5. Silver FH, Ebrahimi A, Snowhill PB. Viscoelastic properties of self-assembled type I collagen fibers: Molecular basis of elastic and viscous behaviors. *Connective Tissue Research*. Oct-Dec 2002;43(4):569-580.

6. Silver FH, Seehra GP, Freeman JW, DeVore D. Viscoelastic properties of young and old human dermis: A proposed molecular mechanism for elastic energy storage in collagen and elastin. *Journal Of Applied Polymer Science*. Nov 21 2002;86(8):1978-1985.

7. Zhu W, Iatridis JC, Hlibczuk V, Ratcliffe A, Mow VC. Determination of collagen-proteoglycan interactions in vitro. *J Biomech*. Jun 1996;29(6):773-783.

8. Hsu S, Jamieson AM, Blackwell J. Viscoelastic studies of extracellular matrix interactions in a model native collagen gel system. *Biorheology*. Jan-Feb 1994;31(1):21-36.

9. Redaelli A, Vesentini S, Soncini M, Vena P, Mantero S, Montevecchi FM. Possible role of decorin glycosaminoglycans in fibril to fibril force transfer in relative mature tendons - a computational study from molecular to microstructural level. *Journal Of Biomechanics*. Oct 2003;36(10):1555-1569.

10. Duquette JJ, Grigg P, Hoffman AH. The effect of diabetes on the viscoelastic properties of rat knee ligaments. *J Biomech Eng*. Nov 1996;118(4):557-564.

11. Harrison DE, Archer JR. Measurement Of Changes In Mouse Tail Collagen With Age - Temperature-Dependence And Procedural Details. *Experimental Gerontology*. 1978;13(1-2):75-82.

12. Sell DR, Monnier VM. Age-related association of tail tendon break time with tissue pentosidine in DBA/2 vs C57BL/6 mice: The effect of dietary restriction. *Journals Of Gerontology Series A-Biological Sciences And Medical Sciences*. Sep 1997;52(5):B277-B284.

13. Richard S, Tamas C, Sell DR, Monnier VM. Tissue-Specific Effects Of Aldose Reductase Inhibition On Fluorescence And Cross-Linking Of Extracellular-Matrix In Chronic Galactosemia - Relationship To Pentosidine Cross-Links. *Diabetes*. Aug 1991;40(8):1049-1056.

14. Svendsen KH, Thomson G. A New Clamping And Stretching Procedure For Determination Of Collagen Fiber Stiffness And Strength Relations Upon Maturation. *Journal Of Biomechanics*. 1984;17(3):225-229.

15. Degenhardt TP, Thorpe SR, Baynes JW. Chemical modification of proteins by methylglyoxal. *Cellular And Molecular Biology*. Nov 1998;44(7):1139-1145.

16. Tessier FJ, Monnier VM, Sayre LA, Kornfield JA. Triosidines: Novel maillard reaction products and crosslinks from the reaction of triose sugars with lysine and arginine residues. *Biochem J.* Oct 14 2002;Pt.

17. Ahmed MU, Frye EB, Degenhardt TP, Thorpe SR, Baynes JW. N-epsilon-(carboxyethyl)lysine, a product of the chemical modification of proteins by methylglyoxal, increases with age in human lens proteins. *Biochem. J.* 1997;324:565-570.

18. Sell DR, Klaus BK, Oliver R, Vincent MM. Glucosepane is a major glycation crosslink of the extracellular matrix in diabetes and aging. *Diabetes.* Jun 2004;53:A205-A205.

19. Silver FH, Christiansen DL, Snowhill PB, Chen Y. Role of storage on changes in the mechanical properties of tendon and self-assembled collagen fibers. *Connective Tissue Research.* 2000;41(2):155-164.

20. Vogel S. *Comparative biomechanics: life's physical world.* Princeton, NJ: Princeton University Press; 2003.

21. Ayad S, Boot-Handford RP, Humphries MJ, Kadler KE, Shuttleworth CA. *The Extracellular Matrix FactsBook.* second ed. London: Academic Press Limited; 1998.

22. Sell DR, Biemel KM, Reihl O, Lederer MO, Strauch CM, Monnier VM. Glucosepane is a major protein cross-link of the senescent human extracellular matrix - Relationship with diabetes. *Journal Of Biological Chemistry.* Apr 1 2005;280(13):12310-12315.

23. Mentink C, Hendriks M, Levels AAG, Wolffenbuttel BHR. Glucose-mediated cross-linking of collagen in rat tendon and skin. *Clinica Chimica Acta.* Jul 2002;321(1-2):69-76.

24. Elgawish A, Glomb M, Friedlander M, Monnier VM. Involvement of hydrogen peroxide in collagen cross-linking by high glucose in vitro and in vivo. *Journal Of Biological Chemistry.* May 31 1996;271(22):12964-12971.

25. Airaksinen KE, Salmela PI, Linnaluoto MK, Ikaheimo MJ, Ahola K, Ryhanen LJ. Diminished arterial elasticity in diabetes: association with fluorescent advanced glycosylation end products in collagen. *Cardiovasc Res.* Jun 1993;27(6):942-945.

26. Baynes JW, Monnier VM. *The Maillard Reaction in Ageing, Diabetes and Nutrition.* New York: A. R. Liss; 1989.

27. Bruel A, Oxlund H. Changes in biomechanical properties, composition of collagen and elastin, and advanced glycation endproducts of the rat aorta in relation to age. *Atherosclerosis.* Dec 20 1996;127(2):155-165.

28. Davson H. *The Eye.* Vol 1. fifth ed. New York: Academic Press; 1990.

29. McCance DR, Dyer DG, Dunn JA, et al. Maillard reaction products and their relation to complications in insulin-dependent diabetes mellitus. *J Clin Invest.* Jun 1993;91(6):2470-2478.

30. Melling M, Pfeiler W, Karimian-Teherani D, et al. Differential scanning calorimetry, biochemical, and biomechanical analysis of human skin from individuals with diabetes mellitus. *Anatomical Record.* Jul 1 2000;259(3):327-333.

31. Sims TJ, Rasmussen LM, Oxlund H, Bailey AJ. The role of glycation cross-links in diabetic vascular stiffening. *Diabetologia.* Aug 1996;39(8):946-951.

32. Silver FH, Horvath I, Foran DJ. Viscoelasticity of the vessel wall: The role of collagen and elastic fibers. *Critical Reviews In Biomedical Engineering.* 2001;29(3):279-301.

Appendix A – Internal Review Board letter of approval for use of human tissue

CALIFORNIA INSTITUTE OF TECHNOLOGY
Committee for the Protection of Human Subjects

Principal Investigator(s): Dr. Julie Kornfield with Charles Nickerson (graduate student)

Title of Project: Exploration and Engineering of the Chemical and Mechanical Properties of the Vitreous Humor

Funding Agency (if applicable)/identification number: Vitreo Retinal Technologies, Inc.

The above application:

☒ is judged to be exempt under paragraph(s) Sec.101(b)(4). Once ratified, no further interaction with the Committee is necessary unless there is a change in protocol affecting the human participants in this research and/or the project terminates.

☐ was provided with expedited review and approval on _____ with the following qualifications:

_____.

This project will be submitted to the Full Committee for ratification at its next meeting scheduled for Fall 2003. Unless exempt, it will be reviewed annually, but in any event, changes in protocol are to be submitted for further review and approval and the Committee must be advised should any complications arise that adversely affects, or has the potential to adversely affect, the human subjects. As applicable, a current copy of any partner organization's IRB approval must be obtained for this Committee's files.

We certify that this review was carried out in accordance with the requirements of Part 46, "Protection of Human Subjects" of Title 45 of the Code of *Federal Regulations* and the "U.S. Department of Health and Human Services (DHHS) Federal-Wide Assurance (FWA) for the Protection of Human Subjects for Domestic (U.S.) Institutions," California Institute of Technology Assurance #FWA00003897.

Name: Charles R. Plott

Title: Chairman, Committee for the Protection of Human Subjects

Signature: Charles R Plott Date: July 14, 2003

* * * * * * * * * * * *

Name: Richard P. Seligman

Title: Senior Director, Office of Sponsored Research

Signature: Richard P. Seligman Date: July 15, 2003

cc. HSC Files

Appendix B – Experimental Protocol for in vivo tests in Mexico

Eye Test Protocol

Proposed Initial experiments for in vivo studies in Mexico City

Summary of Experiment

Quantify the degree of liquefaction in pig eyes 1 and 15 days after injection with 100 ul of 12% carbamide solution pH~6. (8 animals required) and with 100 ul of 24% carbamide solution pH ~9 (3 animals required) compared to untreated animal eyes (2 animals required). Total = 13 animals required.

Experimental Protocol

Animals #1, #2, #3, and #4 – On day 1 (September 7) treat L. eye with 12% carbamide, pH ~6, R. eye with 0.9% saline, slaughter 15 days later (day 16-Sept. 23): Animal #H1 and #H2- On day 1 treat L. eye with 24% carbamide, pH ~9, R. eye with 0.9% saline, slaughter 15 days later (day 16-Sept. 23).

Animals #5, #6, #7, and #8 – On day 14 (September 21) treat L. eye with 12% carbamide, pH ~6, R. eye with 0.9% saline, slaughter 1 day later (day 15-Sept. 22): Animal #H3- On day 14 treat L. eye with 24% carbamide, pH ~9, R. eye with 0.9% saline, slaughter 1 day later (day 15-Sept. 22).

Animal #9 and #10 – On day 15 (September 22) slaughter animals (to give the opportunity for final instrument check and test runs)

Tests to run

Day 15 (Sept. 22) – I will test the rheology of the 1-day treatment eyes (animals #5-#8 and #H3) and the untreated eyes (animal #9&#10). Please have a clinician test the IOP of the animals prior to slaughter and try to gauge liquefaction using their methods.

Day 16 (Sept. 23) – I will test the rheology of the 15-day treatment eyes (animals #1- #4, #H1, and #H2). Again, please have a clinician test the IOP and liquefaction of the animals prior to slaughter.

Daily Schedule:

Day	1 (Sept. 7)	14 (Sept. 21)	15 (Sept. 22)	16 (Sept. 23)
Treatment	Animal #1-#4- L. eye 12% urea, pH ~6 R. eye saline Animal #H1&#H2 L. eye 24% urea, pH ~9 R. eye Saline	Animal #5- #8- L. eye 12% urea, pH ~6 R. eye saline Animal #H3 L. eye 24% urea pH ~9 R. eye Saline		
Collection			Animals #5- #10 & #H3 - Please check IOP & liquefaction then sacrifice the animals	Animals #1- #4, #H1 & #H2 - Please check IOP & liquefaction then sacrifice the animals

* Note: All injections should be 100 µl. I will arrive on day 13 and leave on day 17

INDEX

Charles S. Nickerson

307 S. Wilson Avenue #9, Pasadena, CA 91106 CSN@CALTECH.EDU
Home (626) 793-6169, Lab (626) 395-4634

EDUCATION

California Institute of Technology, Pasadena, CA Fall 2005
PhD Chemistry (GPA 3.8)

North Carolina State University, Raleigh, NC Spring 2001
BS Physics & BS Chemistry with minor in German (GPA 3.8)

RESEARCH EXPERIENCE

PhD, California Institute of Technology 2001 – 2005

- Developed therapeutic strategies for preventing blindness by combining analytical chemistry, polymer physics, and biochemistry to gain a molecular-level understanding of the bio-networks of ocular tissues
- Collaborated with two diverse research teams that includes biochemists, polymer chemists, polymer physicists, retinal surgeons, and MBA's
- Invented tooling (patent pending) and developed/validated method for adapting traditional Rheological analysis technology for use with slip-prone materials
- Negotiated the acquisition of a suite of instruments and service contracts for the research group at a savings of more than $300,000
- Gained proficiency in numerous chemical and mechanical analysis methods including HPLC, Fluorescence, UV-Vis, and NMR spectroscopies, protein assays, and rheological methods

Undergraduate, North Carolina State University 1997 – 2001

- Excelled in multidisciplinary academic pursuits in chemistry and physics on full scholarship, completing both degrees in 4 years
- Expanded fluent written and spoken German language skills to include technical writing and scientific communication

LEADERSHIP EXPERIENCE

President, Elders quorum, LDS Church, Pasadena 2003 – present

- Responsible for every aspect of 80 member service organization
- Organized members into 22 companionships that visit and report on the needs of ~90 households on a monthly basis
- Motivate participation in service projects and increased attendance

Mentor, Summer undergraduate research program 2003

- Trained an undergraduate in analytical techniques, data analysis, technical writing and creating presentations

Instructor/TA, Introductory chemistry lab 2001 – 2002

- Lectured on fundamental aspects of synthetic and analytical chemistry
- Taught good lab practices and report writing and evaluated performance

Commencement Speaker, NCSU Chemistry department 2001

- Elected as speaker for the chemistry department commencement ceremony by more than 65 graduating peers

President, Sigma Gamma Chi service fraternity, NCSU chapter 1998

- Nearly doubled membership by marketing organization with service projects and social events

PROFESSIONAL EXPERIENCE

Technical Consultant, PriaVision, Inc., Menlo Park, CA Jun 2004-present

- Demonstrate the efficacy of their therapeutic strategy using my invention to quantify its mechanical impact
- Adapt cutting-edge research and technologies for product design

Curriculum Consultant, NC Dept of Public Instruction, Raleigh, NC 2001

- Wrote and evaluated reference materials and test questions for standardized math, physics, and chemistry Exams

Intern, Stockhausen Chemical, Greensboro, NC Summers 1998 and 1999

- Assembled, debugged, and instituted a new multi-media system for evaluating the performance of baby diapers (Anacolour video system)

PATENT

Sole author of US provisional patent (application #4103-P) This invention is under licensing consideration and has lead to several collaborations

RECENT PRESENTATIONS

Presenter, Assoc. for Res. in Vision & Ophthalmology, Ft. Lauderdale, FL 2005

Speaker, Society of Rheology Annual meeting, Lubbock,TX 2005

Speaker, International Congress on Rheology, Seoul, Korea 2004

Speaker, Polymer Networks Group conference, Bethesda, MD 2004

Speaker, Graduate Seminar Lecture, Chemical Engineering, Caltech 2004

Presenter, Assoc. for Res. in Vision & Ophthalmology, Ft. Lauderdale, FL 2004

Speaker, Society of Rheology Annual meeting, Minneapolis, MN 2002

Presenter, Society of Rheology Annual meeting, Bethesda, MD 2001

PUBLICATIONS

- **Nickerson CS**, Kornfield JA, Rheological Properties of the Vitreous Humor and the Role of Hyaluronic Acid, Journal of Biomechanics 2005, *in review*.
- **Nickerson CS**, Kornfield JA, A "Cleat" Geometry for Suppressing Wall Slip, Journal of Rheology 2005, 49 (4), 865–874.

- **Nickerson CS**, Karageozian HL, John Park J, Kornfield JA, Internal Tension: A Novel Hypothesis concerning the Mechanical Properties of the Vitreous Humor, Macromolecular Symposia 2005, 227, 183–189.
- Novak JP, **Nickerson C**, Franzen S, Feldheim DL, Purification of molecularly bridged metal nanoparticle arrays by centrifugation and size exclusion chromatography, Analytical Chemistry 2003, 73, 5758–5761.

SELECTED AWARDS AND FELLOWSHIPS

- **Phi Beta Kappa**
- Graduated **Summa Cum Laude** from NCSU University Honors program
- **ARCS Foundation fellow** 2002 – 2005
- **Tannenbaum-Sternberger Foundation fellow** 1999 – 2001
- 1st prize, NCSU undergraduate physics research colloquium
- Merck Index award, NCSU 2000
- Hypercube award, NCSU 2001
- Sigma Pi Sigma
- NCSU University Scholar, 2001
- Golden Key national honor society
- Eagle Scout